NATIONAL ADVISORY COMMITTEE FOR AERONAUTICS

TECHNICAL MEMORANDUM 1376

EXPERIMENTS ON TAIL-WHEEL SHIMMY

By O. Dietz and R. Harling

Translation of "Experimentelle Untersuchungen über das Spornradflattern." Zentrale für wissenschaftliches Berichtswesen über Luftfahrtforschung des Generalluftzeugmeisters (ZWB), Forschungsbericht Nr. 1320, Berlin-Adlershof, Nov. 25, 1940.

Washington
October 1954

NATIONAL ADVISORY COMMITTEE FOR AERONAUTICS

TECHNICAL MEMORANDUM 1376

EXPERIMENTS ON TAIL-WHEEL SHIMMY* [1]

By O. Dietz and R. Harling

ABSTRACT

Model tests on the "running belt" and tests with a full-scale tail wheel were made on a rotating drum as well as on a runway in order to investigate the causes of the undesirable shimmy phenomena frequently occurring on airplane tail wheels, and the means of avoiding them. The small model (scale 1:10) permitted simulation of the mass, moments of inertia, and fuselage stiffnesses of the airplane and determination of their influence on the shimmy, whereas by means of the larger model with pneumatic tires (scale 1:2) more accurate investigations were made on the tail wheel itself. The results of drum and road tests show good agreement with one another and with the model values.

Detailed investigations were made regarding the dependence of the shimmy tendency on trail, rolling speed, load, size of tires, ground friction, and inclination of the swivel axis; furthermore, regarding the influence of devices with restoring effect on the tail wheel, and the friction damping required for prevention of shimmy.

Finally observations from slow-motion pictures are reported and conclusions drawn concerning the influence of tire deformation.

---

*"Experimentelle Untersuchungen über das Spornradflattern." Zentrale für wissenschaftliches Berichtswesen über Luftfahrtforschung des Generalluftzeugmeisters (ZWB), Forschungsbericht Nr. 1320, Berlin-Adlershof, Nov. 25, 1940, pp. 1-101.

[1]Furthermore, a film on "Tail-Wheel Shimmy" has been made by the Forschungsinstitut für Kraftfahrwesen und Fahrzeugmotoren an der Technischen Hochschule Stuttgart (Research Institute for Automobilism and Vehicle Motors at the Technical Academy Stuttgart) with the cooperation of the Reichsanstalt für Film und Bild in Wissenschaft, Erziehung und Unterricht (State Institute for Film and Pictures in Science, Education, and Instruction), Berlin. This film may be found in the film and photo archive of the ZWB as standard silent film and as microfilm (16 mm).

OUTLINE

I. Problem of the Investigations

II. Test Method and Model Laws

III. Comparison of Full-Scale and Model Tires

IV. Test Organization and Values Used
- (A) Model tests
  - (1) Airplane fuselage torsionally rigid about longitudinal axis
  - (2) Airplane fuselage torsionally flexible about longitudinal axis; consideration of mass distribution
- (B) Full-scale tests
  - (1) On the rotating drum
  - (2) On flat runway

V. Test Performance

VI. Test Results
- (A) Model tail wheel
  - (1) Preliminary tests
    - (a) Influence of the vertical motions of the airplane mass
    - (b) Influence of the wheel mass
    - (c) Influence of the torsional flexibility of the airplane fuselage and of the mass distribution
  - (2) Main tests
    - (a) Without damping
      - (α) Trail
      - (β) Inclination of swivel axis
      - (γ) Rolling speed and trail
      - (δ) Ground friction
      - (ϵ) Load
      - (ζ) Stiffness of tires
    - (b) With damping
      - (α) Friction
      - (β) Spring restoring
      - (γ) Restoring by cam plate
- (B) Full-scale tail wheel
  - (1) Tests on the rotating drum
  - (2) Road tests
- (C) Comparison of results for full-scale and for model tail wheel

VII. Considerations and Observations on the Origin of Shimmy

I. PROBLEM OF THE INVESTIGATIONS

The laterally swiveling nose or tail wheel on an airplane which adjusts in rolling into a stable equilibrium position sometimes shows a tendency toward undesirable shimmying motions. In this shimmy the wheel axis performs oscillatory movements in the lateral direction about a swivel axis which is usually vertical or slightly inclined in the travel direction. The wheel continues rotating about its axis, the tire partly slides on the runway, as shown by the rubbing tracks of a shimmying tail wheel on a tar-macadam runway, figure 1. The consequences are: considerable wear on the tire; frequently noticeable, undesirable vibrations in the airplane due to mass forces of the tail wheel; and the danger for this wheel of having steering members ripped off.

Investigation of the causes of these shimmy phenomena and of the means to their elimination fulfills an urgent requirement. It is true that individual shimmy control measures have become known and have been applied. The fundamental relationships, however, were unknown. The greatest influence is, doubtlessly, exerted by the wheel trail, the rolling speed, the wheel load, and the damping of the rotary motions of the swivel axis.

II. TEST METHOD AND MODEL LAWS

In order to obtain a general idea of the conditions for tail-wheel shimmy, the simpler model method is used instead of the expensive and more time-consuming tests with full-scale dimensions. Therein, the axis of the tail wheel stands still while the "running road" represented by an endless belt (ref. 1) moves contrary to the direction of travel. This method has been used successfully several times at the Stuttgart Institute for Automotive Research; very good agreement with actual full-scale conditions resulted (ref. 2). The present experiments also were supplemented by full-scale tests, and the correctness of the model method was thereby further confirmed.

The first condition for use of the model method is observance of geometrical similitude. The applicable model laws and their relationships have already been basically developed (ref. 1). The ratios between model and full-scale values are indicated below.

The scale of length λ is fixed. The scales of the remaining parameters must be made to agree with the given physical relations and the possibilities of practical execution. It is advantageous if the ratio of the accelerations can be 1:1 since then in occurring vertical motions the effect of gravity is the same for actual and model size. The unequal pressures of the tire on the ground alter somewhat the directivity of the wheel; according to experience (ref. 1), however, the effect on the oscillation process is slight.

For investigation of tail-wheel shimmy, two model apparatus with "running belts" were available. One of them permitted investigation, with higher accuracy, of the behavior of the tail wheel in the scale of length 1:2 without influence of vertical motions of the airplane mass; the other apparatus permitted extensive simulation in the scale of length 1:10 of all airplane parameters, such as fuselage stiffness, mass, and moments of inertia, and of their effects on shimmy.

The scale factors for both scales are (with the ratios denoted by Greek letters):

Lengths λ	1:2	1:10
Accelerations $\beta = \frac{\lambda}{\tau^2}$	1:1	1:1
Times $\tau = \lambda^{1/2}$	1:1.41	1:3.16
Speeds $\varphi = \frac{\lambda}{\tau} = \lambda^{1/2}$	1:1.41	1:3.16
Masses (specific weights $\mu = \frac{\lambda^3\gamma}{\beta} = \lambda^3$ 1:1)	1.8 $\mu = a\lambda^3 = \lambda^2$	1:100
Forces $\chi = \mu\beta = \lambda^3$	1.8 $\chi = a\lambda^3 = \lambda^2$	1:100
Moments of inertia $\Theta = \lambda\chi\tau^2 = \lambda^5$	1:32 $\Theta = \lambda a\lambda^3\lambda = \lambda^4$	1:10000
Torsional rigidities $\delta = \frac{\chi\lambda}{1/\lambda} = \lambda^5$	1:32	1:10000
Relative torsional rigidities referred to unit length $\delta_r = \chi\lambda = \lambda^4$	1:16	1:1000
Spring rigidities $\epsilon = \frac{\chi}{\lambda} = \lambda^2$	1:4	1:10
Stresses $\sigma = \frac{\chi}{\lambda^2} = \lambda$	1:2	1:1

Pressures	$\pi = \frac{\lambda^3}{\lambda^2} = \lambda$	1:2	$\pi = \frac{a\lambda^3}{\lambda^2} = 1$	1:1
Moments	$\Psi = \chi\lambda = \lambda^4$	1:16	$\Psi = a\lambda^3\lambda = \lambda^3$	1:1000

The value a is a conversion factor with the aid of which the ratio of forces can be varied. In the same ratio, there vary then also all parameters related to the forces. The forces transmitted from the runway by means of the friction contact with the tire to the tail-wheel system which is capable of oscillation - chiefly lateral directing forces perpendicular to the wheel plane - vary in this case. However, they are in the same proportion to the remaining forces (in model as well as in actual full-scale conditions) only when equal ground pressures of the tires prevail. According to the table set up above the ratio of pressures must then be

$$\pi = \frac{\chi}{\zeta} = \frac{a\lambda^3}{\lambda}$$

wherein ζ signifies unit area. Hence there results the conversion factor $a = \frac{1}{\lambda}$. If the ratio of pressures $\pi = 1$ is not observed, a may be arbitrarily selected, that is, the model dimensions are then fixed according to some other viewpoints.

III. COMPARISON OF FULL-SCALE AND MODEL TIRES

Equal behavior of the wheels, in actual as well as in model size, presupposes identical tire characteristics, such as lateral deformation and elasticity. For this reason, the model tests were carried out with pneumatic tires especially developed for this purpose. A standard automobile-tire valve provided on the model tire makes a simple checking of the tire-inflation pressure possible. The model tire has, according to its inflation pressure, an outer diameter of 120 to 130 mm, the actual tire (tire size 260 × 85) one of 260 mm. Therewith, the ratio between the lengths, of 1:2, is preserved.

From figure 2, one may recognize that the lateral deformations of the two tires agree very well for approximately equal inflation pressure at standstill. The cornering forces of the rolling wheels in figure 3 also show good approximation. We measured the cornering force required for maintaining the wheel at a certain yaw angle with respect to the direction of travel. Therein a test speed of travel of 19 [27][2] km/h and

[2]The numbers in brackets refer to the full-scale magnitude.

a ground-adhesive friction coefficient $\mu_H = 0.7$ were maintained. The cornering force of the model wheel was measured on the "running belt" provided with a rubber contact surface, that of the full-scale wheel on a rotating drum made of steel, of 1.6 m diameter. According to experiences so far, rotating drums of steel and tar-macadam or asphalt runway show good agreement in cornering force.

The elasticities of the tires in case of vertical load also show good agreement. The model tire deflects for 6.5 kg [52 kg] by 4.8 mm [9.6 mm]. Experiments with the full-scale wheel showed, correspondingly, for approximately 50 kg load a deflection of 9 to 11 mm.

IV. TEST ORGANIZATION AND VALUES USED

(A) MODEL TESTS

(1) Airplane Fuselage Torsionally Rigid About Longitudinal Axis

The construction of the model tail wheel with arrangement of swivel axis and load is schematically represented in figure 4. The tail wheel a rests in a stirrup-shaped support b which can be rotated about the point c whereby a variation of lead or trail of the tail wheel is made possible. The swivel axis d is arranged rotatably in roller bearings and permits the tail wheel to be swivelled through 360°. Friction in the swivel bearings is very slight; the damping caused by it may be varied within wide limits by additional damping l.

The bearing housing e of the swivel axis is hinged to the levers of the parallelogram linkage f which are placed on the lever g which in turn is rotatable and can be locked about the fixed point h. The axis through the fixed point h is supported by a fixture adjustable in height which is placed on a table above a "running belt." The running belt attains speeds up to 15 m/s.

Figure 5 shows the various possible inclinations (angle β) of the swivel axis with respect to the perpendicular and the resulting variation in trail i which represents the distance of the point where the extended swivel axis penetrates the runway from the center of contact between wheel and ground. In the case of swivel-axis inclinations with positive angle β the wheel trail increases with growing inclination; for negative angle β, in contrast, the trail decreases and may be transformed into lead. Figure 6 shows a photograph of the test arrangement.

The indicator a shows on the scale b the varying inclination β of the swivel axis. The shimmy angle α of the tail wheel - that is the

deflection angle formed with the direction of travel during a rotational oscillation about the swivel axis - may be read off with the aid of the indicator c and the scale d.

The loading is produced by weights k (figure 4) which act on the crank arm attached to the parallelogram linkage by means of a control line with rope pulley. A tension spring inserted in the control line balances slight vertical motions of the swivel-axis housing and thereby guarantees uniform load also in the case of an inclination of the swivel axis. The load variations occurring due to the deflection, caused by the then appearing horizontal components, may be neglected.

The shimmy angle could be registered with a recording apparatus which was connected with the swivel axis of the tail wheel via wire line and transmission lever. With the aid of the scale provided on the swivel axis (d in figures 6 and 11), the recording apparatus could be calibrated with respect to the shimmy angle.

In the case of the tail-wheel arrangement investigated first, on an airplane fuselage assumed to be torsionally rigid in the longitudinal axis, four different measures against shimmy were applied:

(a) Friction damping.- Figure 7 shows the test setup with friction damping. A compression spring a presses a molded-plastic disk b bolted to the swivel axis of the tail wheel on to the bearing housing c of the swivel axis. By tightening of the compression spring the damping is increased.

(b) Two restoring springs on a transverse lever (fig. 8).- Two tension springs act by means of a transverse lever b on the swivel axis rigidly connected with the latter so that the wheel is led back into straight-ahead position after deviations. The effect of this restoring springing may be influenced by variation of the spring preloading, spring stiffness, and the length of the transverse lever.

(c) One restoring spring on a longitudinal lever (fig. 9).- A single spring a, acting through a longitudinal lever b, also is capable of exerting restoring moments on the tail wheel. These moments may be varied by application of different spring preloadings and lever-arm lengths. If the wheel, lifted off the ground, is placed obliquely at a certain angle, the restoring moments appearing in rolling may be measured with a calibrated spring balance which acts on a certain lever arm.

Arrangement of the restoring springs is mechanically simpler than the friction device.

(d) Rolling pressure on a cam plate (fig. 10).- A roller a is pressed by means of a spring against a cam plate b which is rigidly

connected with the swivel axis and formed in such a manner that restoring moments always act on the tail wheel. The restoring moment is modified according to arrangement of the cam plate or according to the magnitude of spring pressure.

(2) Airplane Fuselage Torsionally Flexible in Longitudinal Axis; Consideration of Mass Distribution

For investigation of the influence of torsional flexibility of the airplane fuselage on tail-wheel shimmy, the levers g shown in figure 4 were connected with a longitudinal axis a supported in bearings (fig. 11). The fixed point h, according to figure 4, is unscrewed from the support frame for this purpose. The two levers g are rigidly connected with one another by a crosspiece e which is screwed onto the longitudinal axis a, adjustable in height, figure 11. The entire parallelogram guide of the tail-wheel swivel axis therewith now hangs only on this longitudinal axis a and is laterally inclinable with it. The longitudinal axis a is spring-restrained in torque direction by a cross-bar spring (a, fig. 12). With the aid of the clamps b, figure 12, the cross-bar spring stuck through the longitudinal axis may be gripped at various lengths; the torsional flexibility is thereby variable. The torsional angle of twist may be read off the scale c (fig. 12).

To the longitudinal axis a, figure 11, there is screwed, moreover, a crosstube on which the lead weights b may be shifted for adjustment of the moment of inertia about the "longitudinal airplane axis."

This test arrangement, of the model-length scale 1:2, does not permit, it is true, an exact simulation of the parameters which will presumably exert an influence on the shimmy: the values of the relative torsional rigidity of the fuselage ($\frac{C}{l}$ mkg) and of the airplane moment of inertia about the longitudinal axis (J_x mkgs^2).

The reduction scale for J_x and $\frac{C}{l}$ is, for $\lambda = 1.2$, according to the model laws mentioned:

1:32

For a small airplane, one would have to have in the model

$$J_x = \frac{1.9 \times 10^3}{32} = 59.5 \text{ mkgs}^2$$

$$\frac{C}{l} = \frac{GJ_d}{l} = \frac{10^5}{32} = 3130 \text{ mkg}$$

Therein signify:

G	shear modulus
J_d	torsional stiffness constant
$GJ_d = C$	torsional rigidity in m^2kg
l	length of the airplane fuselage stressed with respect to torsion

The maximum possible moment of inertia simulated on the model device with scale 1:2 amounts to $J_x = 0.05$ mkgs^2, the maximum relative rigidity to $\frac{C}{l} = 260$ mkg. Most important, the correct ratio of J_x can therefore not be simulated.

In order to discover, nevertheless, the effects of these airplane parameters and to prove that the simpler rigid clamping of the tail wheel at the parallelogram guide also suffices for investigation of the causes of shimmy, the arrangements schematically represented in figure 13 was used over a running belt. The airplane was simulated at the length scale 1:10. A longitudinal pipe a of 22 mm diameter represents the airplane fuselage; transversely to it a pipe b is mounted for holding the wing masses. Weights c can be shifted on the longitudinal and on the transverse pipe for adjustment of the masses of fuselage and wings.

At one end of the longitudinal pipe a the tail wheel d is mounted the swivel axis e of which is supported in the housing f in roller bearings; the housing itself is rigidly connected with a round bar g supported in roller bearings in the longitudinal pipe a. The round bar is clamped at its other end. In this manner, it acts as torsion-rod spring for simulation of the torsional flexibility of the airplane fuselage.

The recording apparatus h registers the shimmy motions, the recording apparatus i the vertical motions of the airplane fuselage.

In place of wheels, the model airplane has been suspended on springs k which diverge obliquely upward; for low oscillation frequency about the longitudinal fuselage axis, there results thus only an insignificant influence on the tail-wheel shimmy, and a mean position of the longitudinal pipe is maintained. A rope l holds the model on the runway in the direction of travel.

All freedoms of motion the actual airplane possesses have therefore been maintained in the model airplane with its tail-wheel swivel axis. The moments of inertia J_y and J_z about transverse and normal axis therewith also take effect.

The values used on this airplane simulation correspond to a relatively small airplane and amount to:

	Full scale	Model
J_x	320 to 330	0.0337 $mkgs^2$
J_y	640 to 720	0.068 $mkgs^2$
J_z	960 to 1050	0.0995 $mkgs^2$
Flying weight	2200 to 2650	26.5 kgs
Torsional rigidity C/l	1.0×10^5	3 mkgs

The torsional rigidity of the model arrangement amounts to only approximately one-thirtieth of the one required according to the model law.

(B) FULL-SCALE TESTS

(1) On the Rotating Drum

For the full-scale tests which were run parallel to the model tests, a full-scale tail wheel (wheel size 260 × 85) was placed on a drum of the automobile testing field having a diameter of 1.6 m (figs. 14 and 15). The tail wheel with shock-absorber leg was built into a frame and loaded with weights b by means of a crosslever a (fig. 14). The shimmy angle may be read off during the test on a scale c. By initial load of various magnitude, a restoring moment was tentatively exerted on the tail wheel by means of the two tension springs d. The trail of the tail wheel is adjustable. Figure 15 shows various openings in the tail-wheel fork into which the swivel pin is inserted for varying the trail.

(2) On Level Road

For investigation of the shimmy of tail wheels on the road and in the field, a passenger car with front-wheel drive is at disposal; the tail shock-absorber leg may be built in at the free rear end of this car (fig. 16). The adjustable load is applied by means of a control arm a by a compression spring b. A recording apparatus c registers the shimmy variation. The wheel may be unloaded by means of the lever d.

V. TEST PERFORMANCE

The following influences on tail-wheel shimmy had to be investigated:

Lead and trail of wheel
Inclination of swivel axis
Running speed
Friction between wheel and runway
Tail-wheel load
Tire-inflation pressure and tire deformability
Torsional rigidity of airplane fuselage
Moment of inertia about longitudinal axis of airplane
Vertical motions of airplane mass
Damping of the shimmy motions

In order to make a comparison between the single test series possible, first of all the friction between wheel and runway, running speed, and tail-wheel load had to remain always constant. They were varied only in special cases.

The adhesive-friction coefficient in the model and drum tests could be kept within the limits $\mu_H = 0.4$ and $\mu_H = 0.5$ by means of talcum-powder treatment of the runway. In case of grassy ground the coefficient is, according to measurements, lower by about 5 to 10 percent.

The results of the model tests may be transferred, with the aid of the model-conversion factors, to the full-scale tail wheel. One of the main conditions for the transferability is the analogous lateral deformation of the tire; according to experiments, there result then also like cornering forces on the ground in the case of oblique running (refs. 1 and 3). As shown before in figures 2 and 3, this agreement actually occurs. The performance of the measurement is represented in figure 14. The wheel with control line and dynamometer is held in an oblique running position with respect to the actual traveling direction. The same procedure was used for the model wheel.

The wheel load was in most cases 6.3 [50] kg. Only in the special case of investigation of the influence of different wheel loads, the model wheel was loaded up to 9 kg.

The running speed usually maintained was 19 [27] km/hr; at this speed the most violent shimmy occurred. For representation of the landing operation, the running speed was increased up to 48 [70] km/hr.

VI. TEST RESULTS

(A) MODEL TAIL WHEEL

(1) Preliminary Tests

Admissibility of the simplifications made on the model arrangement at the scale 1:2 was clarified in preliminary tests.

(a) Influence of the vertical motions of the airplane mass.- From the arrangement of the swivel-axis guides for the model device at the scale 1:2 (according to fig. 4), there results the fact that the vertical motions of the airplane mass which actually occur in tail-wheel shimmy in case of inclined swivel axis and which show, in consequence, fluctuations in wheel load, are here eliminated up to a certain degree.

In order to learn the influence of such vertical motions of the airplane mass, running tests were performed on the free-suspended arrangement of the airplane fuselage with adjustable weights for fuselage and wing masses according to figure 13. The longitudinal pipe a representing the torsional rigidity and the mass of the airplane fuselage, with the adjustable mass c_1, was fixed in vertical direction by means of a support spanning the running belt. By springing the swivel axis in its housing, the ground pressure was kept constant. Also, the lateral oscillations of the swivel axis were prevented.

The simultaneously recorded motions of shimmy and of the raising and lowering of the fuselage are reproduced in figure 17 for the torsionally flexible and the torsionally rigid fuselage. In the course of the recordings, the vertical freedom of the fuselage was cut out and cut in. There occurs hardly a change in the shimmy recordings. Only for torsionally flexible fuselage, thus for lateral inclination oscillations of the swivel axis, the shimmy angle increases slightly due to the vertical motions of the fuselage.

Thus it may be assumed that no significant modifications of shimmy occur due to the simpler tail-wheel suspension according to figures 4 and 5 at the model-length scale 1:2.

(b) Influence of the wheel mass.- The tests on the simplified model device at the scale 1:2 could be performed only with a wheel, provided with a pneumatic tire and with a steel hub, of 0.91 kg weight and a moment of inertia about the axis of rotation $\Theta = 0.0114$ cmkgs^2. The shimmy oscillations originating for 30 mm trail, [60 km/hr] running speed, and a road-traction coefficient $\mu_H = 0.4$ are recorded in figure 18, at right. With the wheel load increasing from 6 through 9 to 12 kg, the shimmy deflections become larger.

A full-scale wheel to be compared with this model wheel, of a diameter of 260 mm and a width of 85 mm, weighs 1.64 kg and has a moment of inertia $\Theta = 0.104$ cmkgs^2. With the conversion factors valid for a scale 1:2, there hence result model values of $G = 0.21$ kg and $\Theta = 0.0033$ cmkgs^2. The fabricated model wheel is therefore too heavy. In order to discover faults possibly arising from this fact, a wheel of equal size was made with a hub of light metal. It weighs 0.45 kg and has a moment of inertia $\Theta = 0.0068$ cmkgs^2 which therefore still has twice the required magnitude.

Figure 18, left, shows the shimmy phenomena for the wheel with light-metal hub for different wheel loads, obtained under the same conditions as for the wheel with steel hub.

The deflections and oscillation frequencies are approximately the same for various vertical weights.

It may be assumed that a further reduction of the tail-wheel mass by about 50 percent - whereby the values to be compared of the full-scale wheel would be exactly simulated - would not cause a significant change in shimmy tendency, either.

Further model tests were therefore carried out with the model wheel with steel hub.

(c) Influence of torsional flexibility of the airplane fuselage and of the mass distribution.- With the apparatus of the length scale 1:10 simulating an airplane (fig. 13), the influence of the torsional flexibility $\frac{GJ_d}{l}$ of the fuselage, and of the moments of inertia J_x, J_y, and J_z of the airplane was checked.

In two test series, the tail-wheel swivel axis was, one time, fixed so that it could not perform lateral motions; the other time it could freely move, with the longitudinal pipe a representing the airplane fuselage. Figure 19 shows the arrangement of the model-airplane apparatus on a running belt with the swivel-axis housing fixed on a crossbeam. The housing contains the tail-wheel springing which produces the ground pressure corresponding to the airplane loading. The positioning of the swivel axis thus corresponds to that on the larger model (scale 1:2, fig. 4).

In figure 20, the swivel-axis housing is free and the airplane model is now suspended only by two springs, with the tail wheel held against the running belt. This system, capable of oscillation, is like the full-scale airplane with respect to the effects of the moments of inertia of the airplane, of the torsional rigidity of the fuselage, and of the position of the center of gravity.

The recordings of the tail-wheel oscillations thus obtained are represented in figures 21 and 22.

Figure 21, top, shows the shimmy oscillations for fixed swivel axis and constant running speed [40 km/hr]. The shimmy angles are, on the average, 45°, for an oscillation frequency of 24 [7.6] cycles per second. With the slow increase in running speed, shimmying ceases at [55 km/hr], with the oscillation frequency rising to 32 [10.1] cycles per second.

By release of the swivel axis, the shimmy motions become slightly more violent, the shimmy angle increases, at an oscillation frequency of 18 [5.7] cycles per second, to 54° and is damped only at [80 km/hr] with a frequency of 30 [9.5] cycles per second, figure 22.

The oscillation frequencies therefore increase approximately in the same proportion as the running speed.[3]

The first cause of this intensified oscillation is the excess (30 times) bending flexibility of the longitudinal pipe (a in fig. 13) representing the fuselage. The entire swivel axis thus oscillates laterally parallel to itself; torsional oscillations about the fuselage axis could hardly be observed.

However, as far as lateral inclinations of the tail-wheel swivel axis appear due to the torsional flexibility of the airplane fuselage, they will doubtlessly intensify the shimmy motions. It is worth knowing how the two motions affect one another.

The model arrangement at the scale 1:2 permits lateral inclinations of the swivel axis by springing of the longitudinal axes a representing the airplane fuselage (fig. 11) in the torsional direction. The relatively large torsional flexibility used here, of $\frac{c}{l} = 136\,[4.35 \times 10^3]$ mkg results in the case of normal adjustment (load $P = 6.3\,[50]$ kg, running speed $v = 19\,[27]$ km/hr) in the angles of twist of the fuselage or angles of inclination of the swivel axis γ which are plotted against the trail i in figure 23. The moment of inertia of the airplane represents the parameter. For larger Θ (Θ_3 and Θ_4) angles of twist γ averaging 2.5° or 4° appear. The small moments of inertia Θ do not allow an angle of twist γ larger than 2°. Comparing the therein occurring shimmy angles α in figure 24 one finds that up to angles of twist $\gamma = 2°$ corresponding to a moment of inertia Θ of 0.013 [0.41] mkgs^2 the shimmy angles α are only slightly larger than those originated in the case of laterally fixed swivel axis.

Angles of twist γ larger than 2° will hardly occur in an airplane.

---

[3]In the further investigation of tail-wheel shimmy on the steel drum, the oscillation frequency is discussed in more detail.

This effect of fuselage twist on shimmy becomes even clearer in the case of a still more flexible fuselage with $\frac{C}{l} = 56$ [1.8×10^3] mkg, figures 25, 26, and 27. The small moments of inertia Θ_1 and Θ_2 result in angles of twist γ up to 5° (figs. 25 and 26). Up to $\gamma = 5^\circ$, again corresponding to $\Theta = 0.013$ mkgs^2, no real increase of the shimmy angle α can be ascertained, according to figure 27. Only when the angles of twist γ increase to 7° to 12°, with moments of inertia Θ above 0.01 mkgs^2, the shimmy too increases considerably, up to shimmy angles of 100° to 135°.

Since angles of twist up to 3° do not occur in the airplane fuselage, a significant influence on the shimmy by the airplane mass and the fuselage flexibility can thus not be expected as has been proved already by the tests with the smaller model. The further tests may therefore be made with rigidly fixed tail-wheel axis.

(2) Main Tests

(a) Without damping.- The main investigations were made with the laterally not inclinable swivel axis (figs. 4 and 5). Therewith the influence of the torsional flexibility of the airplane fuselage is essentially eliminated. However, the preliminary investigation has shown that this may be done without significant error.

Below, the possible influences on tail-wheel shimmy are individually investigated.

(α) Trail: Probably the greatest influence on tail-wheel shimmy is exerted (as already shown by the preliminary tests) by the magnitude of the wheel trail (i in fig. 5). A tail wheel with lead is always unstable and attempts sudden change to the trailing state. The transitional position i = 0 represents the neutral equilibrium position of the tail wheel. The wheel maintains any position oblique to the direction of travel it has been given. With the appearance of trail, the wheel starts shimmying. With increasing trail, the shimmy is intensified (figs. 28 and 29) and attains in the present case a maximum value at 30 [60] mm trail. The ratio of trail to wheel diameter is $c_{fl} = \frac{i}{d} = \frac{30}{130} = 0.23$. With further increase of trail, the shimmy decreases again, and for 75 to 80 [150 to 160] mm trail stability exists. In this case, the factor $c_{st} = \frac{80}{130} = 0.62$. The general validity of the proportional values c_{fl} and c_{st} will be examined in further tests.

(β) Inclination of swivel axis: Figures 28 and 29 also show the influence of the inclination β of the swivel axis in the running-direction plane perpendicular to the runway. By inclining the swivel axis in running direction (fig. 28), there originates the positive inclination

angle $+\beta$, with the trail i being reduced. Due to this inclination of the swivel axis, restoring forces of the ground pressure about the swivel axis originate. However, the shimmy deflection is thereby modified only insignificantly. The principal influence is produced by the modified trail.

Inclination of the swivel axis contrary to the running direction ($-\beta$), figure 29, also results, for all inclinations investigated, in only a slight influencing of shimmy by the restoring forces.

(γ) Rolling speed and trail: The shimmy tendency is influenced to a great extent by the rolling speed. Shimmying starts at a lower, and ends at an upper speed limit. The speed range with shimmy tendency, in turn, is influenced by the wheel trail.

In figure 30, the shimmy range is represented as a function of rolling speed and trail. Shimmying starts throughout at [5] to [10] km/hr speed and ends in the present example at [60] to [70] km/hr. In the most unfavorable range of trail from 20 [40] to 50 [100] mm, the limiting speeds are spread apart the fartherest. The more the trail deviates from this range, the more closely the limiting speeds converge. Above i = 65 [130] mm trail and below i = 7 [14] mm, no shimmy at all occurs.

The adhesive or sliding friction on the ground therein plays a subordinate role. Only with additional damping about the swivel axis is the shimmying range reduced (fig. 30, long-dashed).

Figure 31 shows how for a trail of i = 20 [40] mm, the shimmy angle varies with the running speed. The speed was reduced slowly from [55] km/hr. Maximum shimmy prevails at [15] to [20] km/hr; afterwards, it decreases rapidly and ceases shortly before the wheel is at standstill.

This dependence of the shimmy tendency of tail wheels also agrees with the results obtained by Kantrowitz (ref. 4) from numerical and experimental investigations which became known only after the writing of the present report. There a maximum shimmying is reached, with increasing running speed, at 14 km/hr; with further increase in speed, the shimmy likewise decreases and ceases at 50 to 55 km/hr.

(δ) Ground friction: Figures 31 and 32 show again the influence of friction between wheel and runway. For an adhesive-friction coefficient $\mu_H = 0.4$, the maximum shimmy angle $\alpha_{max} = 60^\circ$ to 70°, for $\mu_H = 0.7$ it is $\alpha_{max} \approx 80^\circ$. These two friction coefficients probably correspond to grassy ground and to a concrete landing runway in the actual case.

Outside of the range of maximum shimmy tendency, the differences in shimmying are generally very small.

(ε) Load: As already shown by figure 18, shimmy increases with the load. The shimmy angle for three different loads is plotted against the trail in figure 33. The maximum shimmy angle α amounts to 38° for 3 kg load, to 60° for 6 kg, and to 76° for 9 kg. The trail required for elimination of shimmy likewise increases with the load.

By means of the lateral forces at the point of contact between tire and runway the shimmying tail wheel is supplied with energy and the oscillating tail-wheel system is thus excited. With rising wheel pressure the lateral forces increase and feed more oscillation energy into the tail-wheel system, in consequence of which the shimmy must be intensified. This process will be discussed more thoroughly later on.

(ζ) Stiffness of tires: The influence of the tire-inflation pressure which determines the tire stiffness has not yet been fully clarified. In section VII, p. 24, some opinions regarding it are reported.

In figure 34, one can see how, with rising tire-inflation pressure, the shimmy angle α increases. The immediate cause is the improved cornering making its appearance in case of increased lateral stiffness of the tires, thus larger cornering forces for the same angular deflection on the ground.

In the present tests, the maximum shimmy angle α increases from 64° to 81°, for an increase in tire-inflation pressure from 0.5 to 1.5 atmospheres gage pressure.

In contrast, a laterally rigid wooden wheel is completely free from shimmy. Thus, a maximum shimmy tendency must exist for a certain tire hardness. If, therefore, the tire stiffness exceeds the one at which maximum shimmy occurs, its further increase must cause a reduction of shimmy. This is in agreement with data from practice according to which the shimmy of an airplane tail wheel was reduced by increase of tire-inflation pressure.

(b) With damping.- (α) Friction: It suggests itself to prevent shimmy oscillations by frictional damping. According to figure 7, this can be done by braking the rotations of the swivel axis against its bearing housing.

In the following photos, the shimmy without damping corresponds to that of the normal adjustment for 6.3 [50] kg wheel load, 25 [50] mm trail, 19 [27] km/hr speed, and μ_H = 0.4 to 0.5. The shimmy was registered by the recording apparatus and represented in figure 35, curve 5(a). The shimmy angle α therein amounts to 30° to 45°. By means of a mean friction moment of 1 [16] cmkg, the shimmy angle is reduced to one half (curve 5(b)), and by a friction of 1.9 [30] cmkg, a diminishing oscillation (curve 5(c)) is obtained.

The variation of the friction moments required for the damping of shimmy, as a function of the trail i, and for different wheel loads P (6 and 9 kg), is indicated in figure 36. For 9 [72] kg wheel load and unfavorable trail, the friction moment must amount to 4.1 [65] cmkg. The inclinations $\pm\beta$ of the swivel axis do not influence the necessary frictional damping.

(β) Spring restoring: Frequently, the attempt is made to counteract shimmy by spring restoring of the deflected tail wheel to its straight-ahead position. Since a shimmy of the tail wheel must be preceded by a disturbance in the rolling-off of the wheel, and since thus, for instance, also, an oblique ground contact, that is, a deflected tail wheel, has an exciting effect, an excitation of shimmy which could originate in an oblique ground contact of the tail wheel could be avoided in this manner.

The effects of two (fig. 8) and of one restoring spring (fig. 9) were investigated. The restoring-moment characteristics used are plotted in figure 37. They were modified by variation of the spring compression, of the lever arm acting on the swivel axis, and of the spring characteristics themselves.

As figures 38 and 39 show, an effective damping of shimmy by means of restoring springing is attained only with spring compressions of 15 to 20 [120 to 160] kg. In this case, the corresponding full-scale wheel load is only 50 kg. The full-scale wheel, however, may be loaded with 250 kg.

In the upper limiting range of shimmy, thus at speeds of [50 to 60] km/hr, where shimmy may be eliminated by slight changes, all restoring moments indicated in figure 37 had a damping effect of about the same magnitude. The upper limiting speed was then reduced for normal adjustment from [60] to [35 to 45] km/hr.

Tests with 12 [96] kg load yielded, up to 20 [160] kg preloading (curve 20 × 9.3, fig. 37), no damping of shimmy but resulted in strong shaking forces which were transmitted by the restoring springs to the test apparatus, thus for the full-scale case to the airplane.

Where damping was present, it must be assumed that for such large spring forces the increase of friction in the bearings and at the points of rotation had an accompanying damping effect.

(γ) Restoring by cam plate and roller pressure: A restoring of the tail wheel was attained with the apparatus according to figure 10 by means of radial pressure of a spring-loaded roller on a cam plate. The curves plotted in actual size in figures 40(a) and 40(b) yield maximum restoring moments of 15 and 10 cmkg. The basic variation of the restoring moments is represented at right. According to figures 41 and 42, diminishing

shimmy oscillations were attained with both curves. Particularly the curve form according to figure 40(a), with its pronounced self-alinement in straight-ahead position, counteracted shimmy.

(B) FULL-SCALE TAIL WHEEL

(1) Tests on the Rotating Drum

In order to supplement the model tests and to check the transferability of their results to actual conditions, running tests were performed with a wheel of the size 260 × 85 on the rotating drum (figs. 14 and 15).

The results of these tests for vertical swivel axis, different trails, and different loads are represented in figure 43. The running speed was 40 km/hr and resulted in maximum shimmy deflections for a coefficient of lateral adhesion to the ground at standstill of $\mu_H = 0.7$ to 0.8. For the wheel pressures of 50 and 100 kg (250 kg permissible) employed here, the shimmy at first increases with the trail, reaches its maximum for $i = 60$ to 80 mm and diminishes for $i = 120$ mm. The ratio of trail to wheel diameter is for

Maximum shimmy: $C_{fl} = \frac{i}{d} = 0.23$ to 0.30

Stability: $C_{st} = 0.46$

By doubling the wheel pressure, the shimmy angle becomes slightly more than twice as large.

The influence of the running speed v on the shimmy for different trail i is expressed in figure 44. As in the model test, figure 30, the trail i has been plotted against the running speed v. To every trail there pertains here, too, a lower and upper limiting speed. In case of speeds between both, shimmy occurs. Likewise an upper and a lower trail value limit the shimmy range.

In figure 44 the values are plotted for 50 kg wheel pressure and two different adhesion coefficients of the rotating drum of $\mu_H = 0.5$ and $\mu_H = 0.78$. Corresponding to the results obtained so far, a higher wheel pressure widens the shimmy range.

(2) Road Tests

With the test apparatus described according to figure 16, the tail wheel could be towed on the road by a passenger car. The shimmy phenomena are slightly more pronounced than on the rotating drum; the reason probably lies partly in the oscillations of the car body excited by road roughnesses, but mainly in the mounting of the swivel axis with respect to lateral-inclination motions, which is not quite as rigid as on the rotating drum.

Fundamentally, shimmy again at first increases with the trail, figure 45, and then decreases. The influence of the road roughnesses is recognizable in the recordings of the shimmy variations in amplitudes of different magnitude.

The tail wheel placed with the car on the rotating drum also shows these fluctuations of shimmy deflections when - as shown in row III, figure 46 - the car body is set in vertical oscillation, and the tail-wheel pressure is thereby changed. The natural oscillations of the laterally excited car body differ so much from the frequencies of tail-wheel shimmy that no mutual influence can be established.

The basic dependence on the trail does not change compared to the rotating drum; this is shown by the shimmy angles α plotted against the trail i in figure 47. In their magnitude also, the shimmy angles show agreement for operation on the road and on the rotating drum when the shimmy angles of the vertically moved car body on the rotating drum are compared with those measured on the road.

(C) COMPARISON OF RESULTS FOR FULL-SCALE AND FOR MODEL TAIL WHEEL

Since the tail-wheel drum and road tests had shown satisfactory agreement of the shimmy angles dependent on trail and running speed, the comparison of the results of the model tests and the drum tests may be taken to be valid also as a comparison of the values of a model wheel on a running belt and a full-scale wheel on a stationary runway.

In this comparison one must note, above all, the proportionality factors for lengths (1:2), speeds (1:1.41), and forces (1:8). Comparing the influence of the trail on the shimmy angle of the model wheel (figs. 28 and 29) with the corresponding results of the full-scale wheel on the drum (fig. 43), one obtains the following comparative values:

	Model	Full-scale
Load	6.25 [50]	50 kg
Speed	19 [27]	40 km/hr
Adhesive-friction coefficient	μ_H = 0.4 to 0.5	μ_H = 0.6 to 0.8
Most unfavorable trail range	20 to 40 mm [40 to 80]	50 to 80 mm
Maximum shimmy angle	$\alpha = 60^\circ$	26° (60° for 100 kg wheel pressure)
End of shimmy for a trail of	70 to 75 mm [140 to 150 mm]	120 to 130 mm

If one takes into consideration that the running speed in the full-scale test was too high and that the shimmy angle thereby must be smaller, and that on the other hand, the higher adhesive friction under actual conditions increases the shimmy angle only slightly, the agreement of the most unfavorable trail range and of the maximum trail value at which shimmy still occurs, may be called satisfactory.

Figure 48 gives a comparison of the initial and end speeds of shimmy obtained on the model on the running belt and under actual conditions on the drum, which can be altered considerably even by minute influences.

The values of limiting trail obtained with corresponding adjustments result generally in coinciding curve lines. The upper limiting speed is for the model 72 [102] km/hr, for full scale 120 km/hr. The upper limiting value of trail is for the model 62 [124] mm, for full scale 108 mm. The lower limiting values are in good agreement with 10 [20] mm in every given case.

VII. OBSERVATIONS ON THE ORIGIN OF SHIMMY

The energy required for excitation of the shimmy oscillations must be transferred to the tail-wheel system capable of oscillation at the point of contact between wheel and runway.

Due to the wheel's running obliquely to its direction of travel, lateral forces are known to originate (refs. 5, 6, and 7) which cause deformations at the point of contact with the ground. The more obliquely the wheel plane is situated with respect to the rolling direction at the yaw angle φ, the more these lateral deformation forces increase. These lateral forces attempt to restore the obliquely running wheel to the direction of travel. They thus counteract a lateral motion of the wheel as will occur in shimmying.

Shimmy can be maintained only by forces acting in the direction of the shimmy motion. They must be connected with a lateral deformation of the tire which leads the lateral motion of the wheel.

The lateral deformation of the tire which seemingly leads or lags with respect to the lateral motion signifies energy input or energy output of the oscillating system. In first approximation the magnitude of the force K transferred at the point of contact may be assumed to be linearly related to the lateral deformation s_E, figure 49. Thus

$$K \sim s_E$$

The lateral path of the point of ground contact which for rest position of the wheel forms the center of the contact surface is assumed to be s_B. The energy transferred on the infinitesimal path ds_B then is

$$dA = K\, ds_B$$

Since, however, $s_B = s_R + s_E$ where s_R signifies the lateral path of the wheel center, dA becomes

$$dA = K(ds_R + ds_E), \text{ or } dA \sim s_E\, ds_R + s_E\, ds_E$$

The work transferred during an oscillation process may therefore be represented as a diagram in which $K \sim s_E$ is plotted against the path $s_B = s_R + s_E$ of the point of ground contact.

Figures 50 to 52 show slow-motion pictures of shimmying elastic tires with about 800 frames per second against the variation of the lateral tire deformation, for a full-scale as well as a model wheel, both with high and with low tire-inflation pressure. In all cases the change in direction of the lateral deviation occurs only after the wheel has passed through the position of running straight ahead. In case of the harder tire (figs. 50 and 51) the change takes place 0.004 to 0.005s after the crossing, in the case of the softer one (fig. 52) 0.014s after. The shimmy frequency of all these wheels is of the same order of magnitude.

The deformation diagram or energy diagram which was derived from the deformations observed encloses a positive work area (fig. 53) which signifies energy absorption of the oscillating system. The shimmying oscillation excited must therefore be a stable or self-reinforcing oscillation.

One may prove simply also in an analytical manner that the phase shift of the deformation oscillation of the tire with respect to the oscillation of the wheel is decisive for the origin of shimmy. Let the oscillation of the wheel be given by

$$s_R = R \sin \omega t$$

that of the tire deformation by

$$s_E = -E \sin(\omega t - \epsilon)$$

where ϵ is the phase shift of the deformation oscillation with respect to the wheel oscillation. It was determined experimentally that s_E changes its sign, with respect to time only after s_R, that therefore ϵ is positive and smaller than $\frac{\pi}{2}$.

According to the discussion on page 22 the energy transferred to the system is

$$dA = c(s_E \, ds_R + s_E \, ds_E)$$

If one substitutes therein the above expressions for s_R and s_E and integrates over a complete period, one obtains

$$A\int_0^{2\pi} = c\omega ER\pi \sin \epsilon$$

One sees from it that the energy absorbed by the system A becomes positive, that is, that the system can shimmy when $\epsilon > 0$ as was found experimentally and in agreement with the above considerations.

As already shown by the model tests, a tail wheel with only one degree of freedom of movability about the swivel axis does not shimmy. Only another degree of freedom, such as the lateral flexibility of the elastic tire, leads to shimmy. Thus one can explain an energy absorption of the oscillating system with the sole consideration of the lateral deformation of the tire. The slow-motion pictures confirm that the re-formation of the deformation always takes place a few thousandths of a second after the wheel's passage through its straight-ahead running position.

The delay in the re-formation of the deformation will be the greater, the softer the tire. According to the explanations given so far, the softer tire should absorb more energy, with reference to the oscillation phenomenon, and should lead to more pronounced shimmy. However, with increasing softness of the tire, the variation of the cornering force of the tire on the ground also changes as a function of the yaw angle. The cornering characteristic curve of the tire then shows a flatter variation (refs. 3, 8, and 9), that is, for equal lateral deformation and also for equally oblique run the softer tire is, in the range of yaw angle considered, capable of transferring only correspondingly smaller lateral forces and thus less energy. Thus tire deformation and cornering power complement one another, and the most pronounced shimmy will not occur either in the case of the harder or the softer tire but there where both influences complement one another to a maximum amount of transferable energy.

Even though in the model test the shimmy increased with the tire-inflation pressure, it may nevertheless decrease in case of another model wheel or under actual conditions. The decisive factor is, whether the shimmy-test values used have exceeded the most favorable relationship between tire stiffness and cornering values or have fallen short of it.

A calculation taking into consideration such influences which largely determine the shimmy is being carried out separately at the institute, and a separate report on it will be made.

VIII. SUMMARY

The experimental investigations of the causes of shimmy in airplane tail wheels and the means to its prevention were carried out with model wheels on running belts, and with a full-scale tail wheel on a rotating drum and, after installation in a trailer, on the road.

For the model tests, tail wheels with pneumatic tires on the scale 1:2 and elastic solid-rubber wheels on the scale 1:10 were used. The comparatively large model wheel 1:2 permitted more accurate measurements which could be converted more exactly to full-scale conditions, but did not allow an investigation of the influences on shimmy of the airplane mass and its moments of inertia about the principal airplane axes, and of the stiffness of the fuselage. With the small model scaled 1:10, the airplane characteristics mentioned could be simulated and investigated as to their fundamental effect on shimmy.

It was found that the vertical motions of the airplane mass excited by the tail-wheel shimmy increase the shimmy deflections only slightly and extend the shimmy range which is dependent on the rolling speed only insignificantly.

The fuselage stiffness and the moments of inertia of the airplane also affect the shimmy tendency only slightly. Essentially, only the shimmy at the limit of its occurrence range is noticeably affected; particularly the upper limiting speed above which no shimmy occurs is increased by about 10 to 20 percent, due to the shimmy promoting slight lateral inclinations of the tail-wheel swivel axis which are possible owing to the torsional flexibility of the airplane fuselage.

In the speed range with maximum shimmy deflections no noticeable influence of the airplane masses and stiffnesses appears.

Consequently, the investigations on the large model could be performed without the extensive construction required for simulation of the airplane. For a tail wheel without damping in the swivel-axis bearing the following facts were recognized:

Oscillations occur mostly only after a preceding external excitation, for instance, by oblique ground contact between tail wheel and runway, or by runway obstacles. The shimmy tendency is affected very strongly by modification of the wheel trail. For the present design it is most pronounced for a trail of 25 to 35 mm (the ratio of trail to wheel diameter is on the average $c_{fl} = \frac{i}{d} = 0.23$) regardless of whether the swivel axis is inclined in or against the direction of travel. The effective restoring forces about the swivel axis exert only slight influence. Here, too, the oscillating tendency is determined by the thus modified magnitude of trail. With increasing or decreasing trail the shimmy is reduced and ceases altogether for 0 or 78 to 80 mm trail, thus for a ratio trail to wheel diameter of $c_{st} = 0.62$.

The shimmy varies also with the running speed. It occurs in the present case between a lower speed limit of [5] to [10] km/hr and an upper one of [60] to [75] km/hr, with the maximum value at [27] km/hr.

The amount of friction between tire and runway affects chiefly only the shimmy deflections in case of unfavorable values of trail and speed; the shimmy range is only slightly affected by it.

A very large influence is exerted by the load. Not only the shimmy deflections increase with it, but also the ranges of trail and speed in which shimmy occurs.

The effect of the tire-inflation pressure is, on the whole, not decisive.

A certain means for prevention of shimmy is the damping in the swivel axis. However, for 9 [72] kg load and unfavorable values of trail and speed 41.1 [65] cm kg damping moment had to be applied for complete

elimination of shimmy. The investigations of Kantrowitz (ref. 4) confirm the favorable effect of a damping. The damping moment required in the swivel axis may be calculated according to the formula indicated by him. It is, for a wheel of 260 mm diameter, 70 kg wheel load, and an adhesive-ground friction coefficient $\mu_H = 0.65$:

$$\left[30 \text{ to } 80\right] \text{ cm kg}$$

and thus lies in the order of magnitude of the required damping moment determined in the present report by a purely experimental method.

Restoring springs or cam plates with restoring action have only little effect unless a certain self-alinement already exists in zero position.

Results obtained with the full-scale wheel on the rotating drum and on the road were in satisfactory agreement. Considerations of the causes of shimmy of tail wheels, supported by slow-motion pictures of the shimmying phenomenon, led to the finding that in case of laterally rigid position of the swivel axis and rigid tire every excited shimmy oscillation must be damped since the energy supplied is consumed by the friction. A laterally rigid tire may shimmy when the swivel axis shows, for instance, lateral play or freedom of motion. The deformability of the tire gives rise to a condition where the center of the contact area between tire and runway leads the center of the wheel throughout most of the path of the oscillating wheel. Since therein lateral forces act in the direction of the motion of the wheel, new energy is continuously supplied to the oscillating structure; consequently, the oscillation is self-reinforcing.

This leads to the assumption that, fundamentally, the shimmying should increase with increasing softness of the tire. However, due to the flattening of the curve of cornering force against the angle of yaw of the wheel, the energy transferred from the runway to the oscillating system does nevertheless not show any significant increase per oscillation with increasing softness of the tire.

In cooperation with the Reichsanstalt für Film und Bild in Wissenschaft und Unterricht (Reich institute for films and pictures in science and instruction) a film was made of the tests on tail-wheel shimmy which also contains the slow-motion pictures shown here in excerpt; this film presents a valuable supplement to this report.[4]

---

[4]The film "Tail-wheel shimmy" may be obtained from the Reichsanstalt für Film und Bild in Wissenschaft und Unterricht (Reichs institute for films and pictures in science and instruction), Berlin, through the ZWB.

IX. FURTHER TESTS

The model tests resulted in usable agreement with the full-scale wheel 260 × 85. However, this does not yet provide a direct estimate for wheels of arbitrary size.

Since the drum tests had shown good agreement with road tests, tires of other sizes may be investigated in this manner. For the evaluation of theoretical investigations, knowledge of the cornering characteristics of the wheel for different values of yaw angle and tire deformation is important.

The influence of trail and the shimmying range of the rolling speed are to be determined for various tire sizes in order to make extrapolation of values (particularly for even larger tires) possible.

Since a practical application of a friction damping encounters difficulties, further tests are being carried out with fluid dampers. A separate report will be made concerning these results.

Translated by Mary L. Mahler
National Advisory Committee
for Aeronautics

REFERENCES

1. Dietz, O., and Harling, R.: Experimentelle Untersuchungen der Laufeigenschaften und der Steifigkeit eines Flugzeugfahrwerks. Dtsch. Luftf.-Forschg., FB 1189.

2. Huber, L., and Dietz, O.: Fahrversuche zum Vergleich zwischen Fahrzeugmodell und wirklichem Fahrzeug. FKFS-Bericht Nr. 84, 1935.

3. Huber, L.; Die Fahrtrichtungsstabilität des schnellfahrenden Kraftwagens. Dtsch. Kraftf.-Forschg., Heft 44, p. 34, Berlin: VDI Verlag 1940.

4. Kantrowitz, Arthur: Stability of Castering Wheels for Aircraft Landing Gears. NACA Rep. 686, 1940.

5. Kamm, W.: Kraftwagen und Strasse in ihrer Wechselwirkung. Berichtsheft Kraftfahrtechnische Tagung des VDI 1934, Berlin VDI Verlag 1935.

6. Dietz, O.: Pendelerscheinungen an Strassen-Anhängerzügen. Dtsch. Kraftf. Forschg. H. 16, Berlin: VDI-Verlag 1938.

7. Becker, G., Fromm, H., and Maruhn, H.: Schwingungen in Automobillenkungen, Berlin: M. Drayn, 1931.

8. Dietz, O., and Huber, L.: Einradmodellversuche. FKFS-Bericht Nr. 58, 1934.

9. Förster, B.: Versuche zur Feststellung des Haftvermögens von Personenwagenbereifungen. Dtsch. Kraftf.-Forschg. Zwischenbericht Nr. 22, Berlin VDI-Verlag.

Figure 1.- Rubbing track of a shimmying airplane tail wheel on a tar-macadam runway. The tail wheel was built in between the rear wheels of a trailer with front-wheel drive.

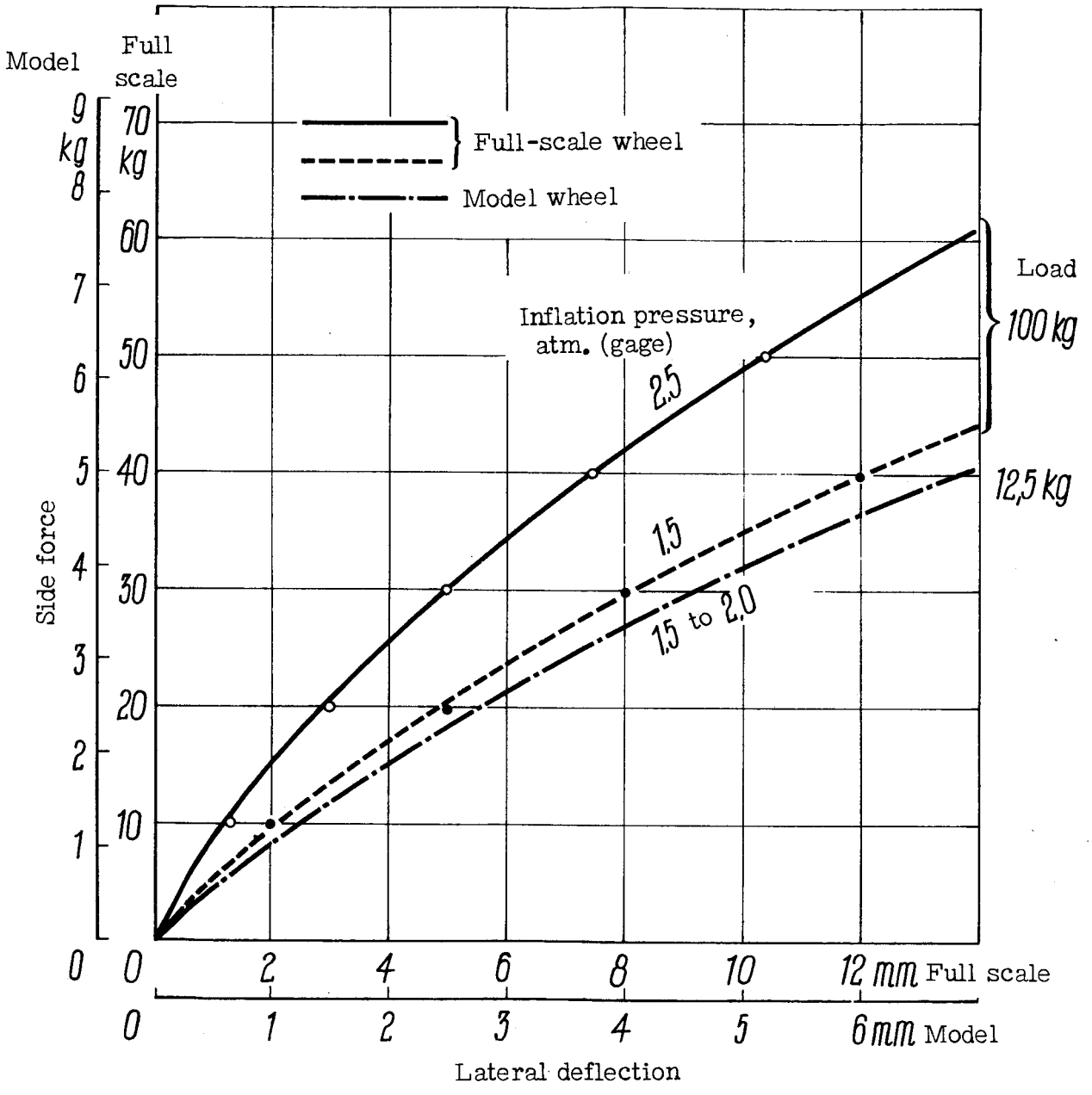

Figure 2.- Lateral deformation of the standing tire of the full-scale tail wheel and of the model wheel. Full-scale wheel 260 by 85; model wheel 120 to 130 mm diameter, for various tire-inflation pressures.

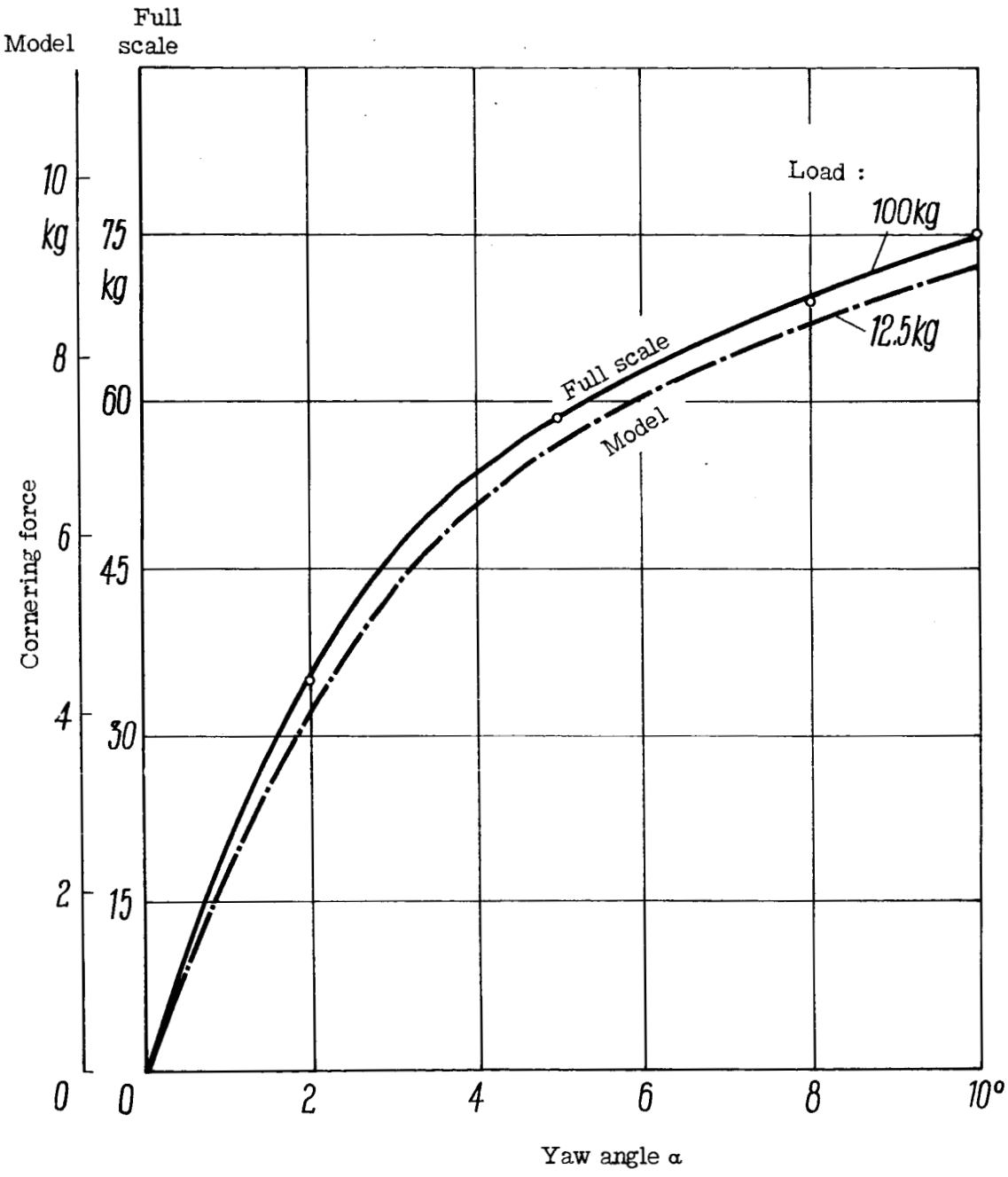

Figure 3.- Cornering forces of the model and of the full-scale wheel. Full-scale wheel 260 by 85; running velocity 19 [27] ; model wheel 120 mm diameter; adhesive-friction coefficient $\mu_H = 0.7$; model scale: forces 1:8, lengths 1:2, velocities 1:1.41.

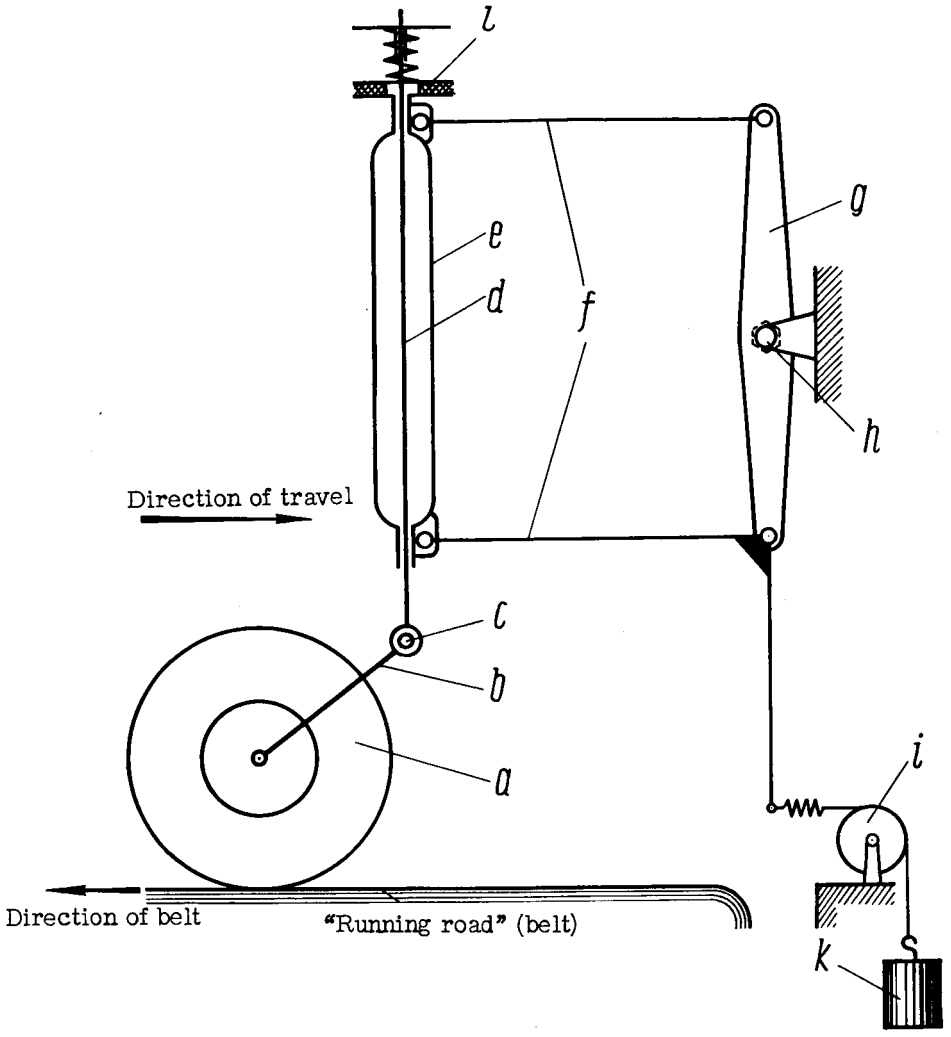

a. Tail wheel
b. Guiding yokes
c. Point of rotation with locking device
d. Swivel axis
e. Bearing housing
f. Parallelogram linkage (the lower arm with crank arm for loading)
g. Pivoting lever
h. Swivel point
i. Rope pulley
k. Loading weight
l. Friction disks

Figure 4.- Schematic representation of the guiding system of the model wheel with load arrangement.

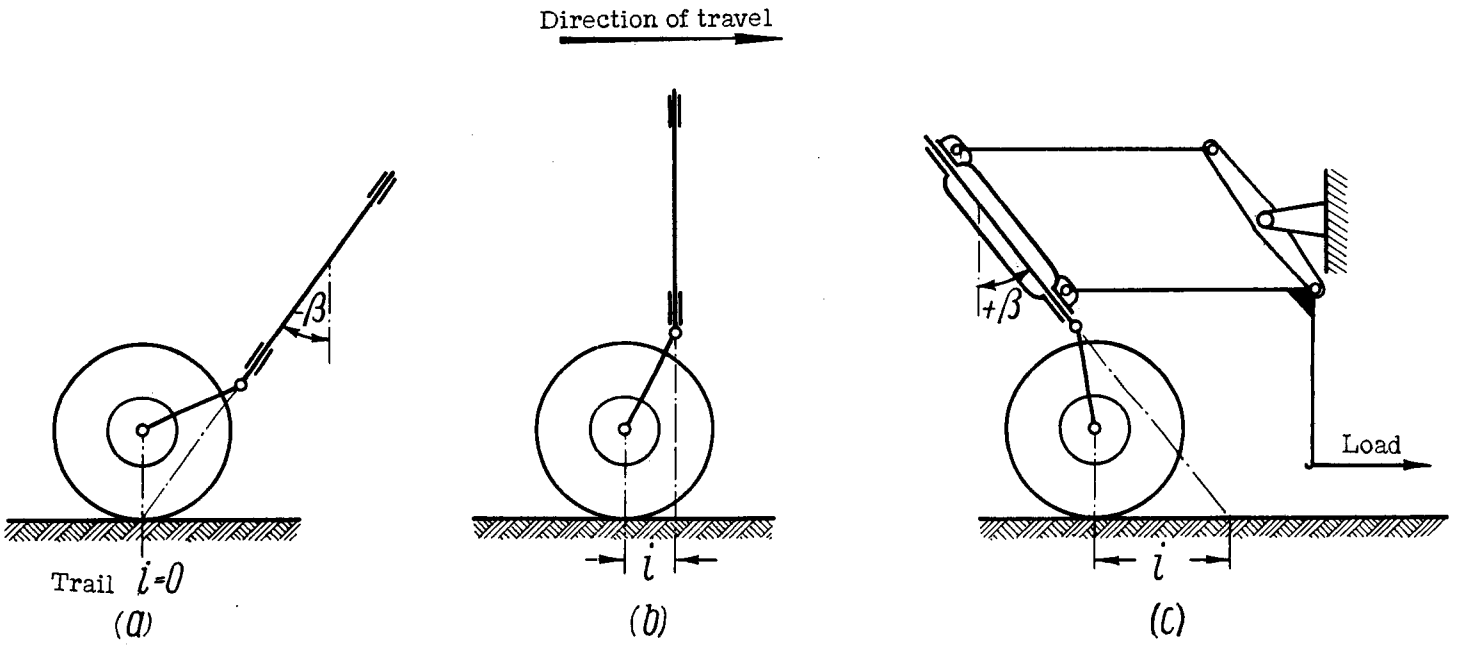

Figure 5.- Trail i of the tail wheel for various inclinations β of the swivel axis. c shows the guiding of the swivel-axis housing by means of parallel linkages.

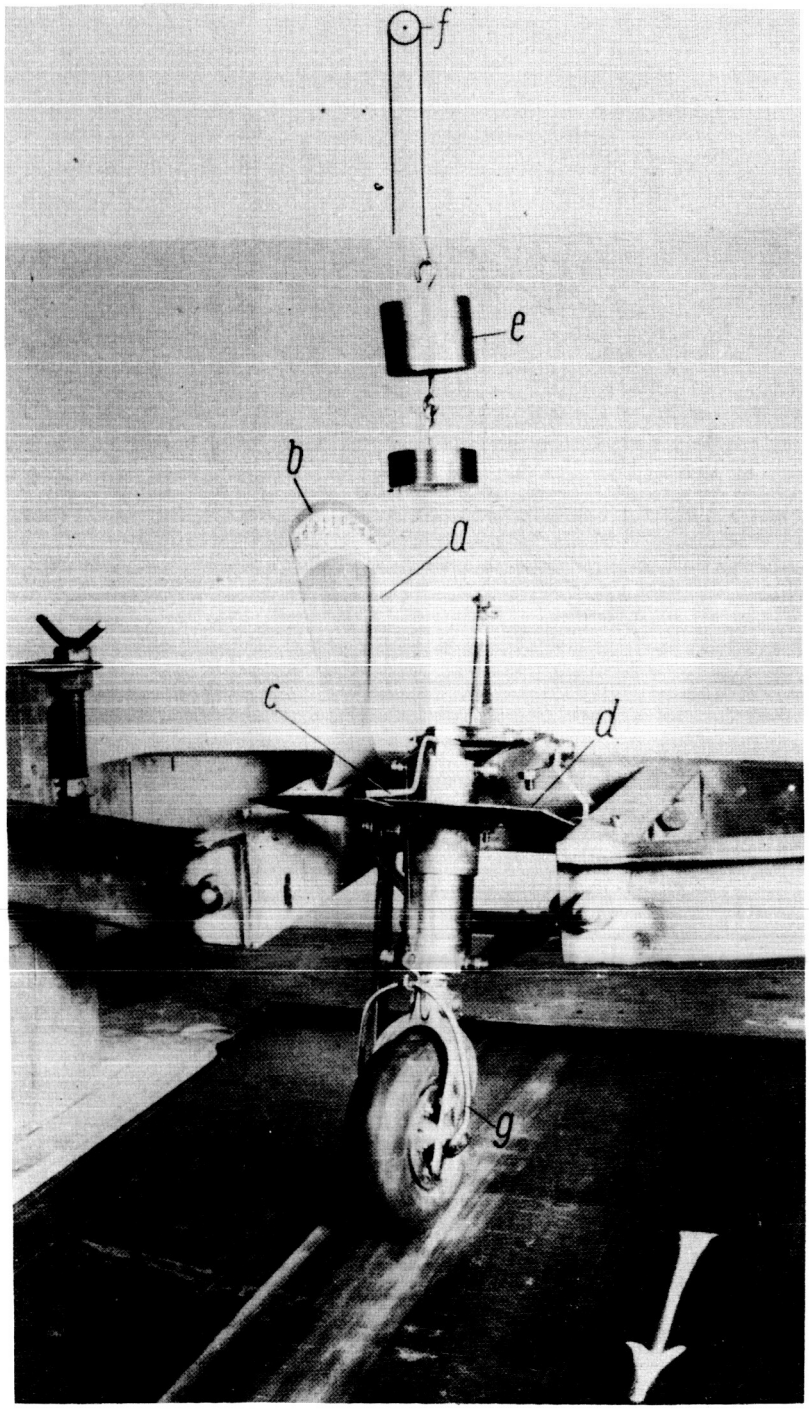

a. Inclinometer (angle β)
b. Inclination scale
c. Shimmy-angle indicator (angle α)
d. Shimmy-angle scale
e. Weights for measurement of ground pressure
f. Rope pulley
g. Lifting yoke

Figure 6.- View of tail wheel with parallelogram linkage and support fixture.

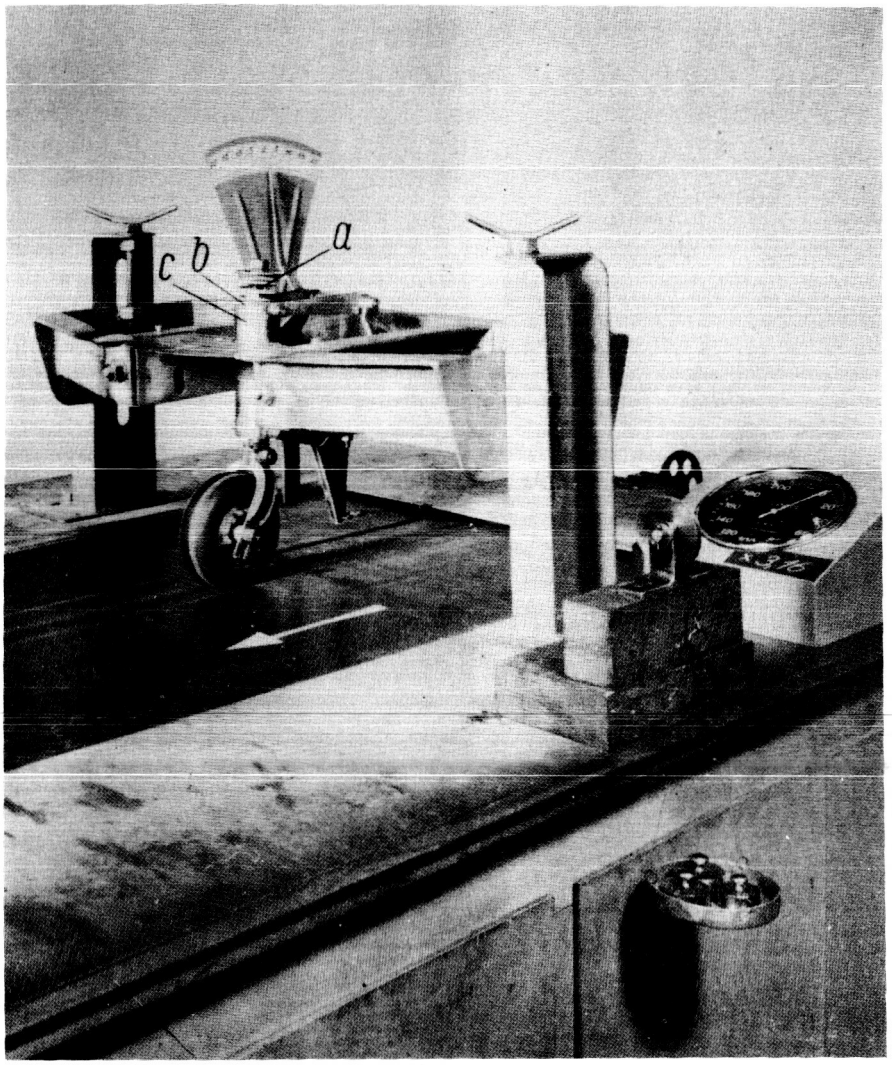

a. Friction damper
b. Friction surface with interlining
c. Swivel-axis housing

Figure 7.- Model tail wheel with swivel axis and friction damping.

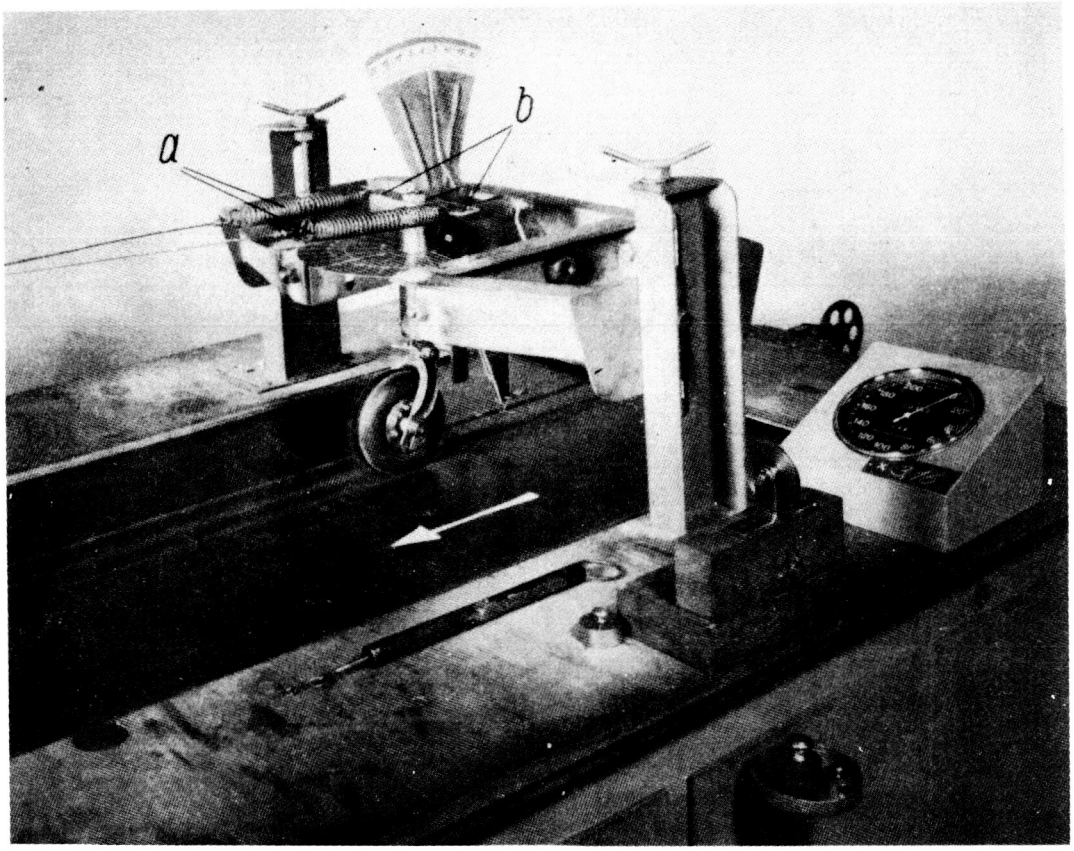

Figure 8.- Restoring of tail wheel to straight-ahead position by two tension springs a on the cross arm b.

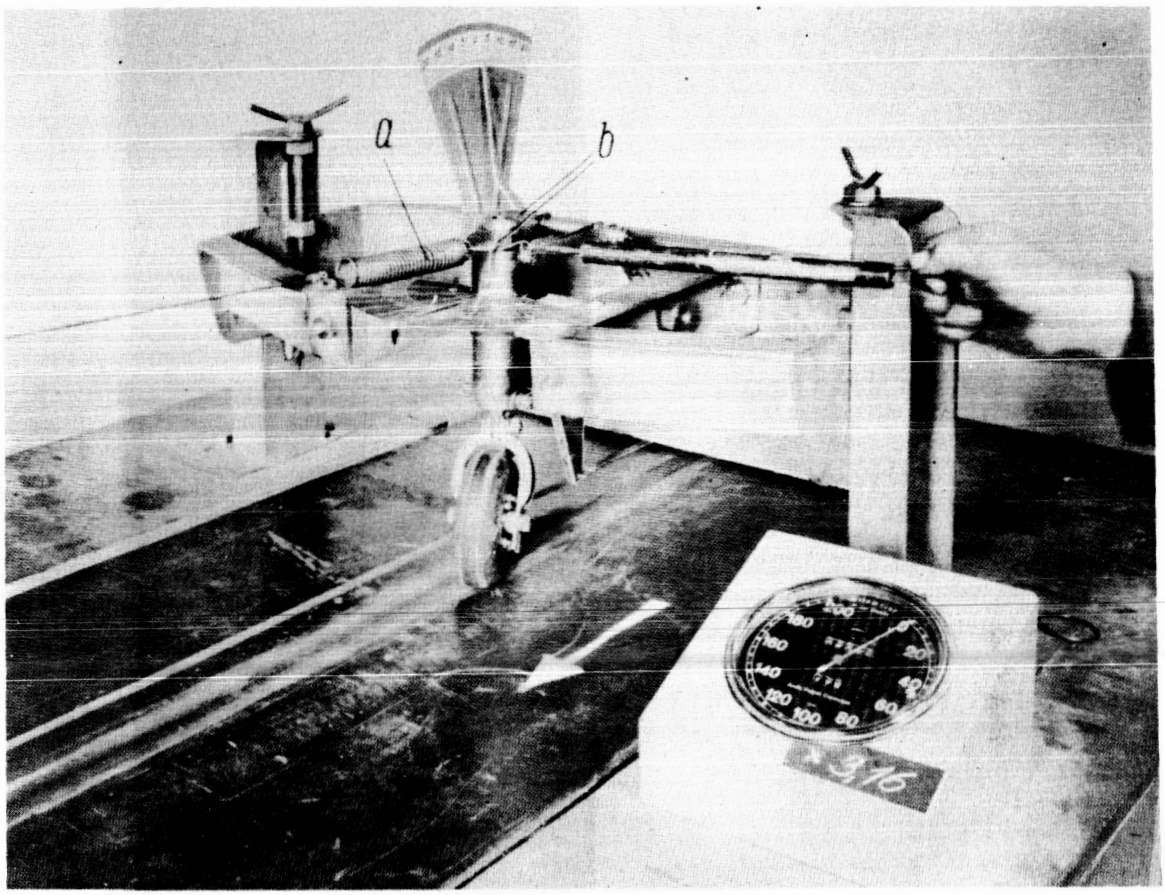

Figure 9.- Restoring of tail wheel to straight-ahead position by one tension spring a on a longitudinal arm b.

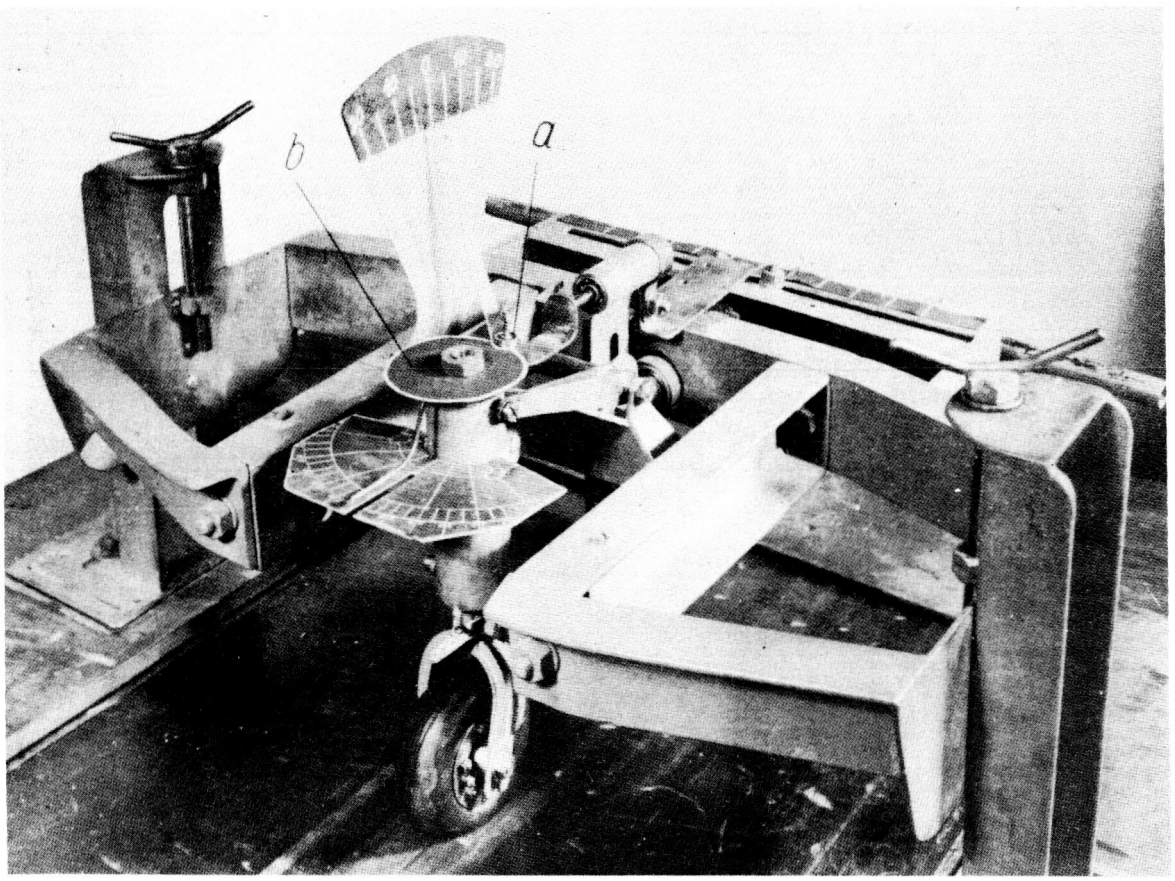

Figure 10.- Restoring of tail wheel to straight-ahead position by roller a and the cam plate b.

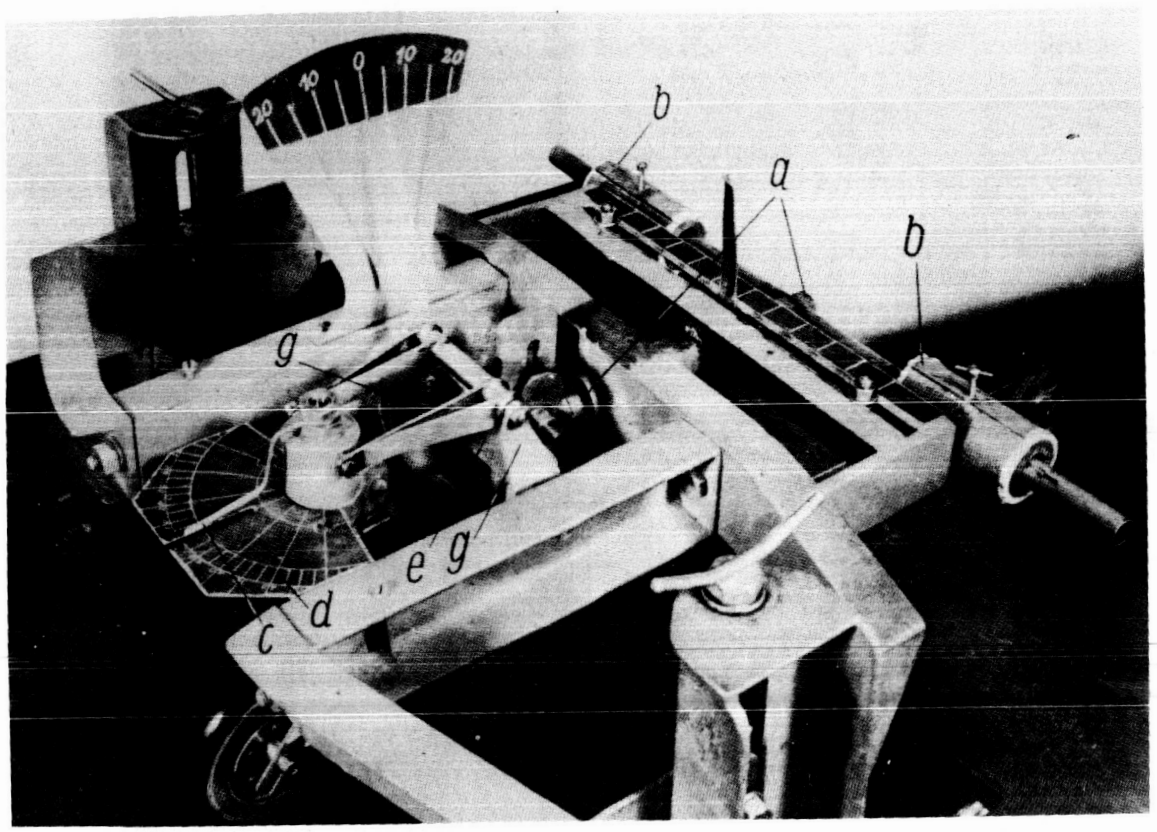

a. Rotatable flexible longitudinal axis
b. Adjustable weights of airplane-moment of inertia
c. Shimmy-angle indicator
d. Shimmy-angle scale
e. Cross connection
g. Lever for hinging the parallelogram linkage (compare fig. 4)

Figure 11.- Model apparatus with simulation of a torsionally flexible airplane fuselage (scale 1:2).

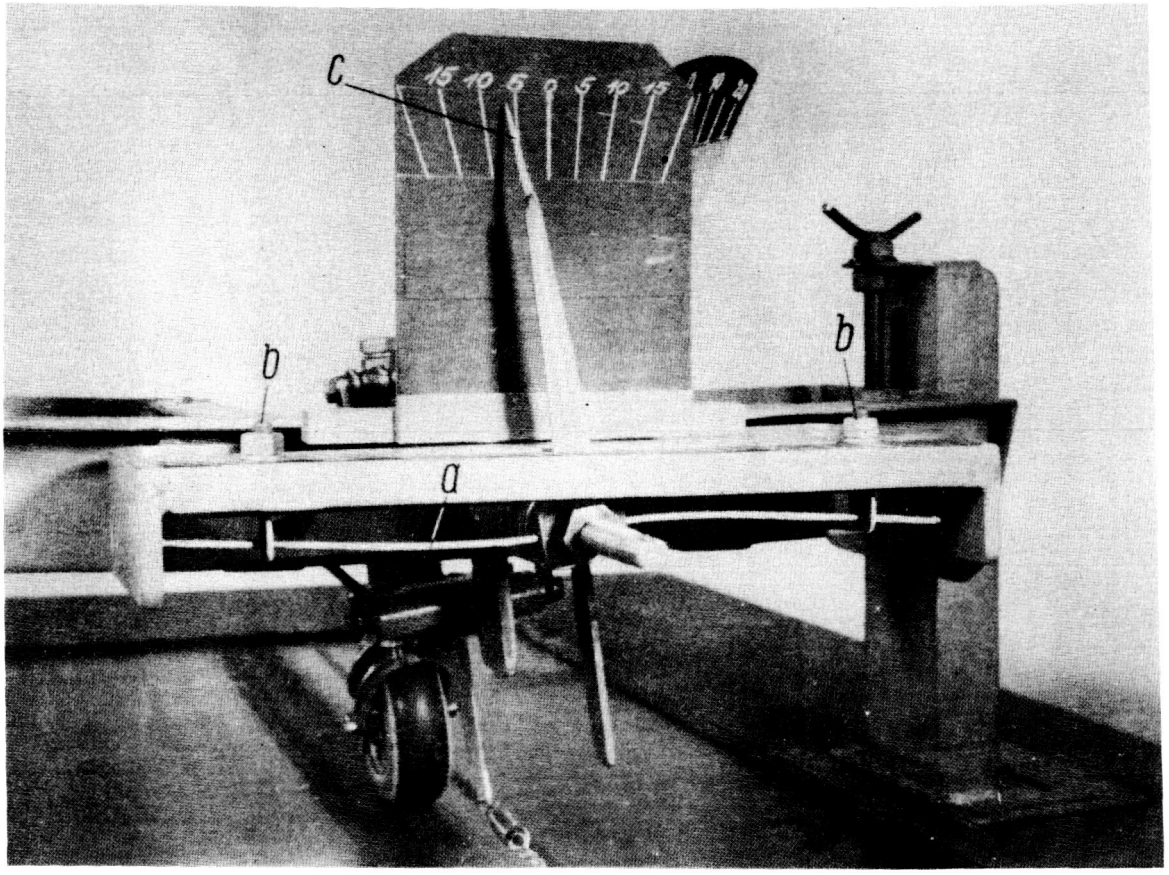

b. Laterally adjustable spring holders
c. Twist scale

Figure 12.- Cross-bar spring a for springing of the longitudinal axis. Torque levers with masses taken off.

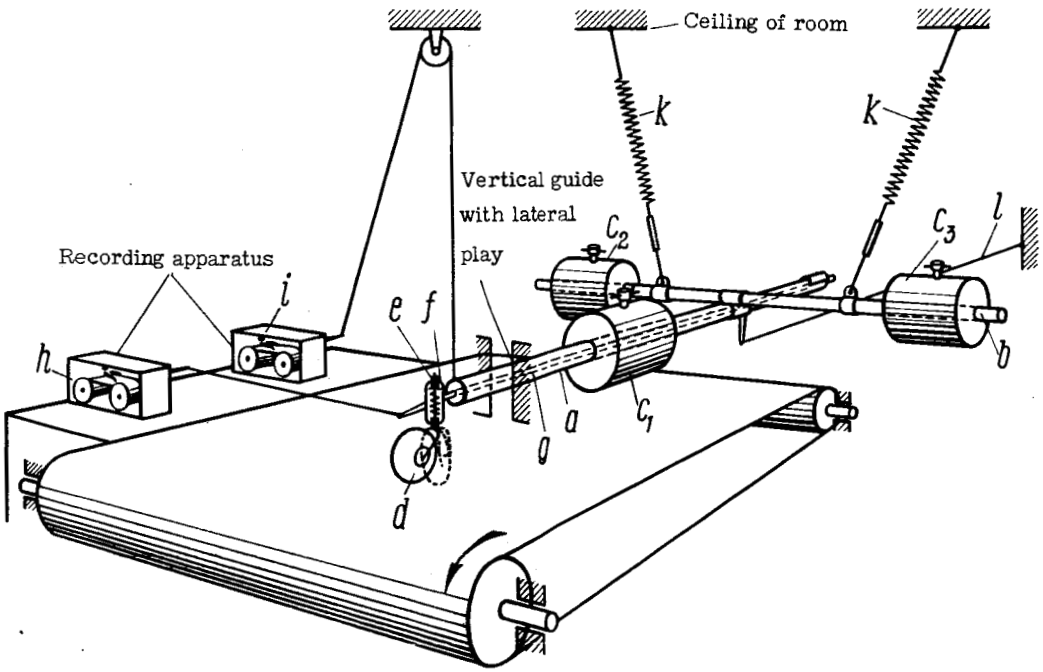

a. Fuselage-longitudinal tube
b. Wing-transversal tube
c_1, c_2, c_3 adjustable weights
d. Tail wheel
e. Swivel axis
f. Housing of tail-wheel bearing
g. Rotatable rod in fuselage tube
h. Recording apparatus for shimmy motions
i. Recording apparatus for vertical motions
k. Suspension springs
l. Restraining line

Figure 13.- Schematic representation of the model tail wheel with horizontally suspended airplane fuselage on a running belt.

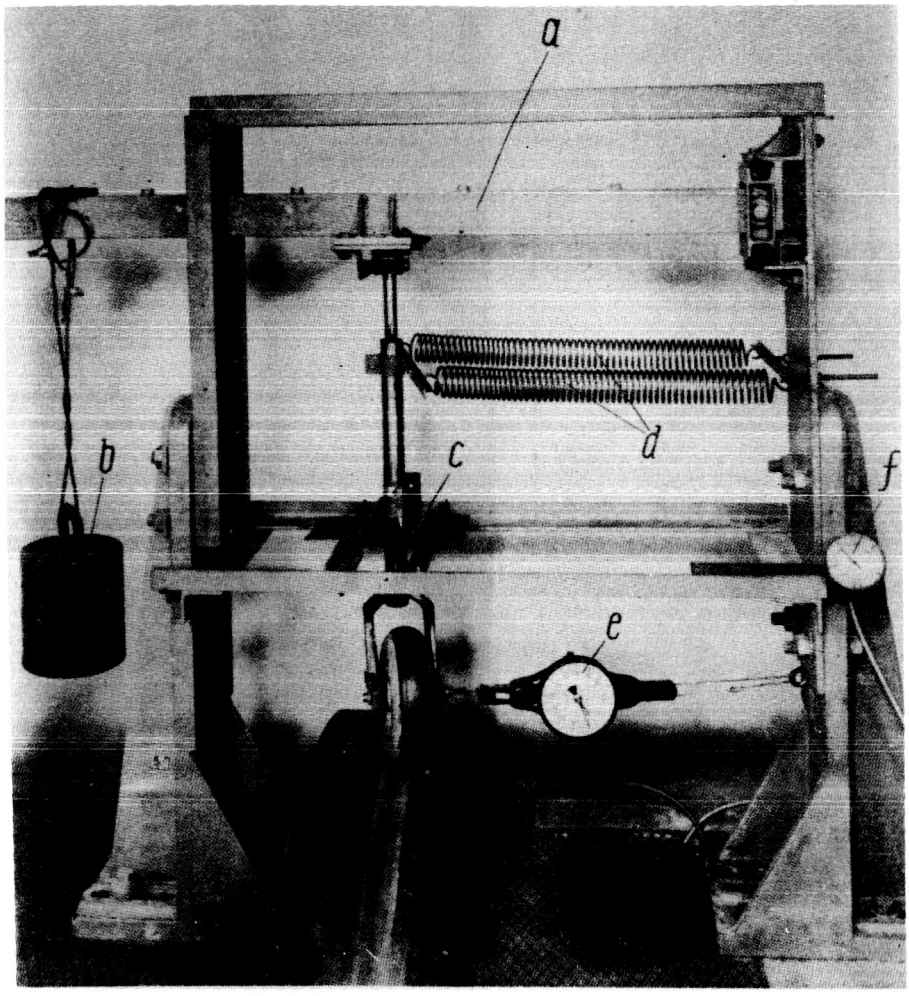

a. Loading lever
b. Loading weight
c. Scale for indication of shimmy angle
d. Restoring springs (built in for experimental purposes only)
e. Cornering-force meter
f. Velocity indicator

Figure 14.- Over-all arrangement of a full-scale tail wheel with shock strut on a rotating drum.

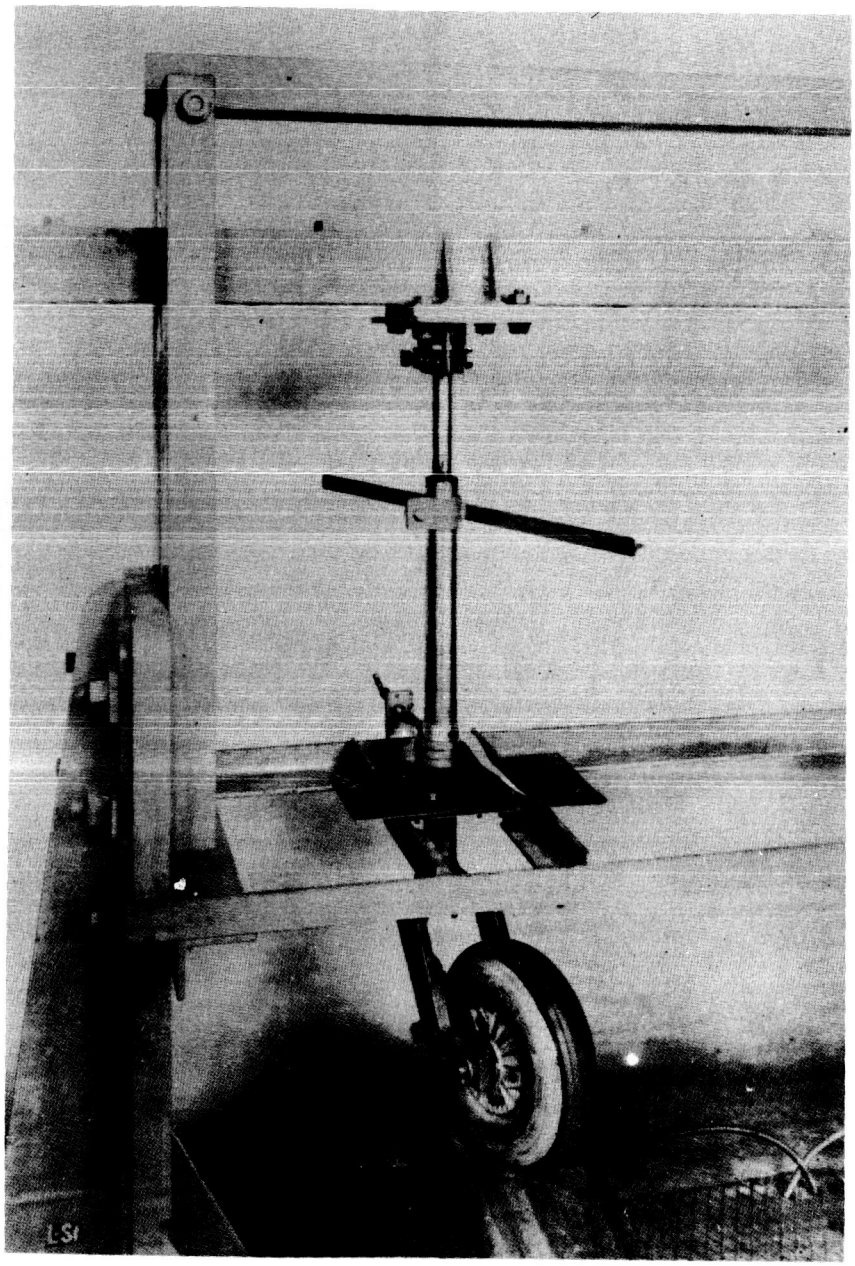

Figure 15.- Full-scale tail wheel on drum. Trail of tail wheel adjustable.

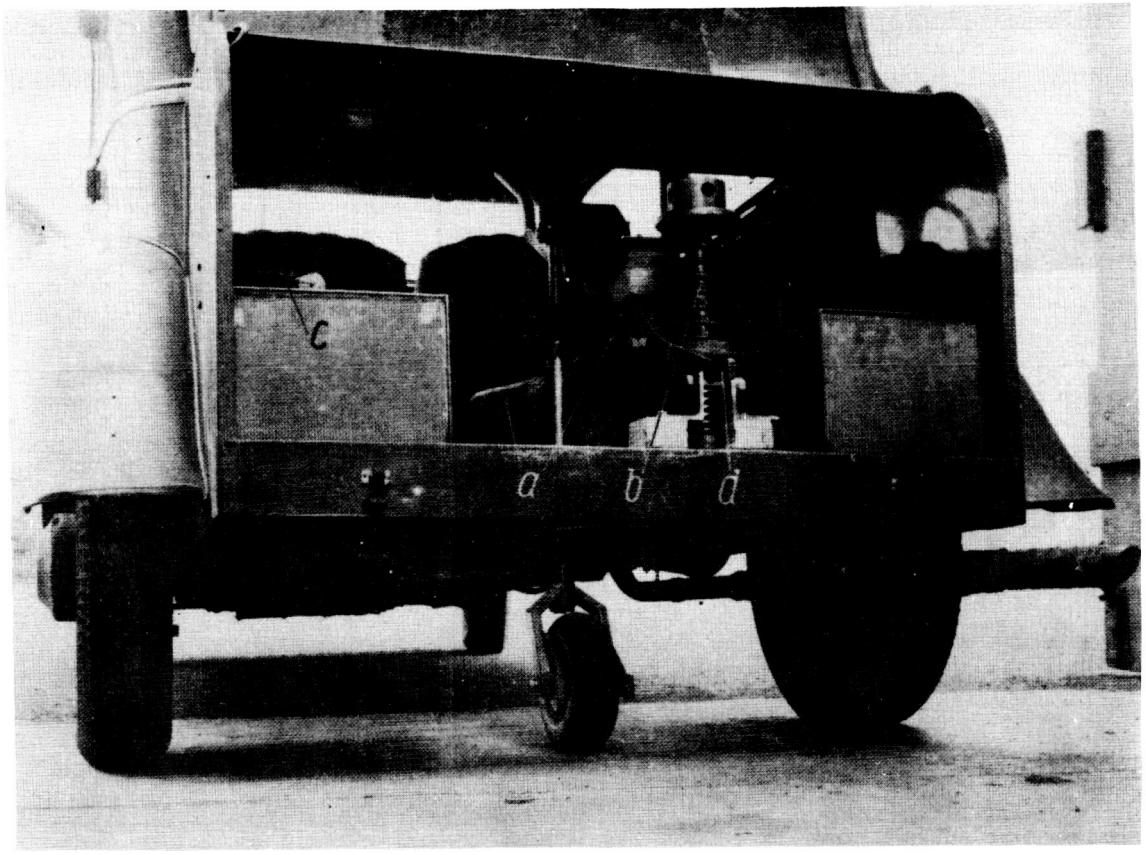

a. Guiding lever
b. Loading spring
c. Recording apparatus for shimmy oscillations
d. Unloading lever

Figure 16.- Full-scale tail wheel with shock-strut, between the rear wheels of a truck with front-wheel drive.

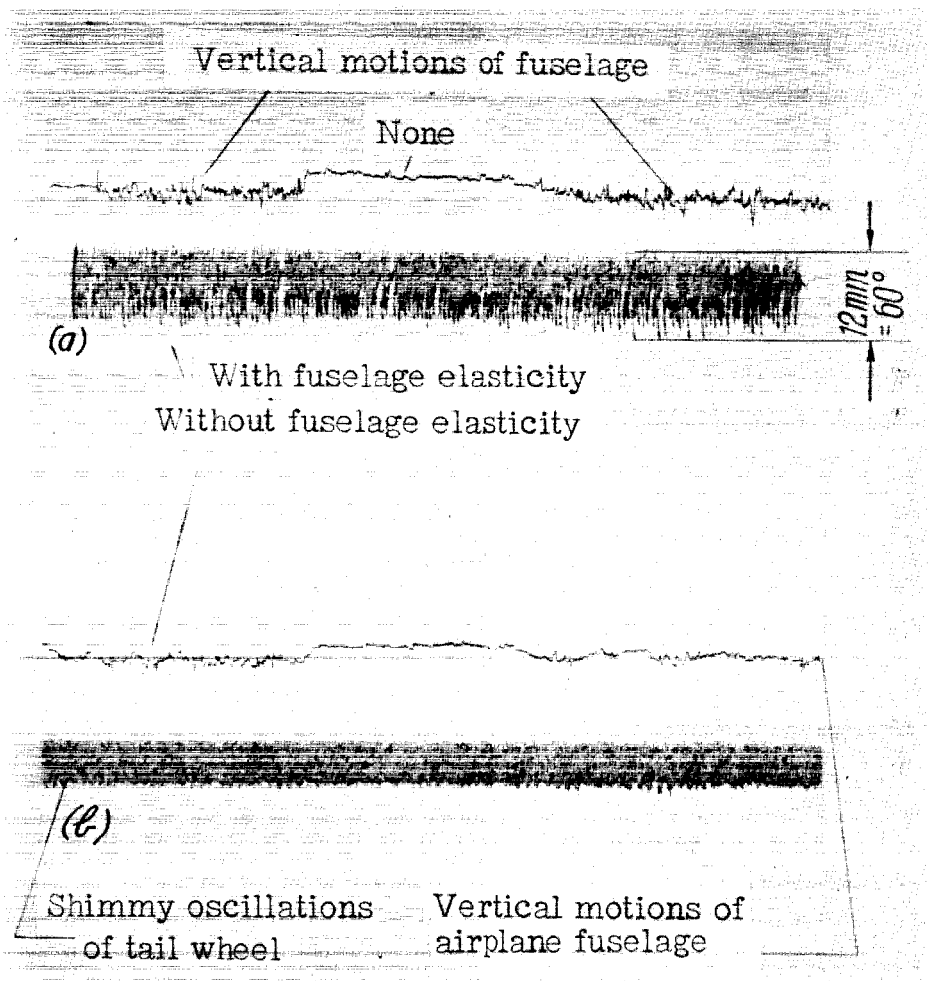

(a) Airplane fuselage torsionally flexible.
(b) Airplane fuselage torsionally rigid.

Figure 17.- Shimmy oscillations of the tail wheel with inclined swivel axis for fixed airplane fuselage freely oscillating vertically.

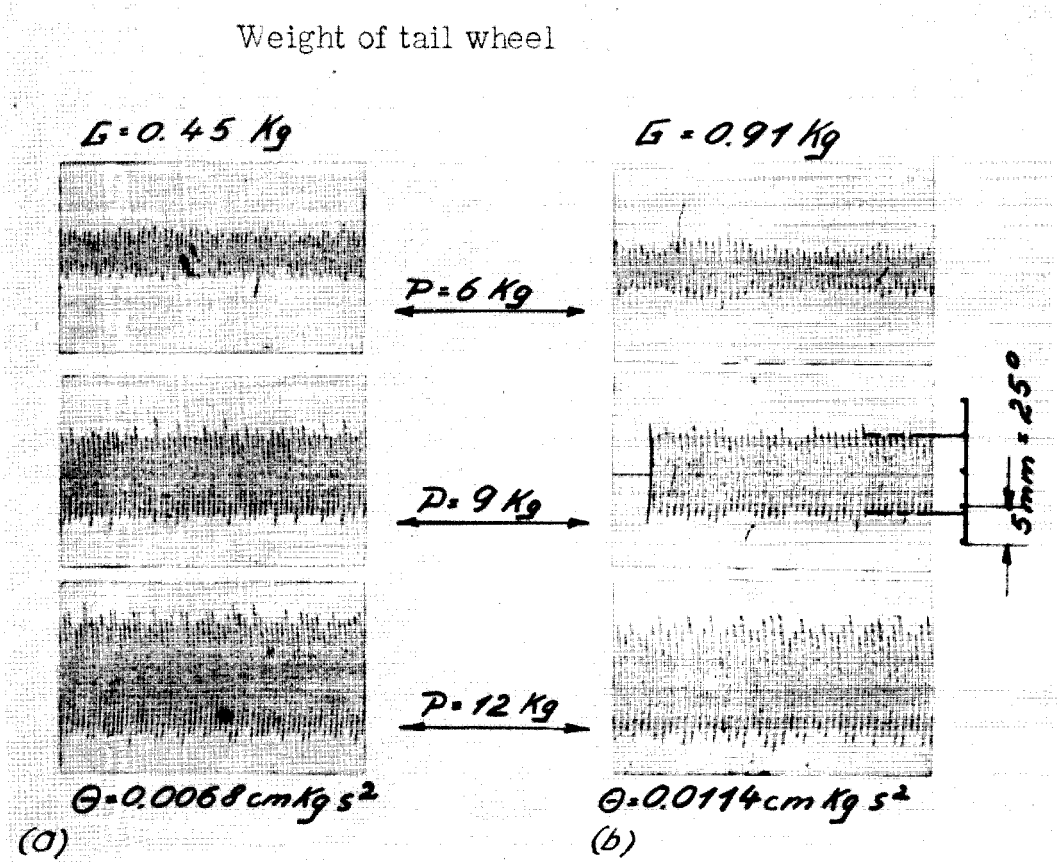

(a) Wheel with light-metal rim (130 mm diameter).
(b) Wheel with steel rim (130 mm diameter).

Figure 18.- Shimmy oscillations for different tail-wheel weights G and three different loads P. Trail, running speed and adhesive-friction coefficient μ_H the same. Scale of length: 1:2.

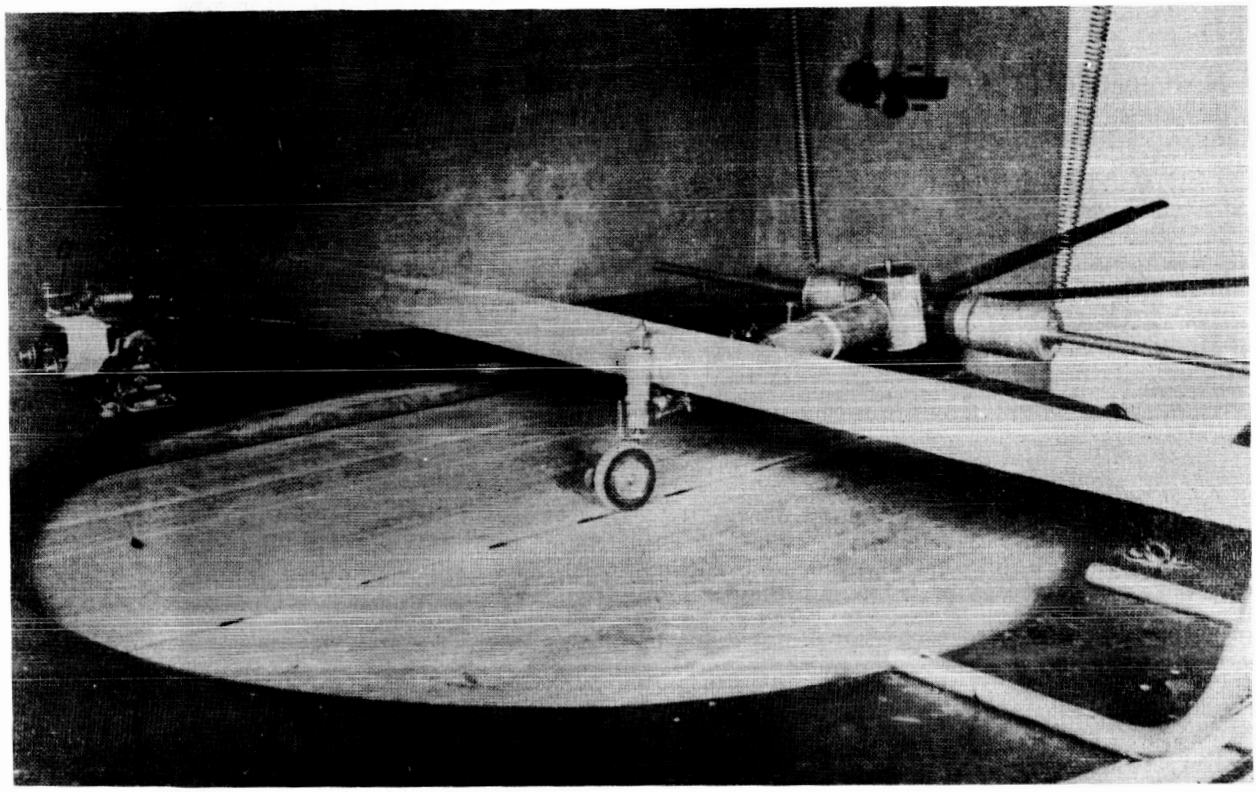

a. Recording apparatus for shimmy oscillations.

Figure 19.- Running belt with model airplane (scale 1:10). Housing of swivel-axis support fixed. Correct wheel-ground pressure (4 kg) by vertical springing in the swivel-axis housing.

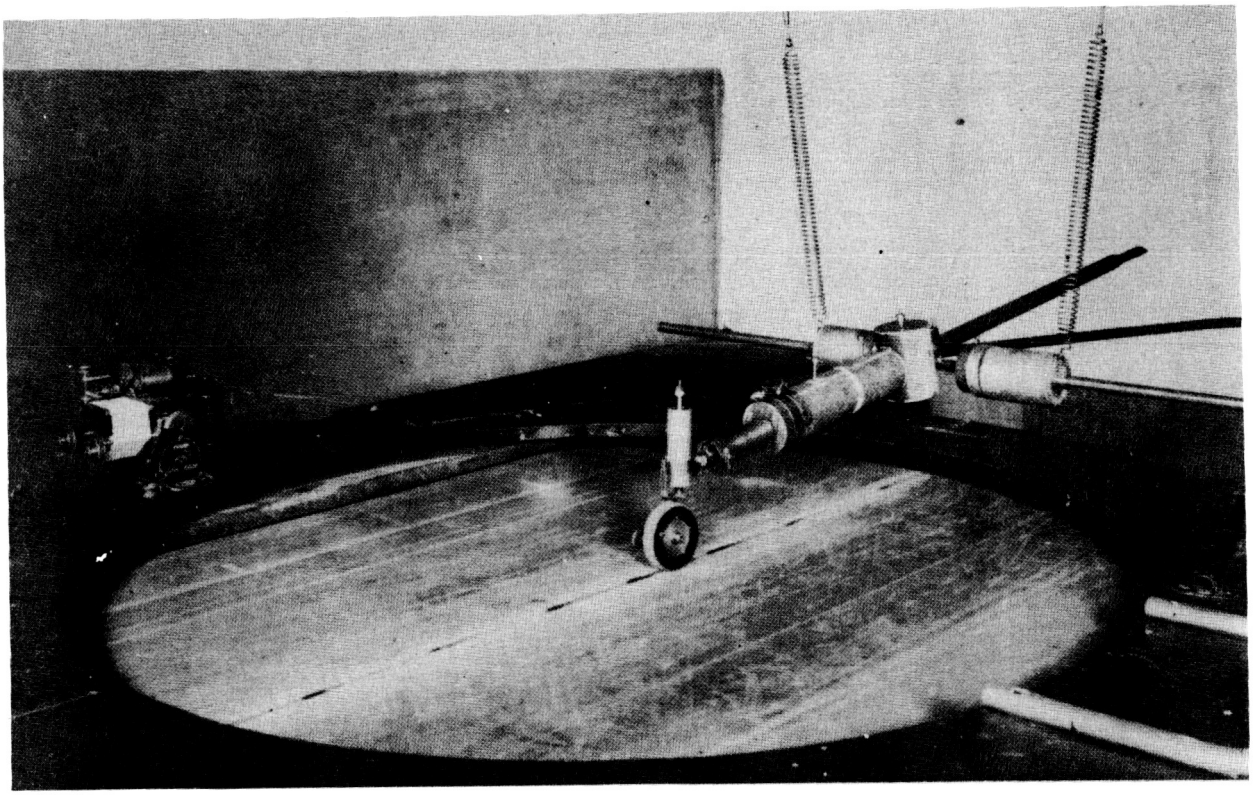

Figure 20.- Running belt with model airplane (scale 1:10). Housing of swivel-axis support free. Twist of fuselage, moment of inertia J_X, J_Y, and J_Z, weights, and position of center of gravity (according to Me 109) affect the tail wheel.

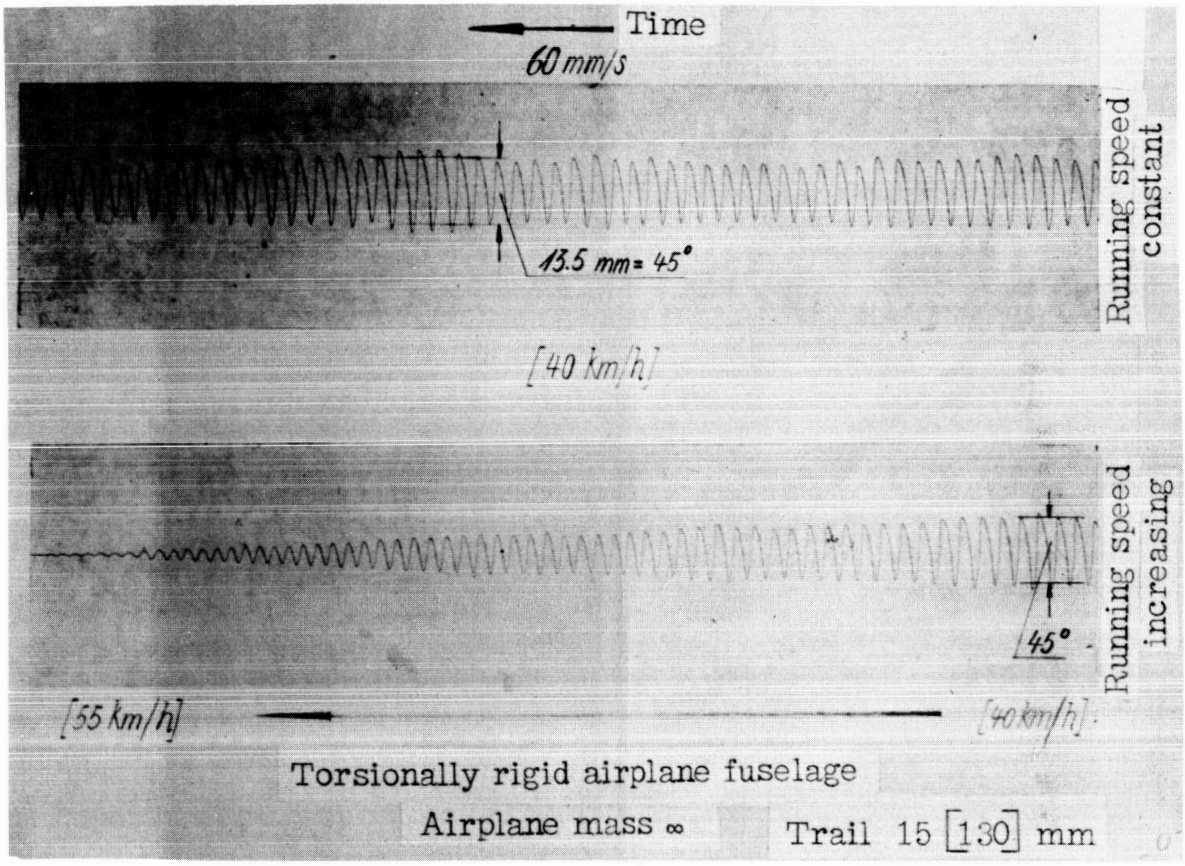

Figure 21.- Recording-apparatus traces of the shimmy motions of the tail wheel. Swivel-axis housing fixed.

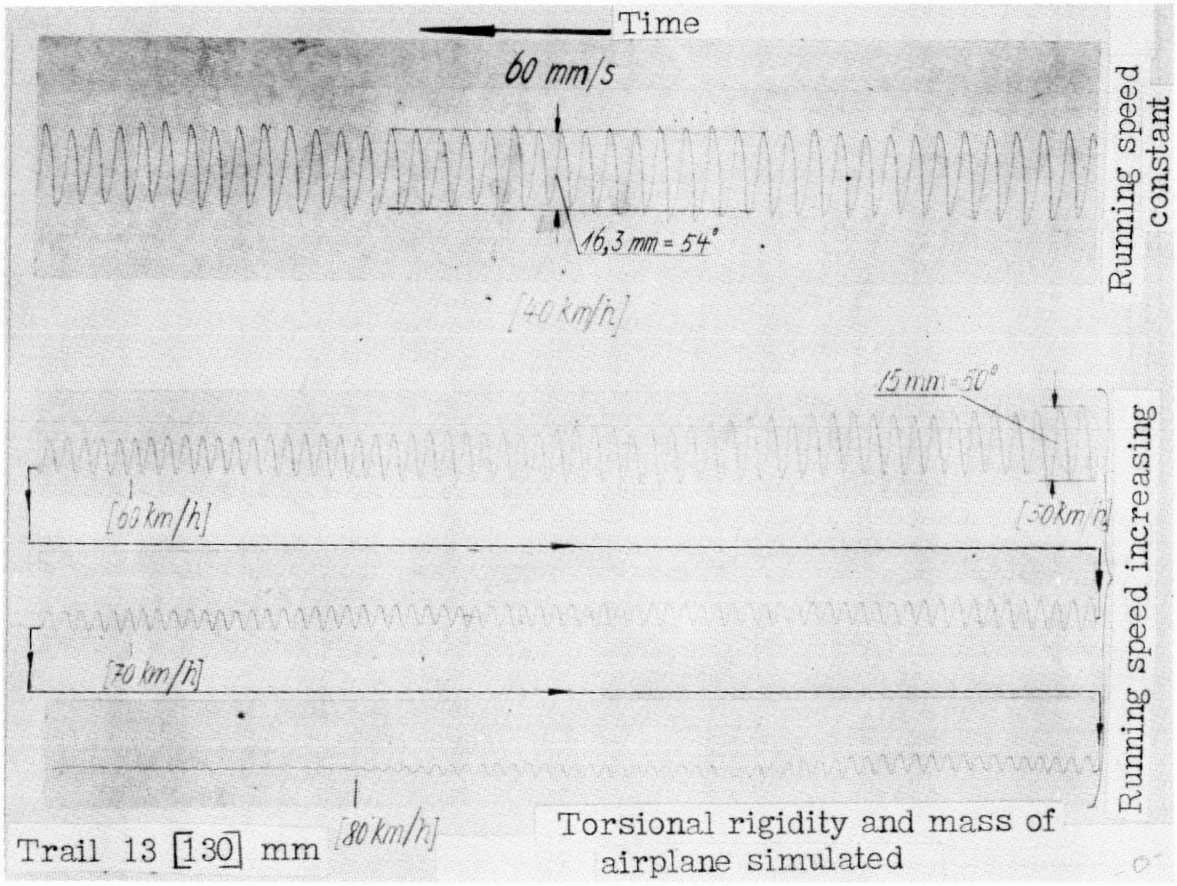

Figure 22.- Recording-apparatus traces of the shimmy motions of the tail wheel. Swivel-axis housing free. Influence of torsional flexibility and mass distribution of the airplane.

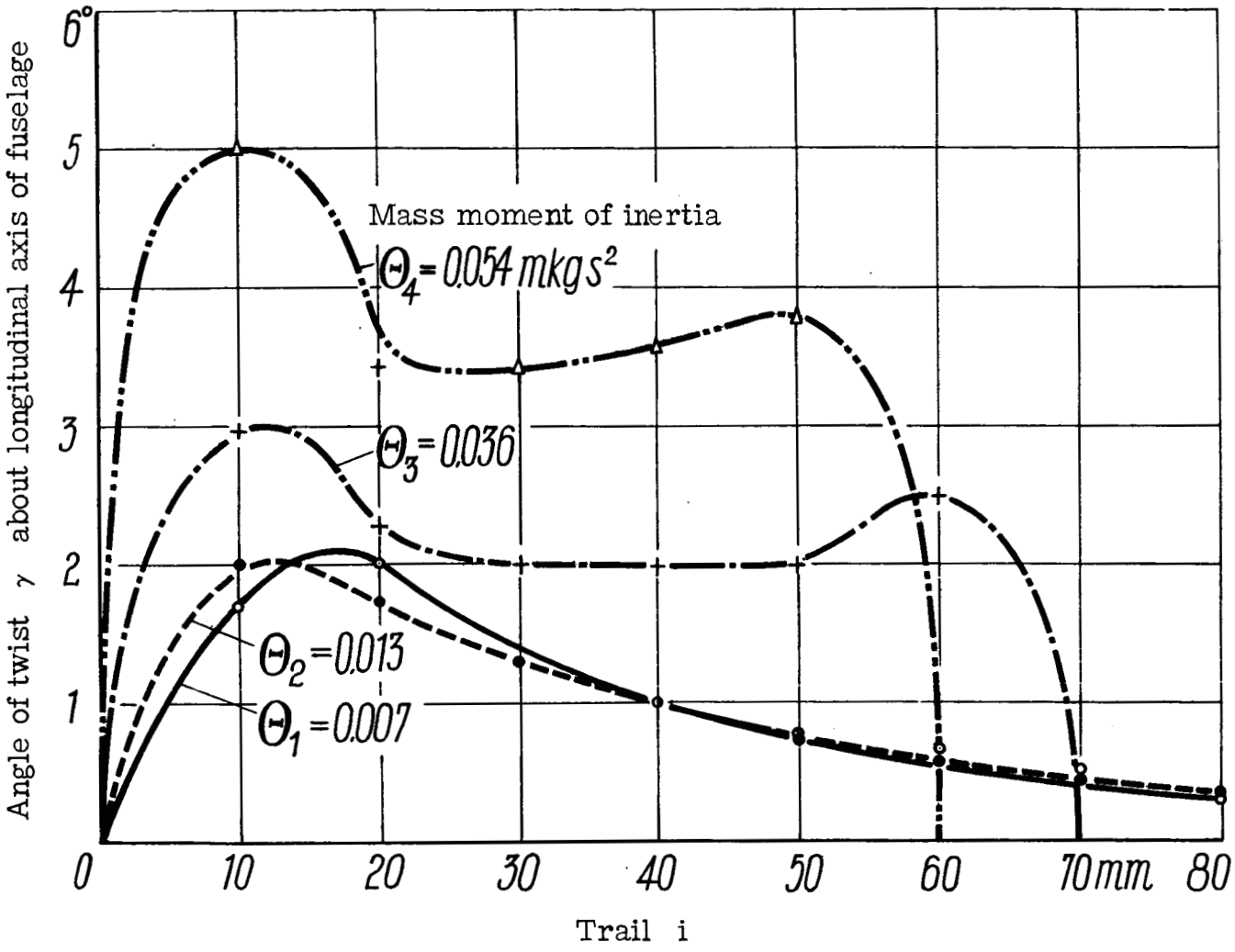

Figure 23.- Angle of twist of the fuselage in tail-wheel shimmy. Torsional rigidity $\frac{c}{l}$ = 136 [4.35×10^3] m kg. Standard adjustment: swivel-axis inclination $\beta = 0^{\circ}$; velocity v = 19 [25] km/hr; load P = 6.3 kg; friction coefficient μ_H = 0.4 to 0.5; tire pressure p = 1.5 to 2.0 atmospheres gage inflation pressure.

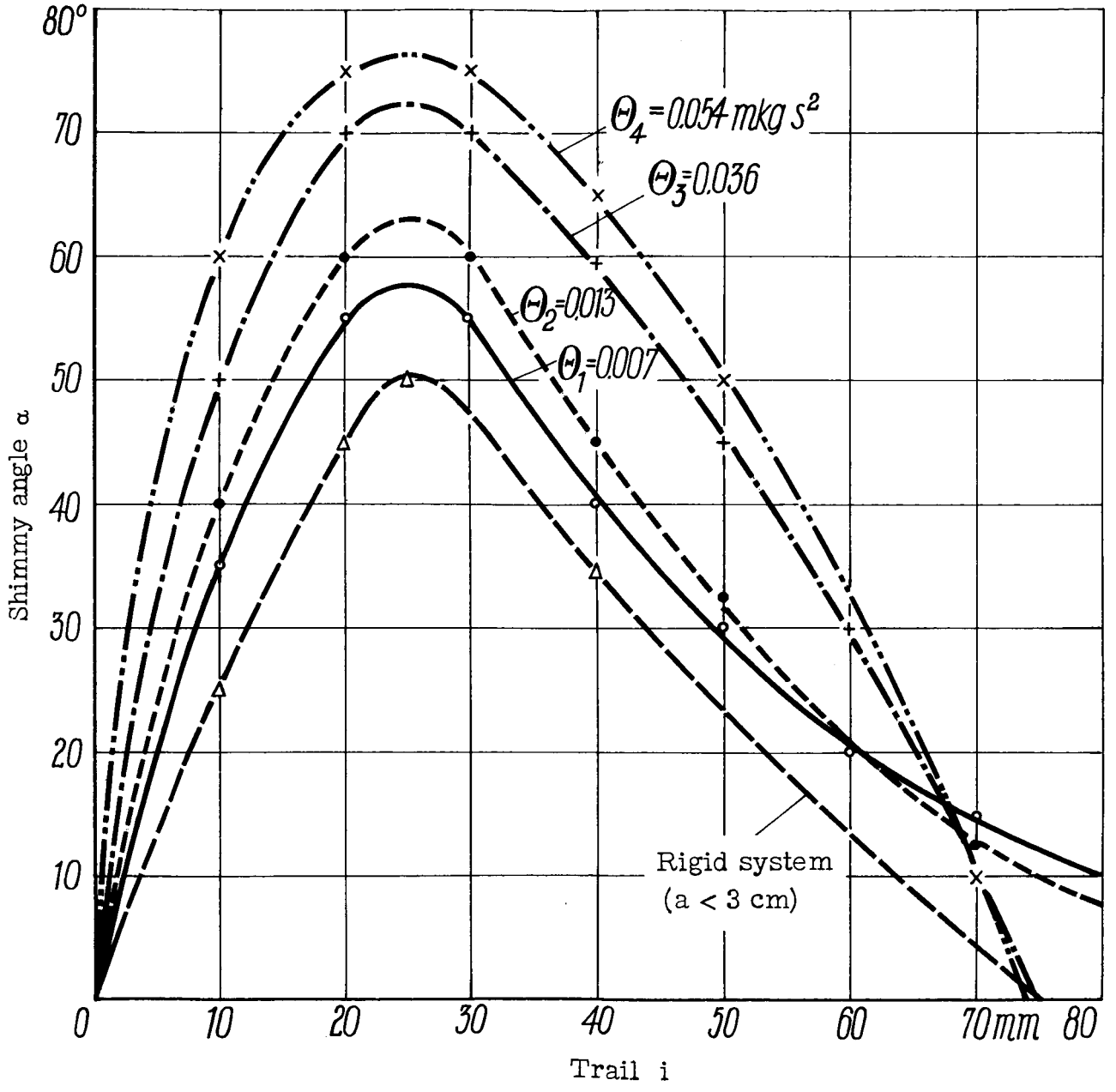

Figure 24.- Tail-wheel shimmy for various moments of inertia about the fuselage axis and for a relative torsional rigidity of the fuselage of $\frac{c}{l} = 136$ [4.35 × 10³] m kg. Swivel-axis inclination $\beta = 0°$; velocity v = 19 [25] km/hr; load P = 6.3 [50] kg; friction coefficient μ_H = 0.4 to 0.5; tire pressure p = 1.5 to 2.0 atmospheres gage inflation pressure.

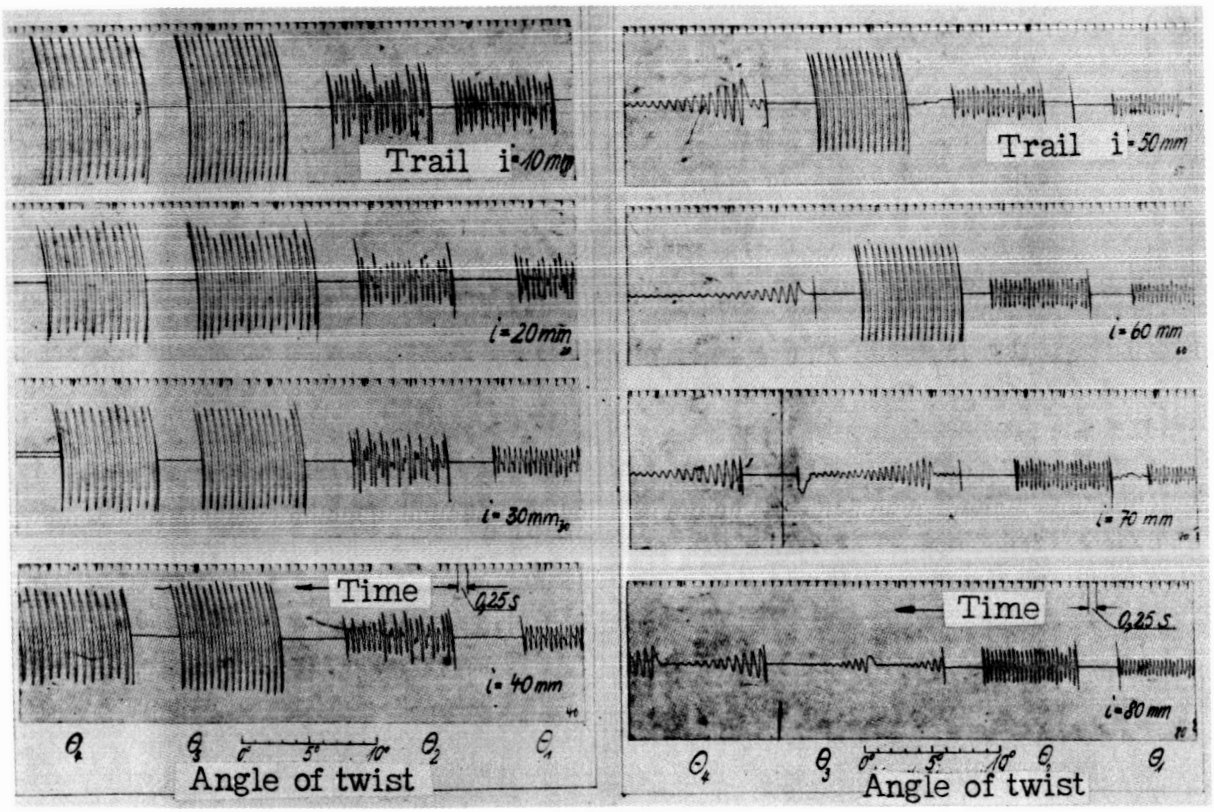

Figure 25.- Recordings of the torsional oscillations of the simulated airplane fuselage for various airplane-moments of inertia about the longitudinal axis of the airplane, and for various trails. $\Theta_1 = 0.007$ m kg s^2; $\Theta_2 = 0.013$ m kg s^2; $\Theta_3 = 0.036$ m kg s^2 (compare fig. 24); $\Theta_4 = 0.054$ m kg s^2.

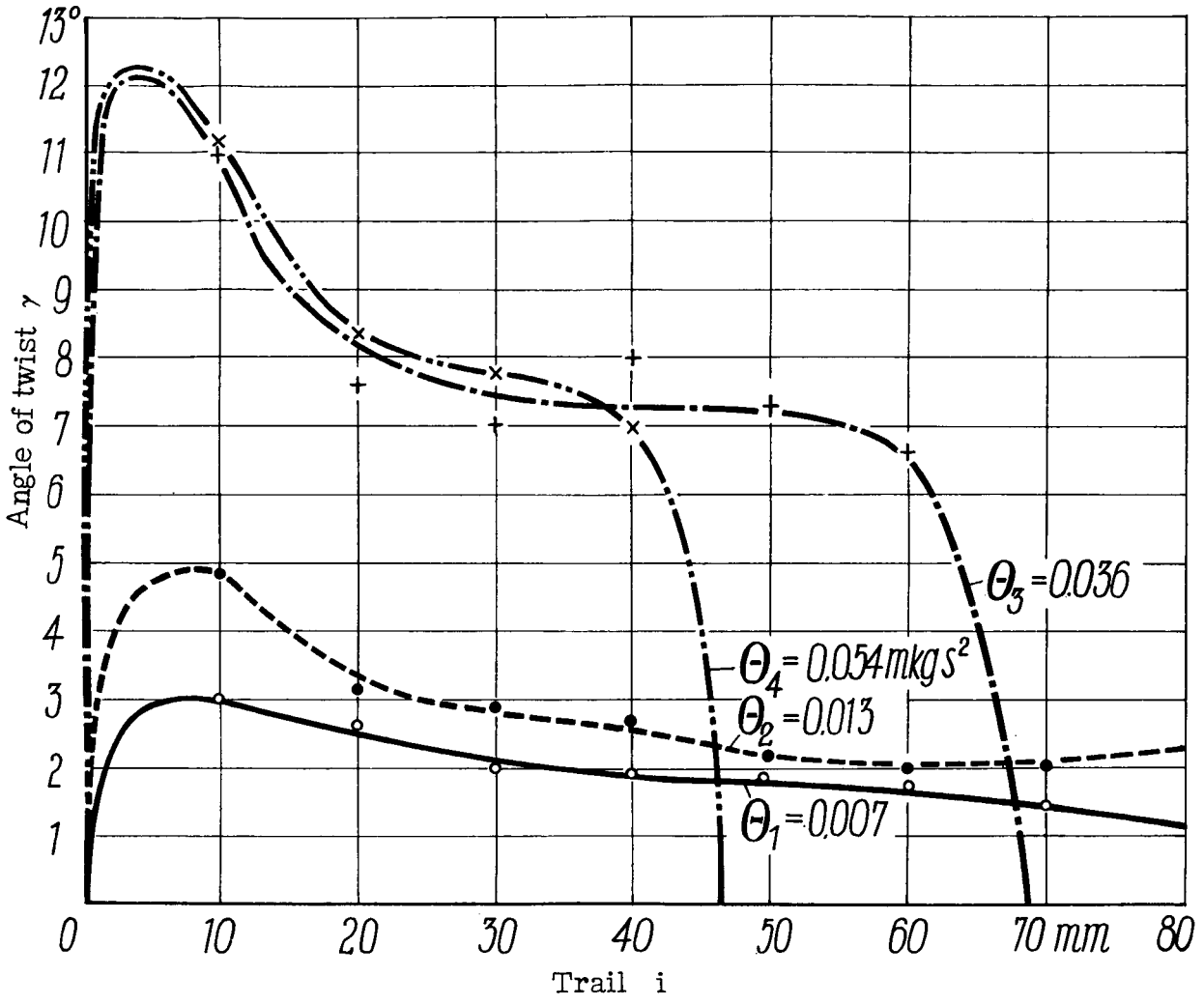

Figure 26.- Angle of twist of fuselage in tail-wheel shimmy for various moments of inertia of the airplane. Torsional rigidity $\frac{c}{l} = 56$ m kg $\left[1.8 \times 10^3\right]$ m kg; velocity $v = 19$ [25] km/hr; load $P = 6.3$ [50] kg; adhesive-friction coefficient $\mu_H = 0.4$ to 0.5.

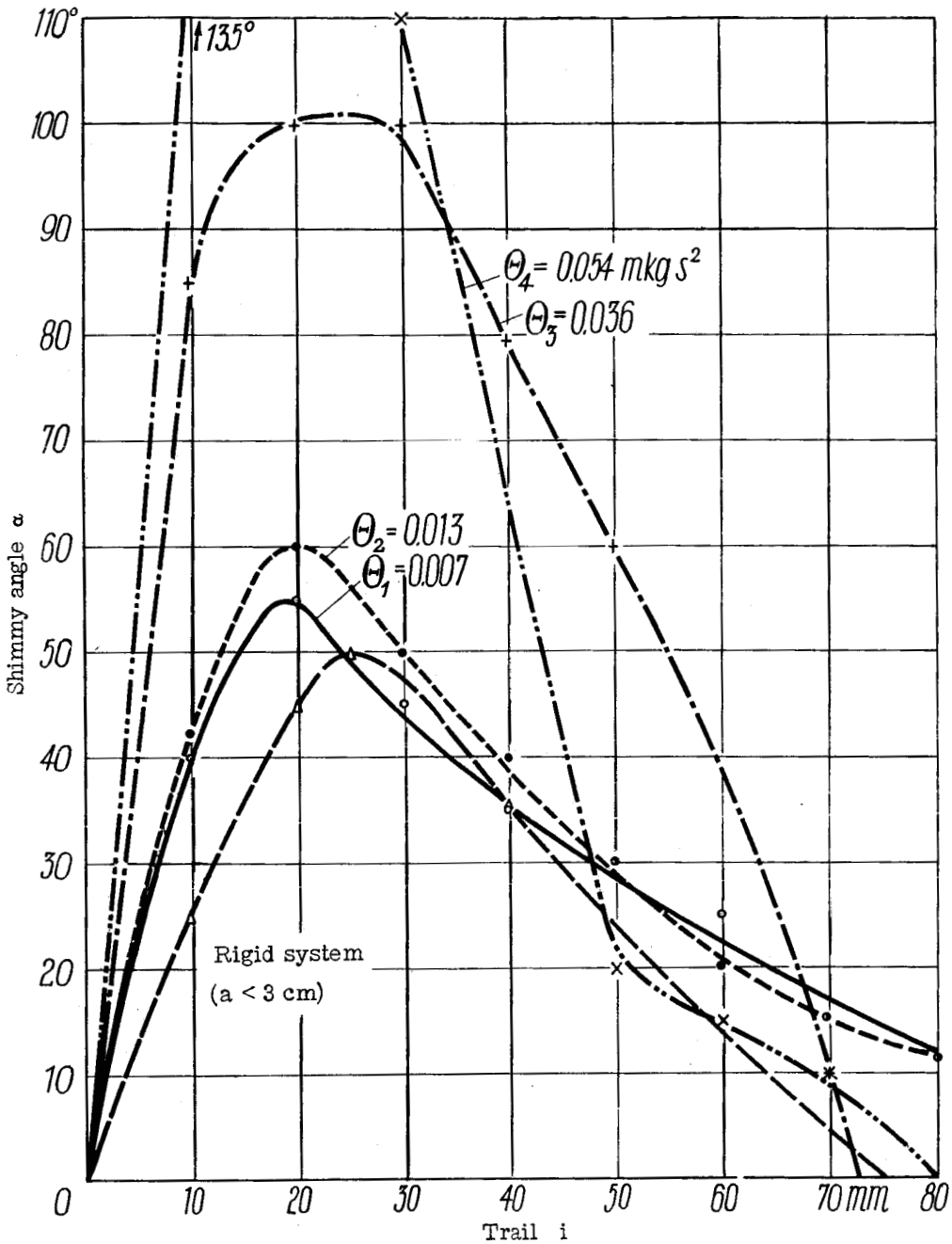

Figure 27.- Tail-wheel shimmy for various moments of inertia. Torsional rigidity $\frac{c}{l}$ = 56 m kg [1800] m kg; swivel-axis inclination $\beta = 0^{\circ}$; load P = 6 kg; adhesion coefficient $\mu_H \sim 0.4$; tire pressure p = 1.5 atmospheres gage inflation pressure; velocity v = 50 km/hr (tachometer).

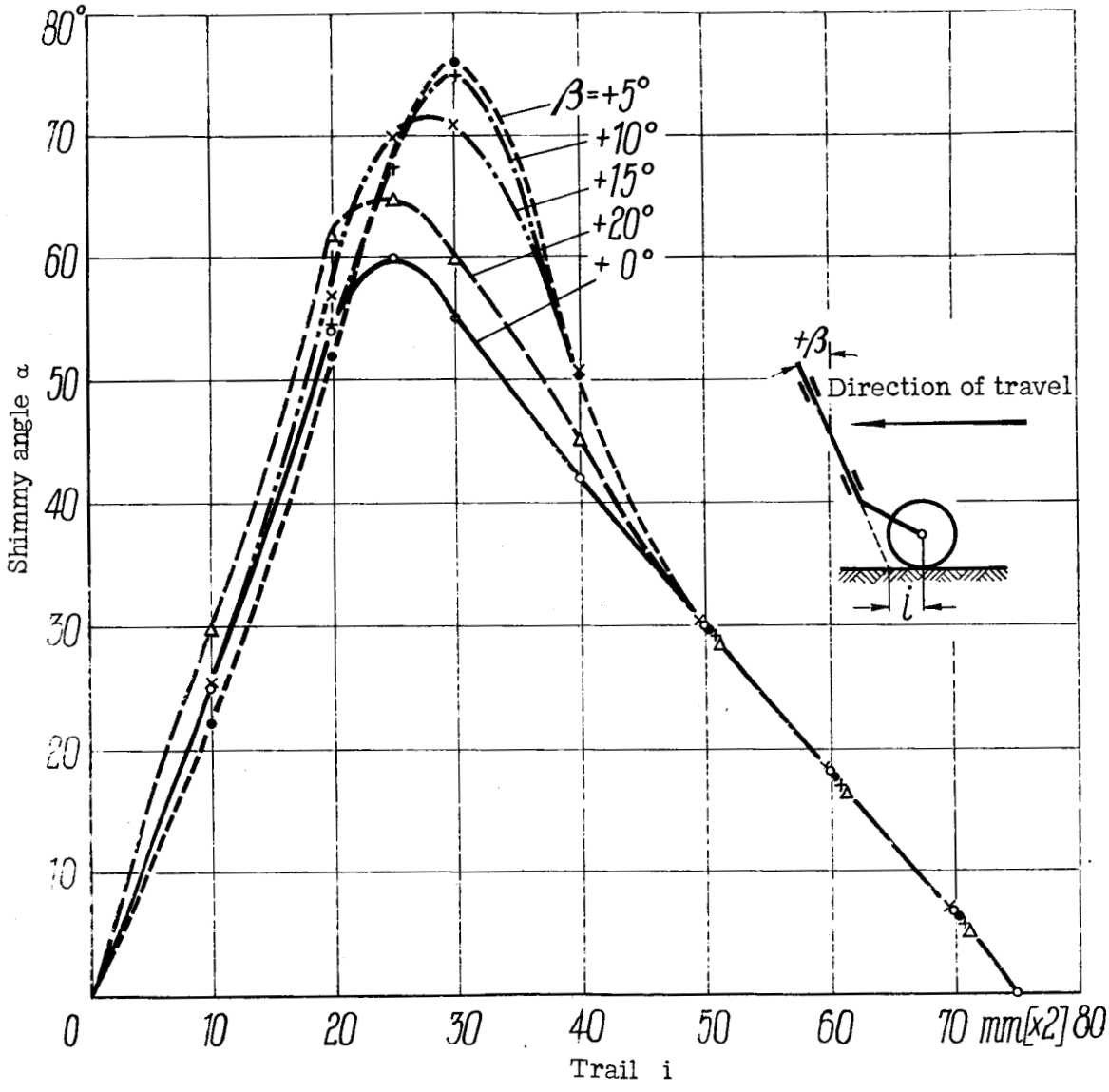

Figure 28.- Influence of the trail i and the inclination angle β of the swivel axis in the direction of travel on the shimmy of tail wheel (β positive). Velocity v = [27 km/hr]; load P = 6.25 [50] kg; adhesive-friction coefficient μ_H = 0.4 to 0.5; tire-inflation pressure p = 1.5 to 2.0 atmospheres gage inflation pressure.

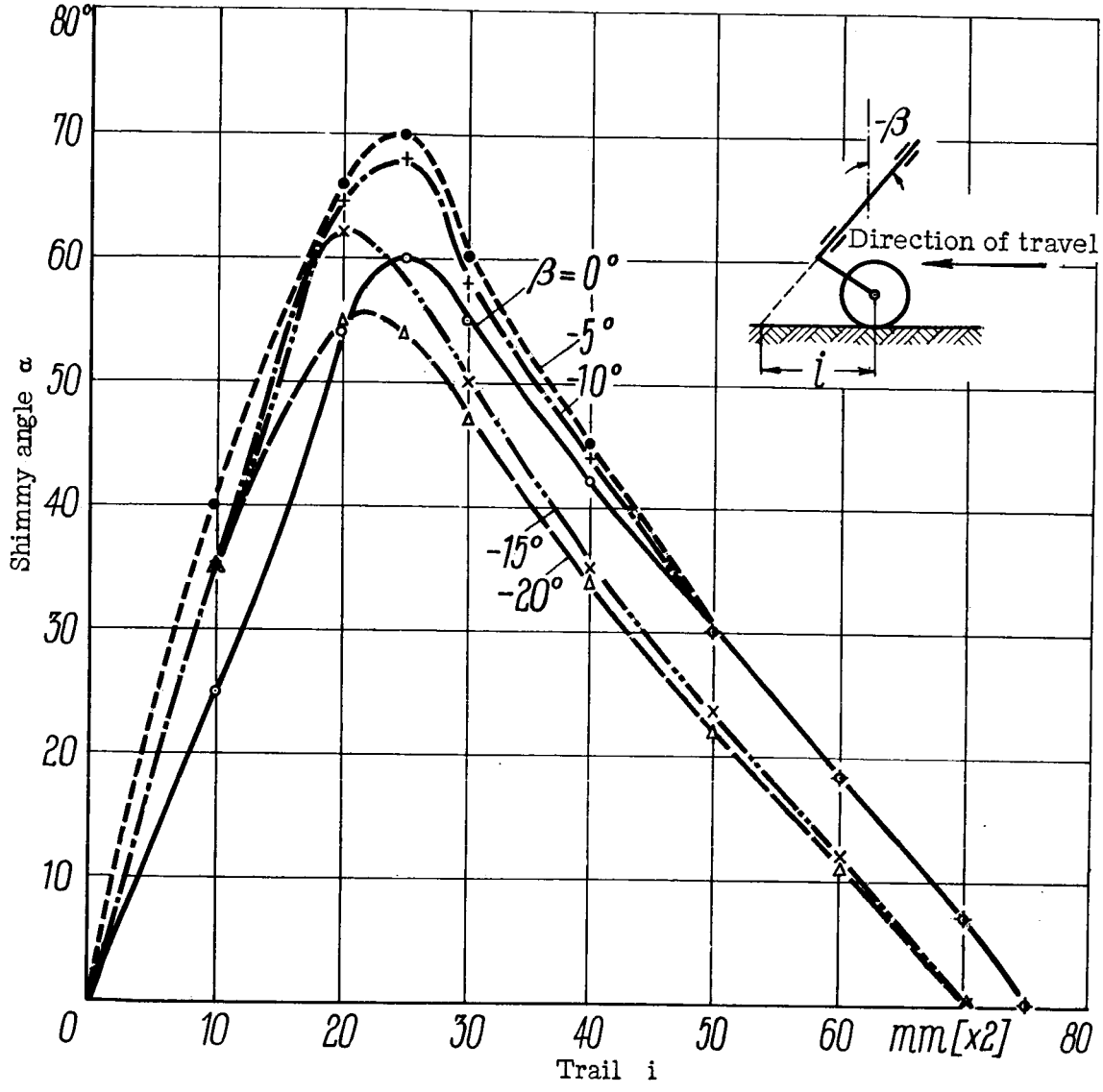

Figure 29.- Influence of trail i and of the inclination angle β of the swivel axis against the direction of travel on tail-wheel shimmy (β negative). Velocity v = [27 km/hr]; load P = 6.25 [50] kg; adhesive-friction coefficient μ_H = 0.4 to 0.5; tire-inflation pressure p = 1.5 to 2.0 atmospheres gage inflation pressure.

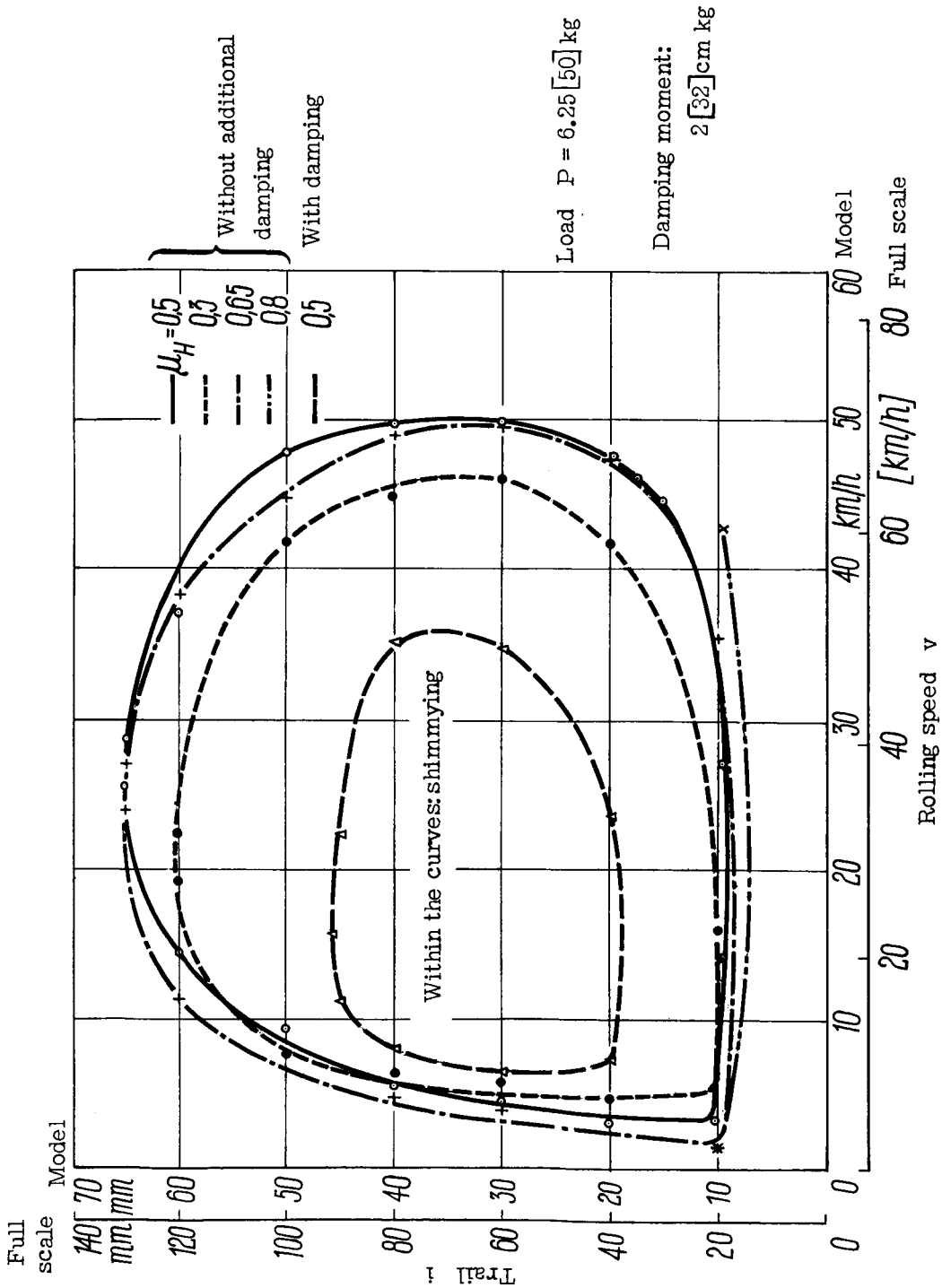

Figure 30.- Shimmying tendency as a function of trail i and rolling speed v. Swivel axis vertical.

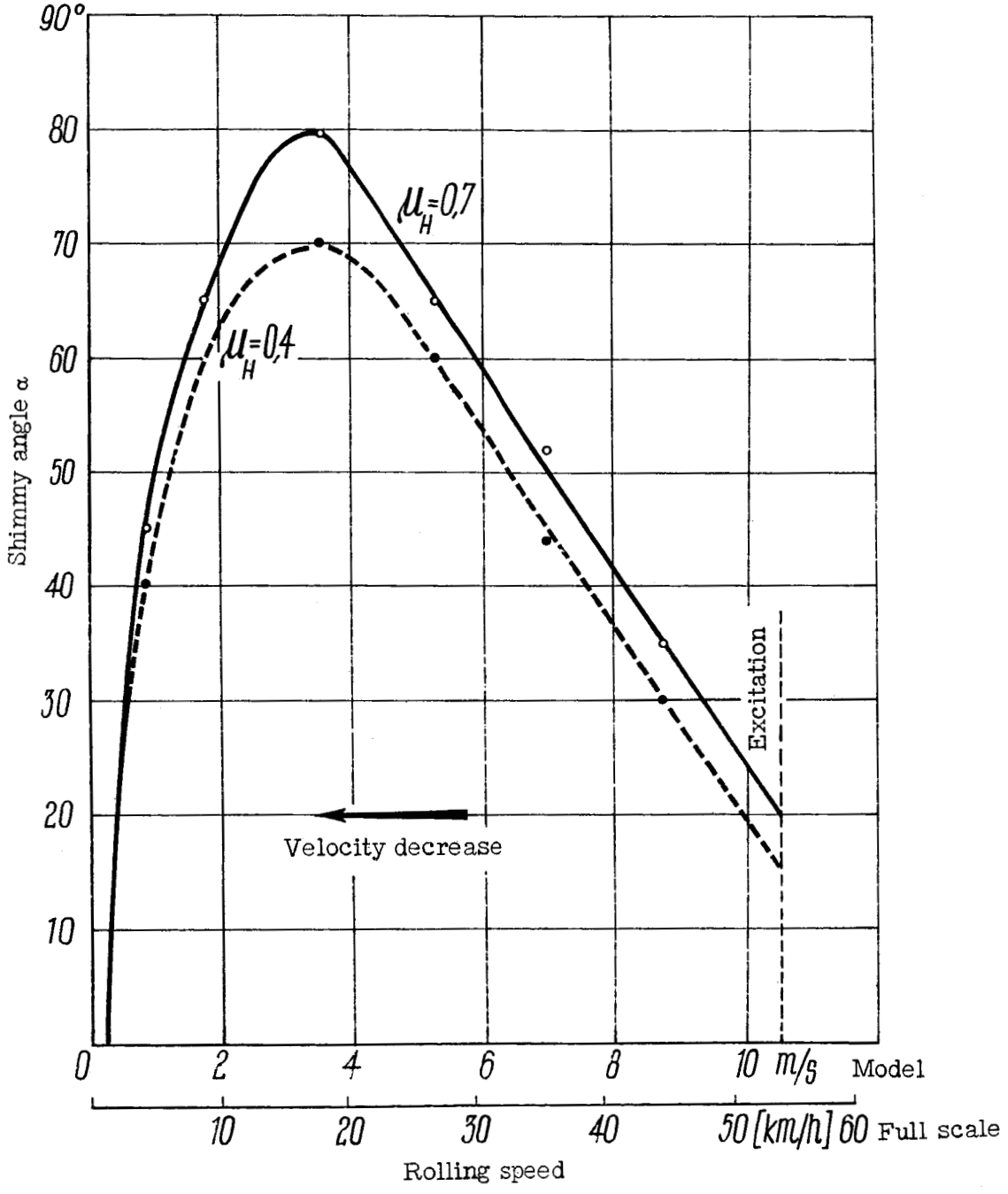

Figure 31.- Influence of velocity on the shimmy of tail wheels for i = 20 [40] mm trail. Load P = 6.25 [50] kg; tire-inflation pressure p = 1.5 atmospheres gage; swivel axis vertical.

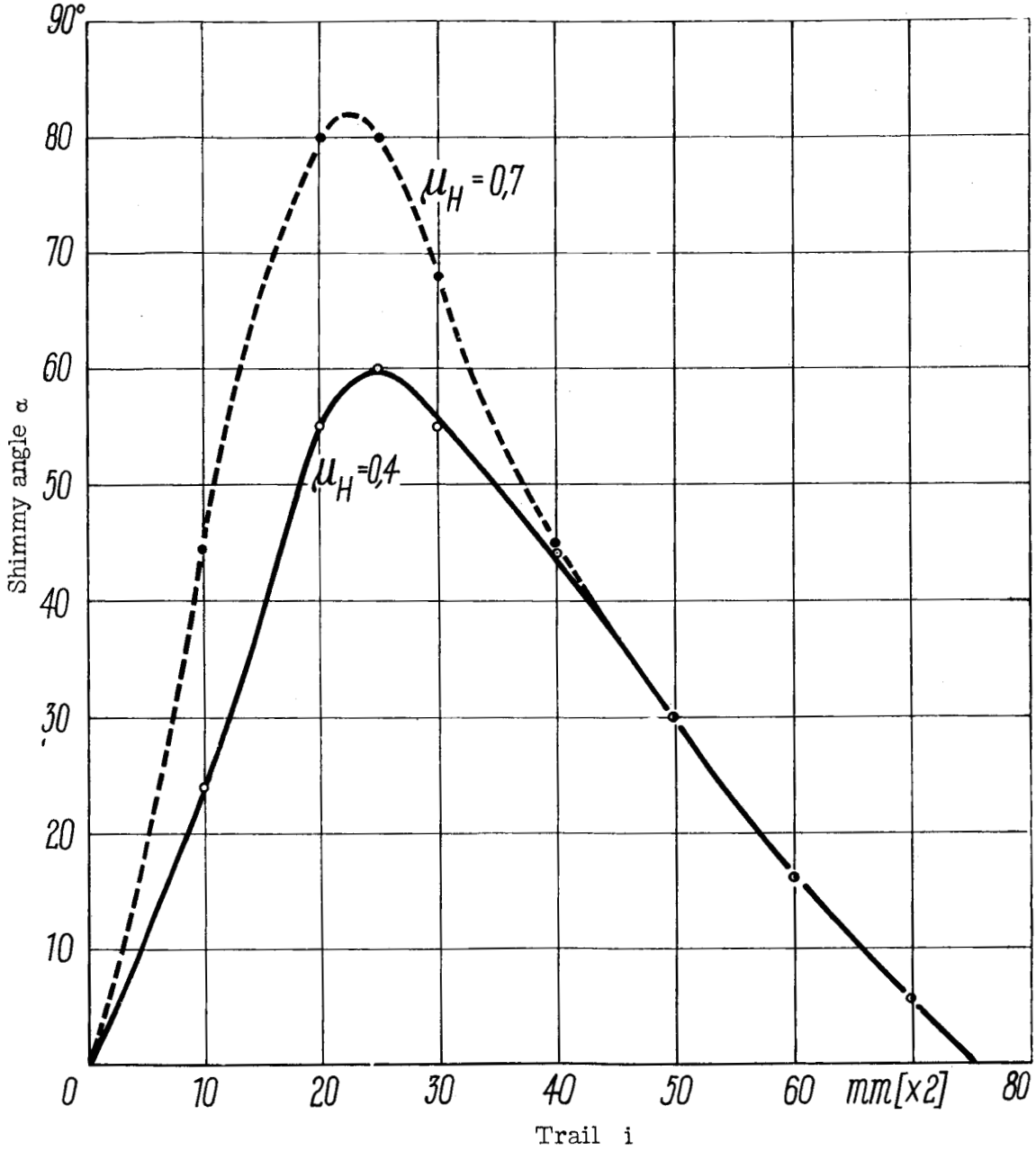

Figure 32.- Influence of friction on tail-wheel shimmy. Velocity v = [27] km/hr; load P = 6.3 [50] kg; tire pressure p = 1.5 atmospheres gage inflation pressure.

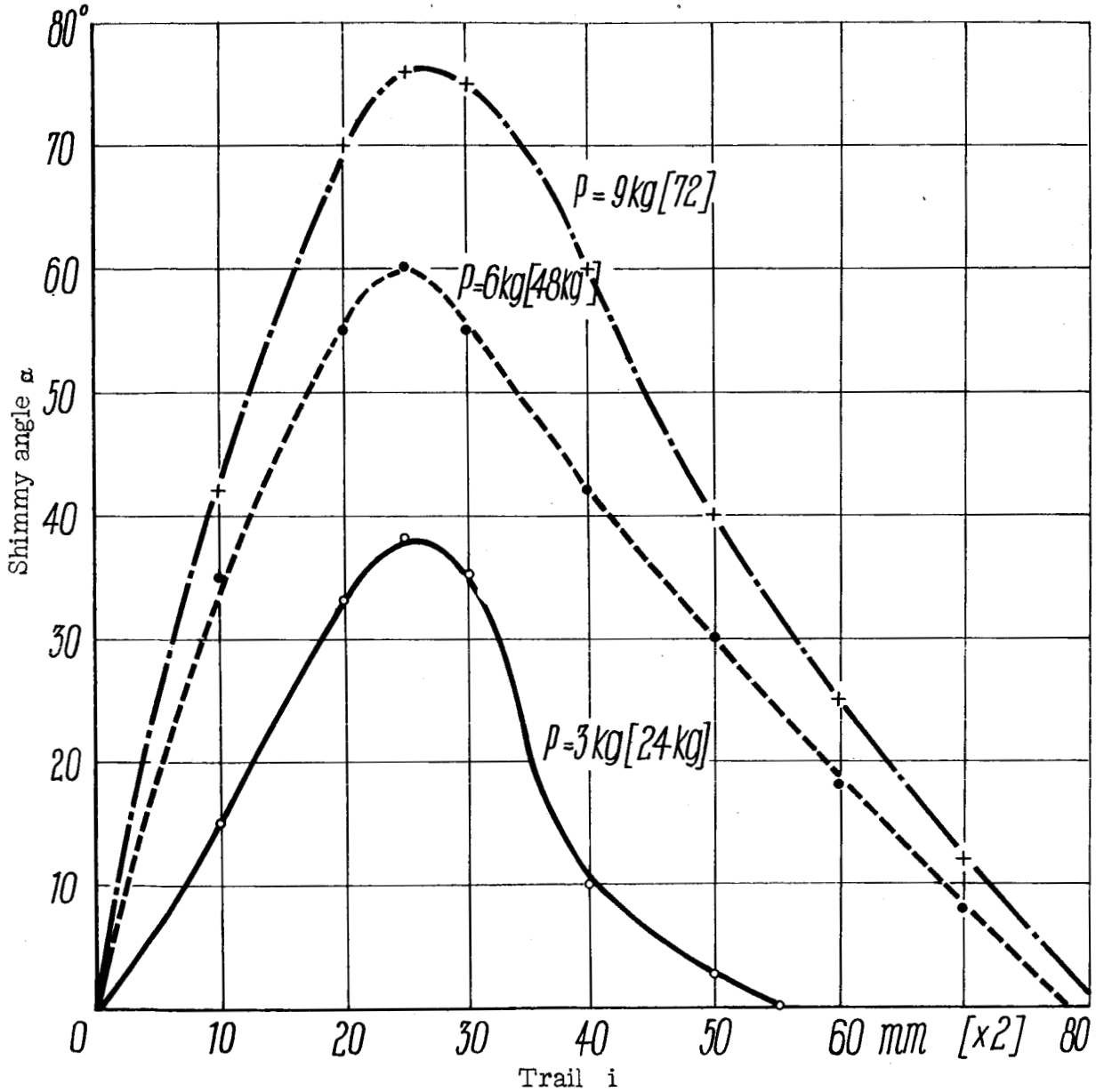

Figure 33.- Influence of load P on tail-wheel shimmy. Tire pressure p = 1.5 atmospheres gage inflation pressure; inclination of swivel axis $\beta = 0^{\circ}$; friction coefficient $\mu_H = 0.4$.

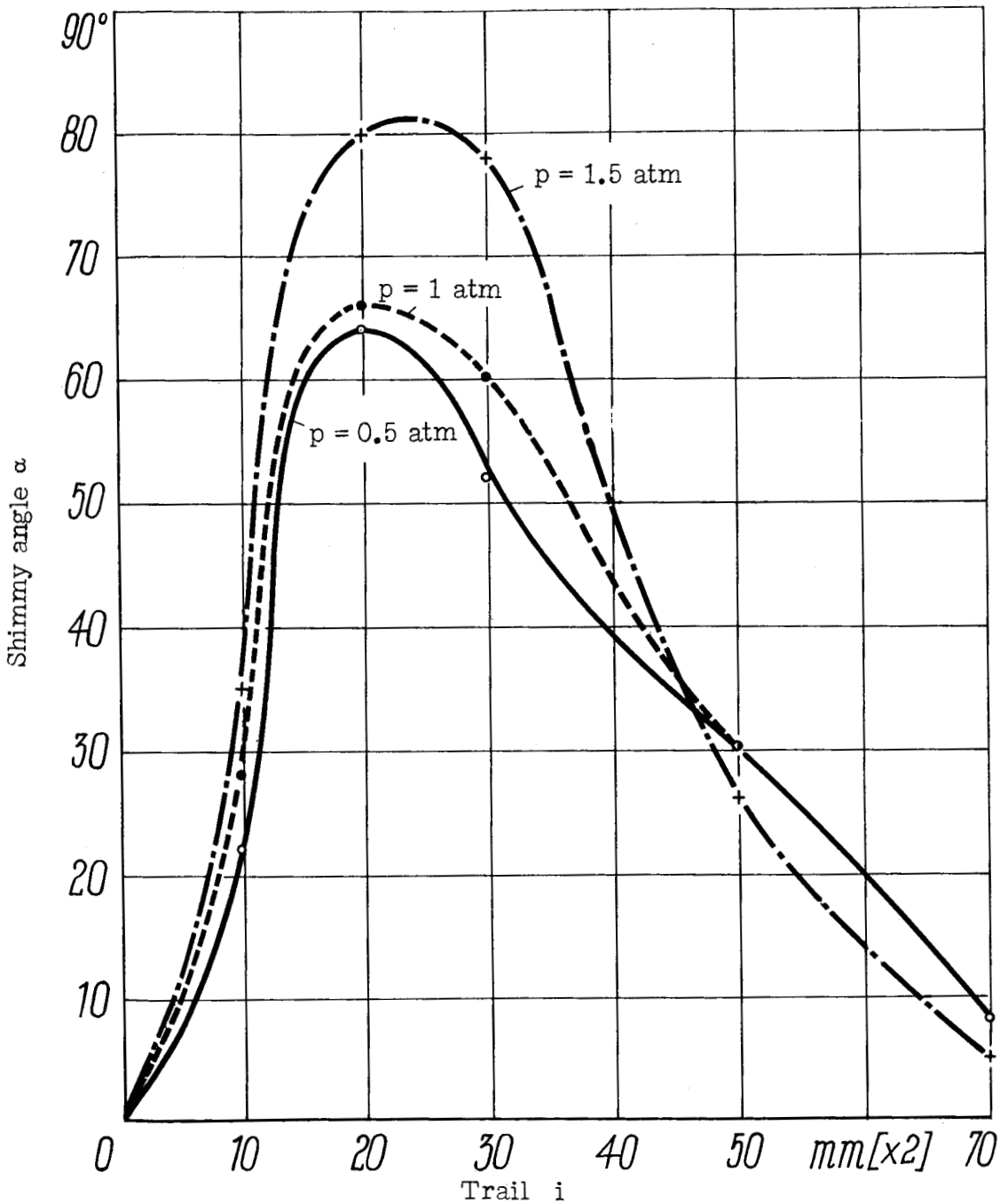

Figure 34.- Shimmy angle for various tire-inflation pressures. Load P = 6.3 kg [50] kg; adhesion friction $\mu_H = 0.4$.

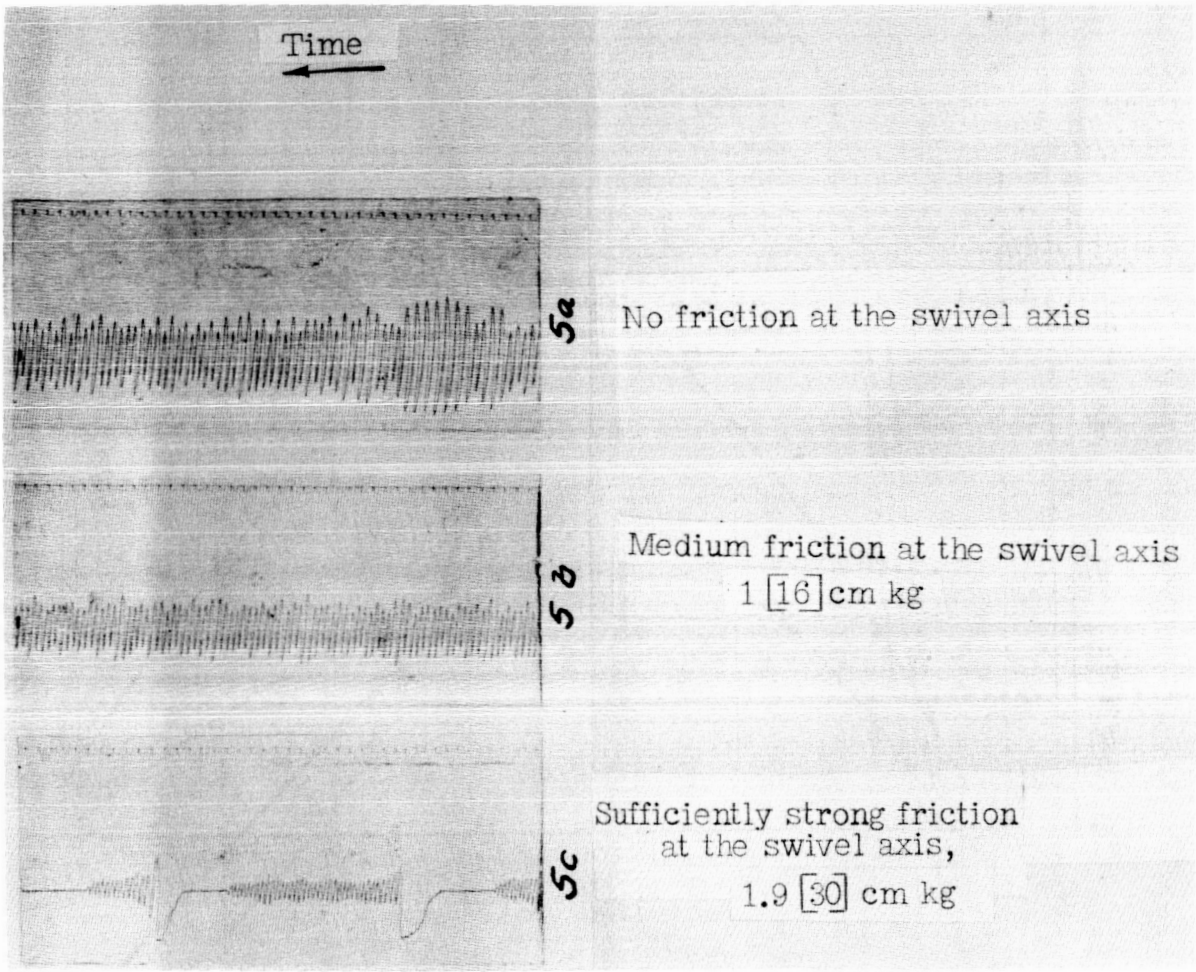

Figure 35.- Damping of shimmy motions by friction (compare fig. 7).

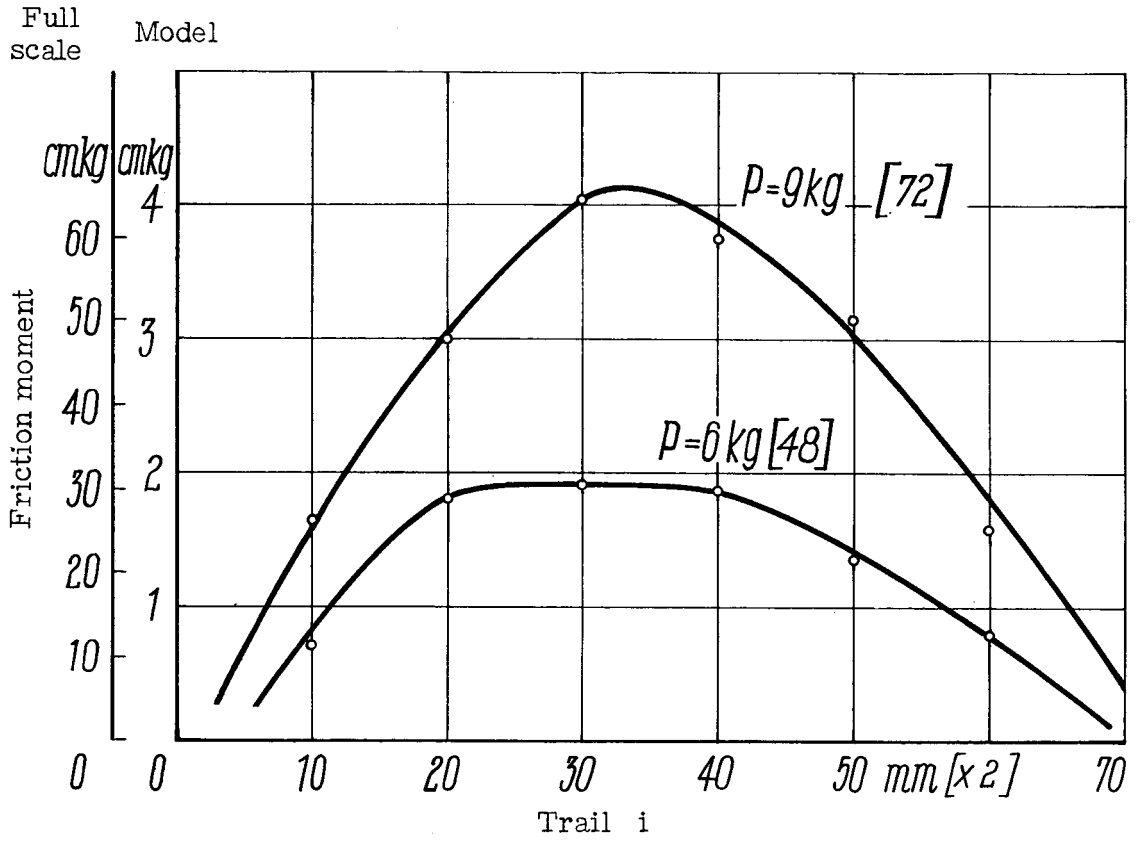

Figure 36.- Friction moment at the swivel axis of the tail wheel required for avoidance of shimmy. Velocity v = 19 [27] km/hr; adhesive-friction coefficient μ_H = 0.4 to 0.5; swivel axis vertical.

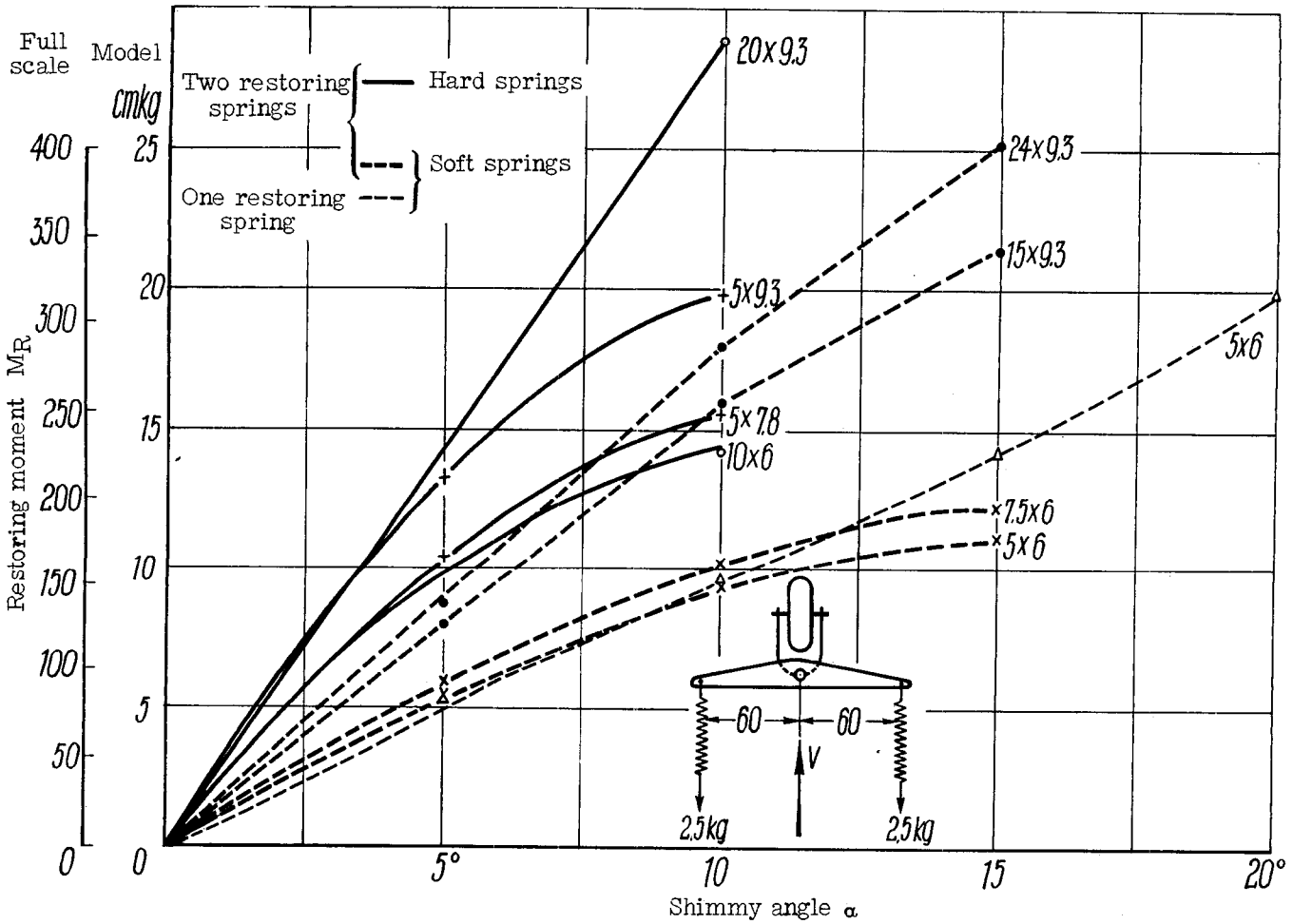

Figure 37.- Characteristics of the restoring moments about the swivel axis. Two-spring restoring. Variation of the spring compression and spring stiffness. 5 × 6 signifies: 5 kg total compression for 6 cm lever arm.

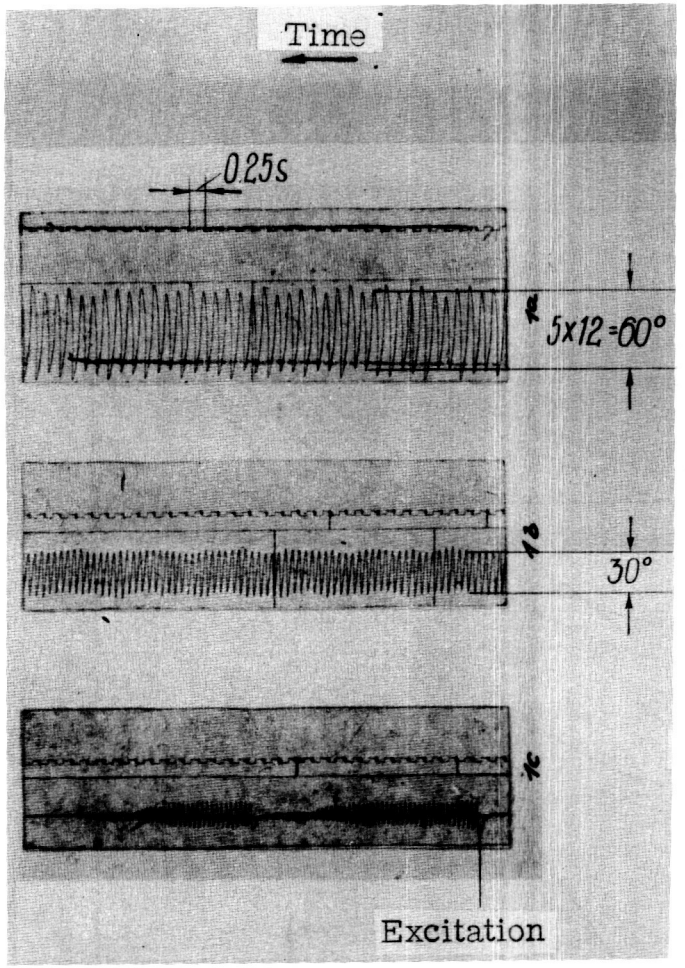

No restoring springing

Restoring springing 10 x 6 (see fig. 37)'
10 [80] kg compression

Restoring springing 20 x 9.3 thus
20 [160] kg compression

Figure 38.- Shimmy damping by two restoring springs.

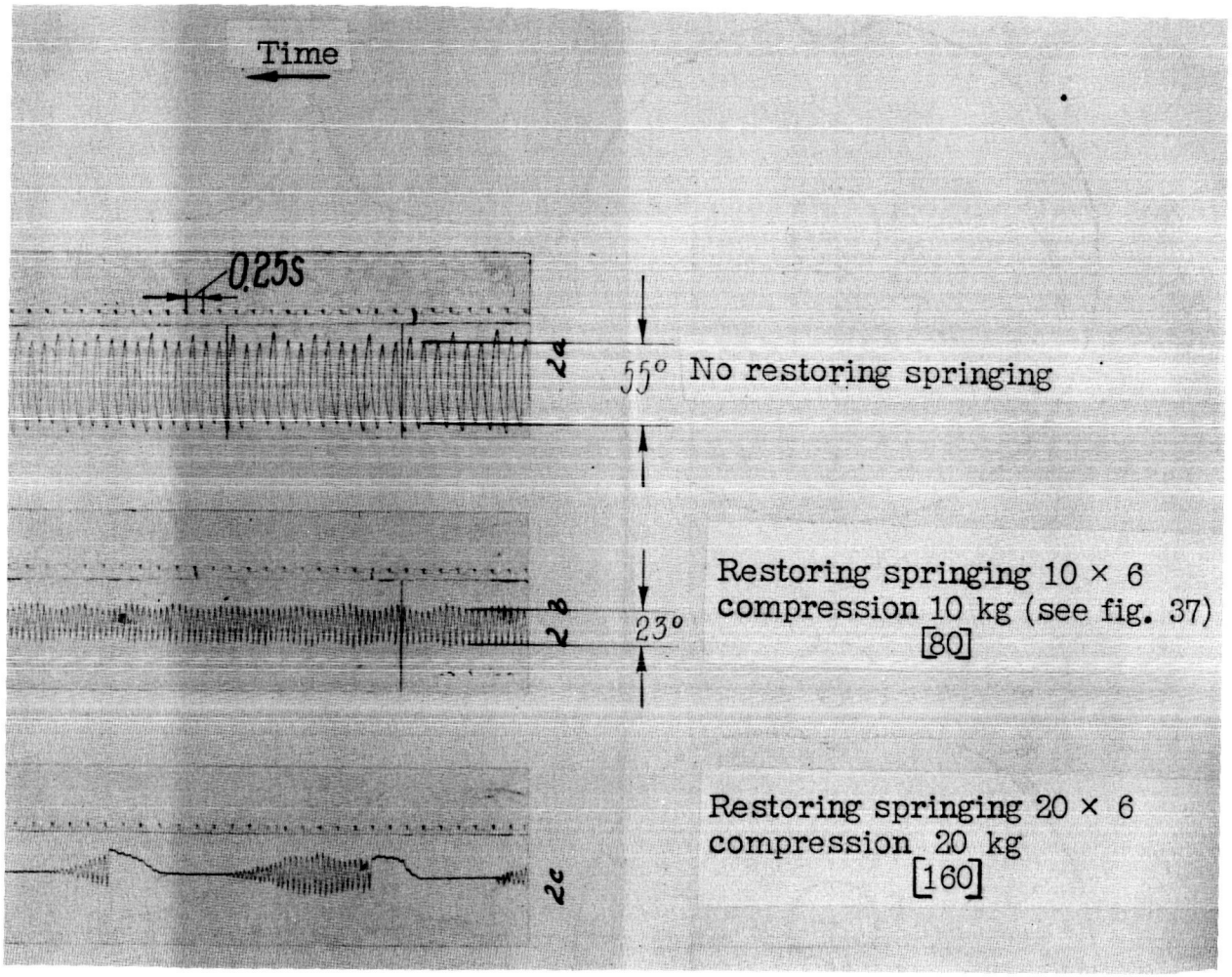

Figure 39.- Shimmy damping by one restoring spring.

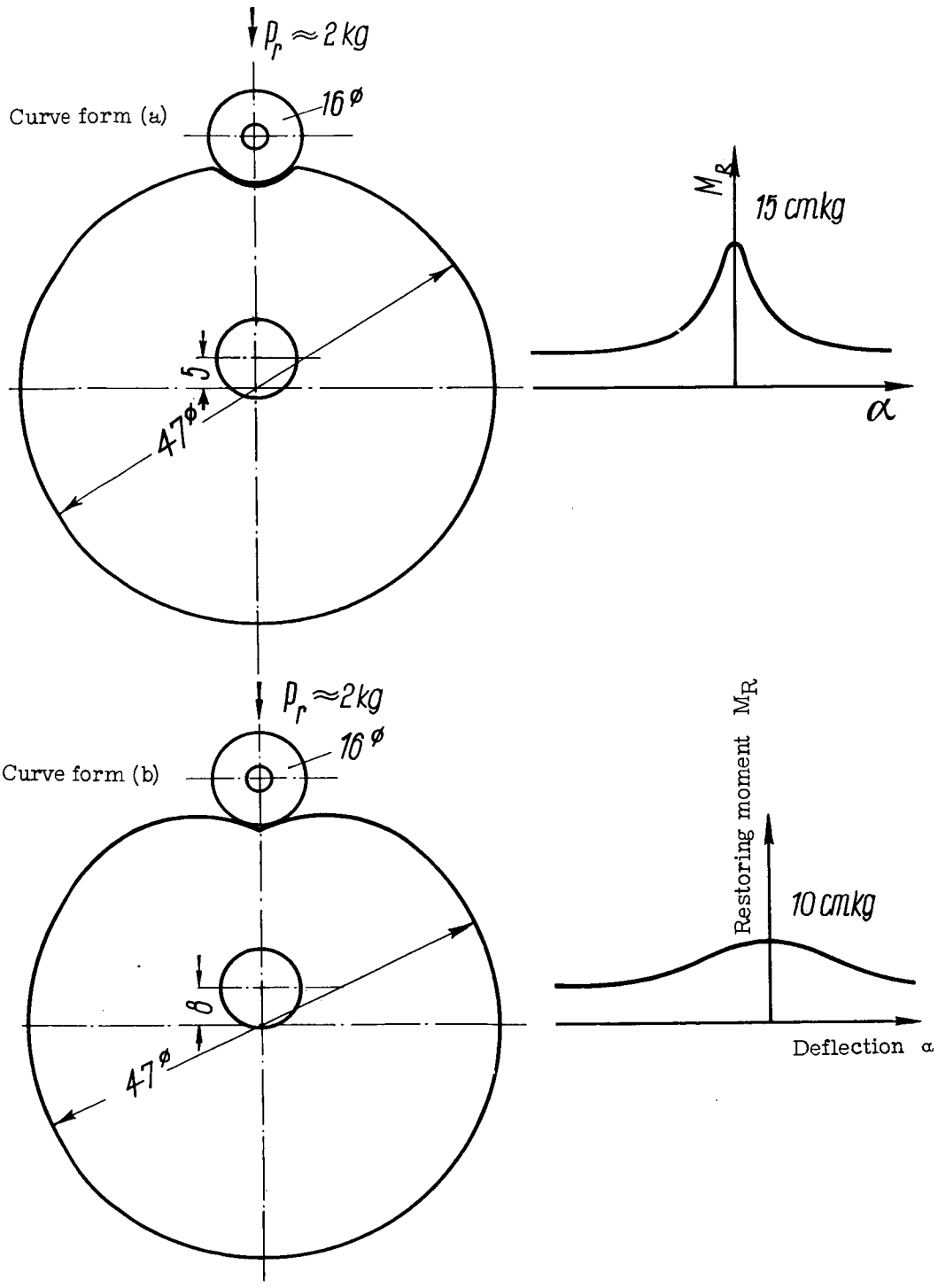

Figure 40.- Cam plates for test arrangement according to figure 10 (to scale) with the characteristics of the restoring moments.

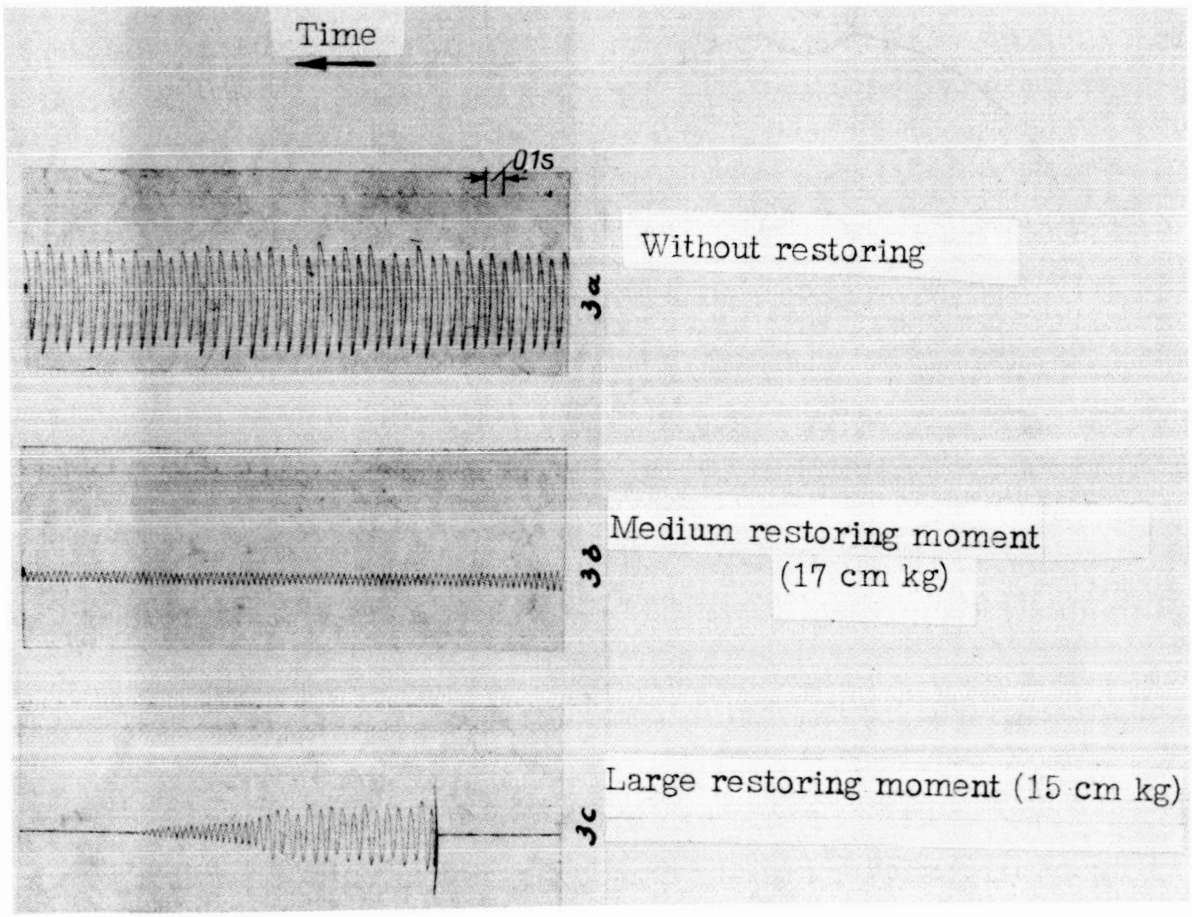

Figure 41.- Damping with cam plate and pressure roller. Curve form according to figure 40a.

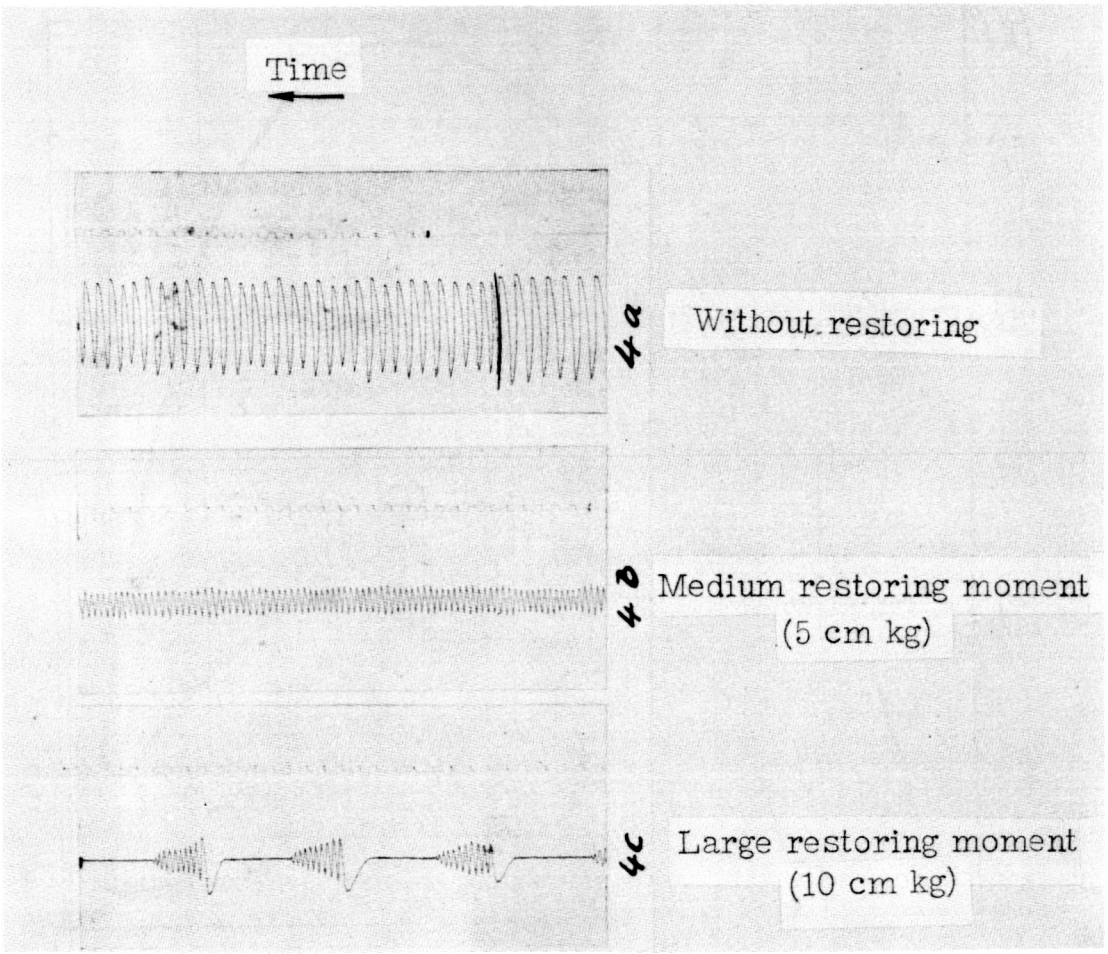

Figure 42.- Damping with cam plate and pressure roller. Curve form according to figure 40b.

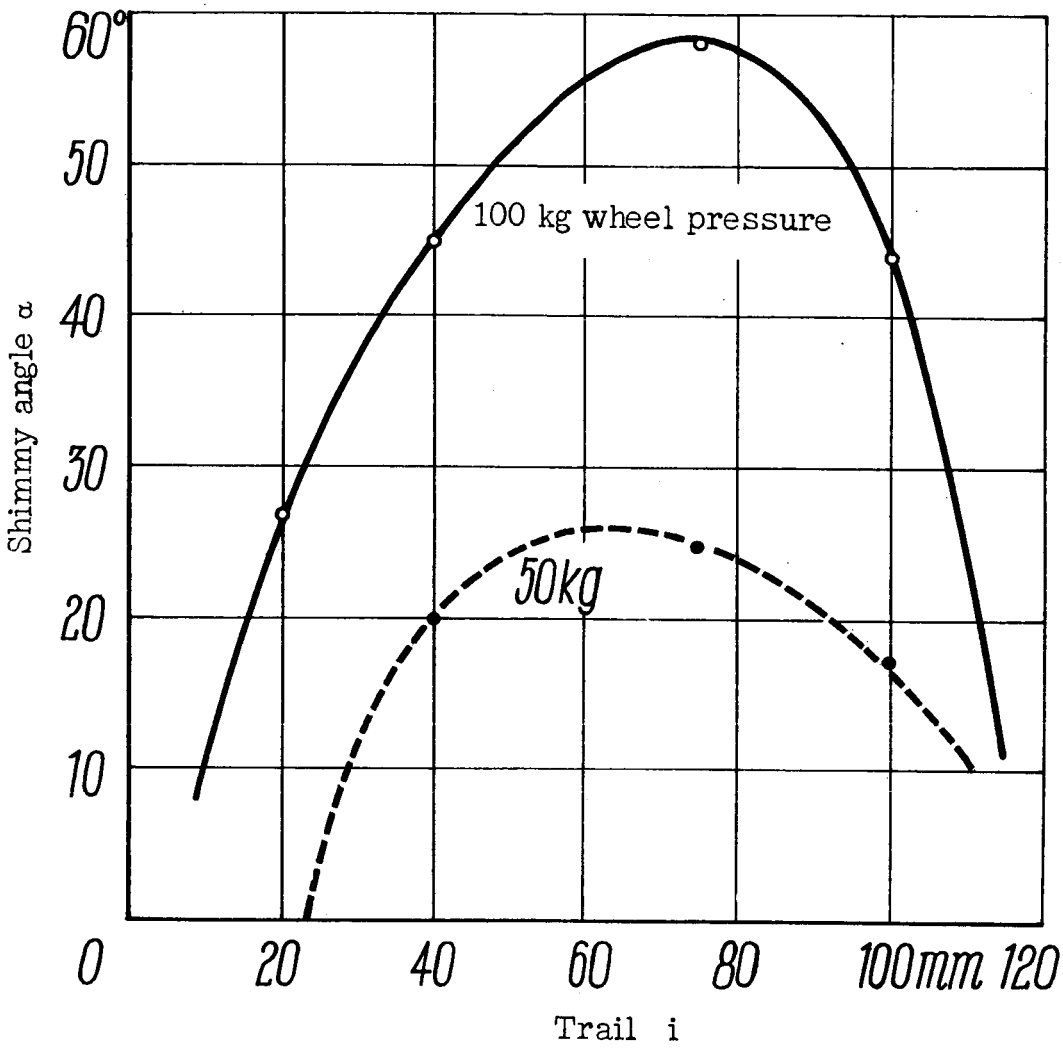

Figure 43.- Shimmy angle α and trail i of a full-scale tail wheel in tests on the rotating drum. Tire size 260 × 85; adhesive-friction coefficient μ_H = 0.7 to 0.08; swivel axis vertical; velocity v = 40 km/hr.

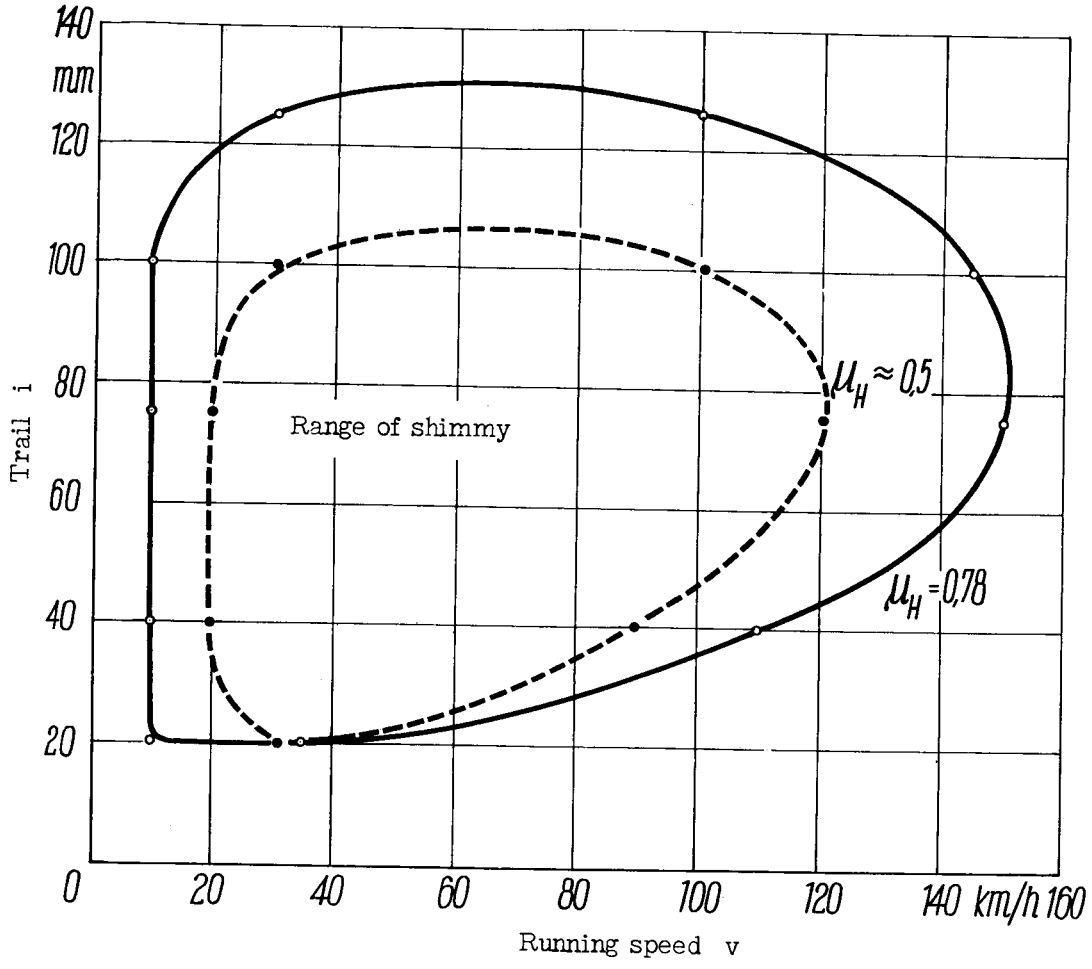

Figure 44.- Connection between trail and running speed for shimmy. Tests on the rolling-field drum, swivel axis vertical. Tire 260 × 85; load 50 kg.

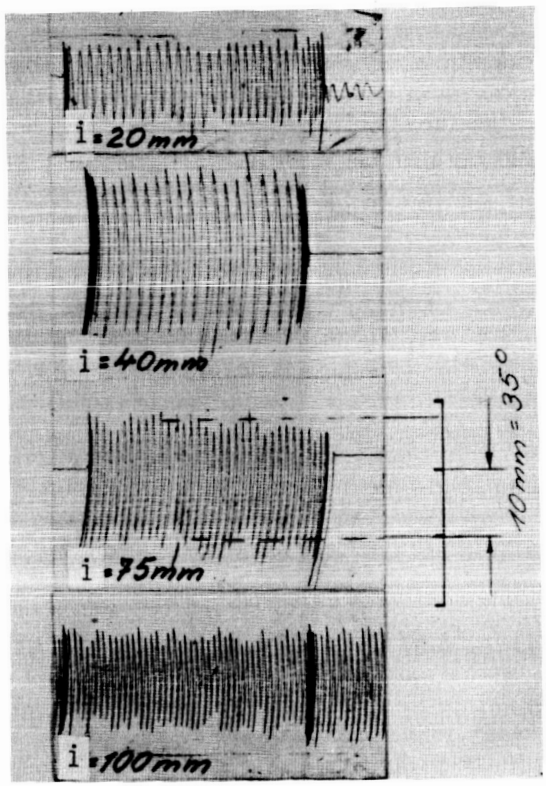

Figure 45.- Shimmy on the road with full-scale tail wheel. Installation in a passenger car (compare fig. 16). Trail i = 20, 40, 75, and 100 mm; tire 260 × 85; runway: asphalt, dry, $\mu_H = 0.72$; load P = 100 kg; velocity v = 40 km/hr.

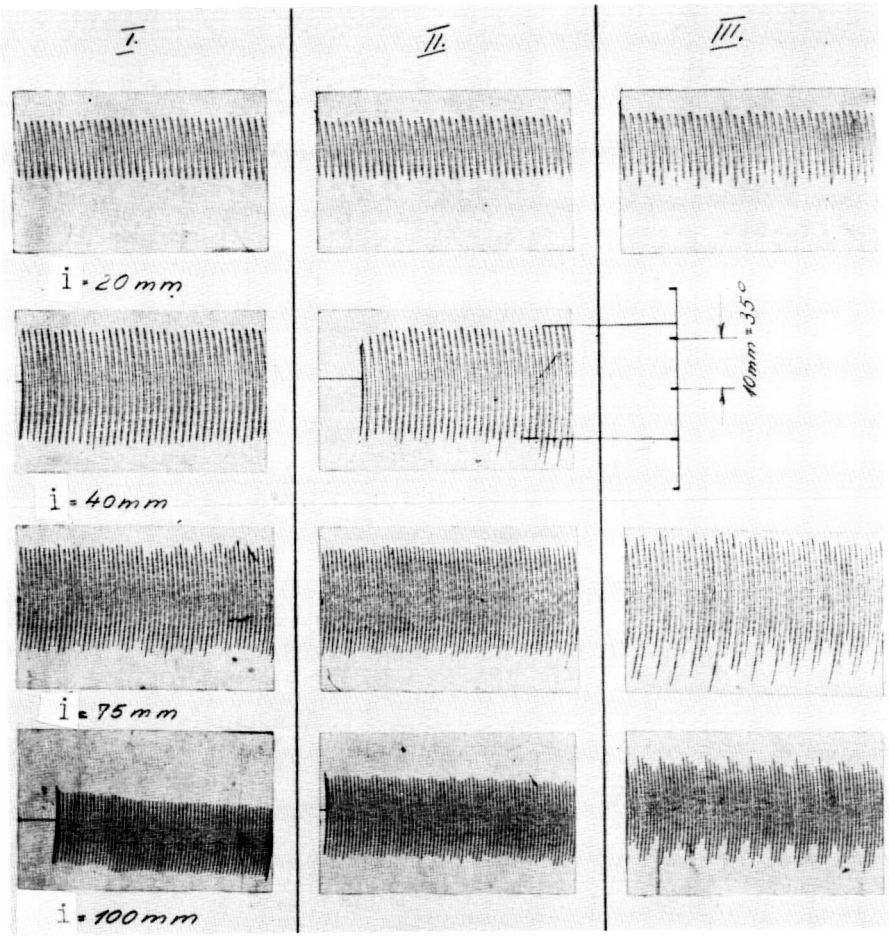

I. Vehicle stationary
II. Vehicle laterally excited
III. Vehicle vertically excited

Figure 46.- Shimmy of the full-scale tail wheel on the rolling field (passenger car with built-in tail wheel). Trail i = 20, 40, 75, and 100 mm; tire 260 x 85; adhesive-friction coefficient μ_H = 0.75; load P = 100 kg; velocity v = 40 km/hr.

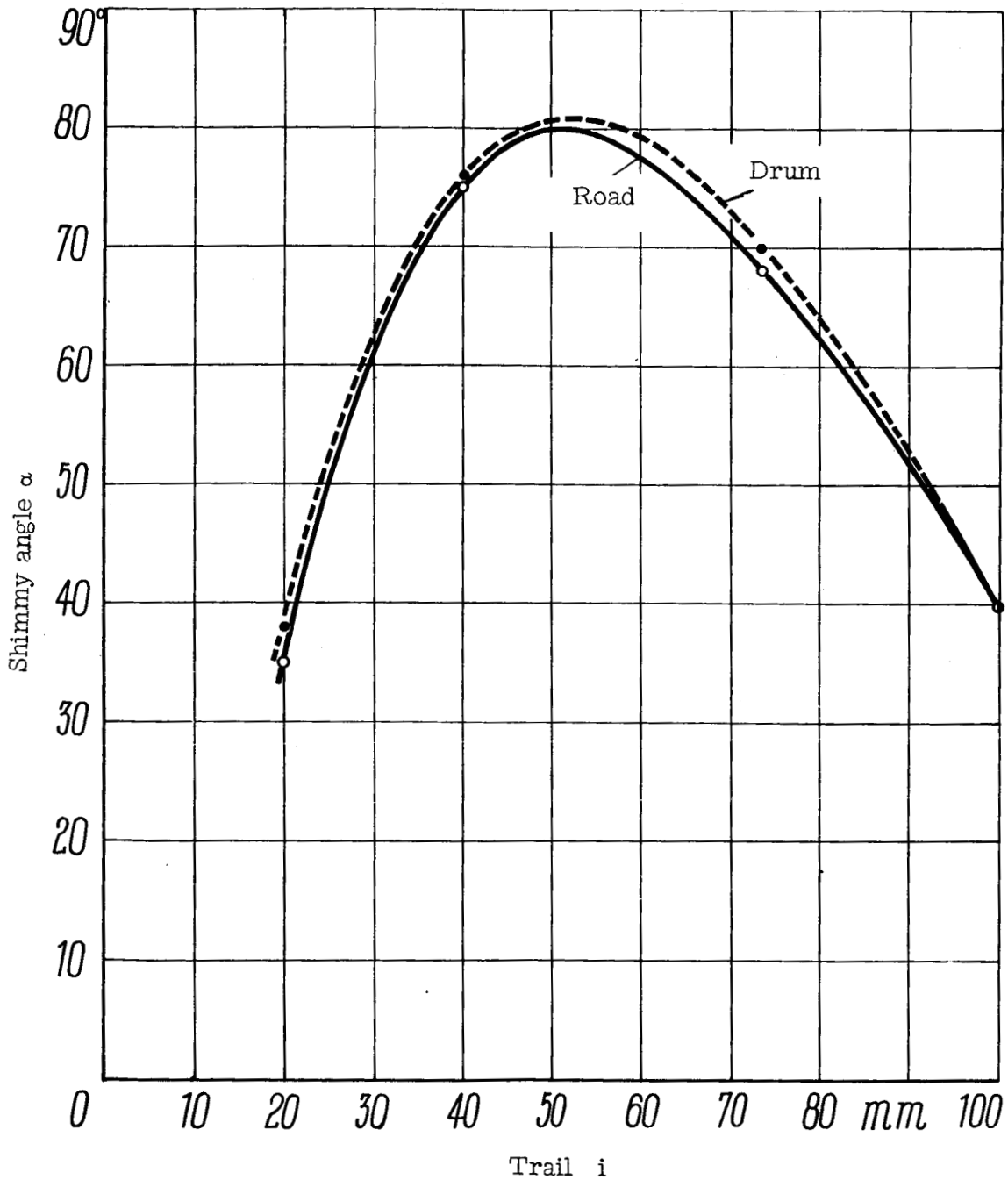

Figure 47.- Comparison of the test results obtained with the full-scale tail wheel on drum and road. Drum: iron, $\mu_H = 0.75$; road: asphalt, $\mu_H = 0.72$; wheel size: 260 × 85; load P = 100 kg; velocity v = 40 km/hr.

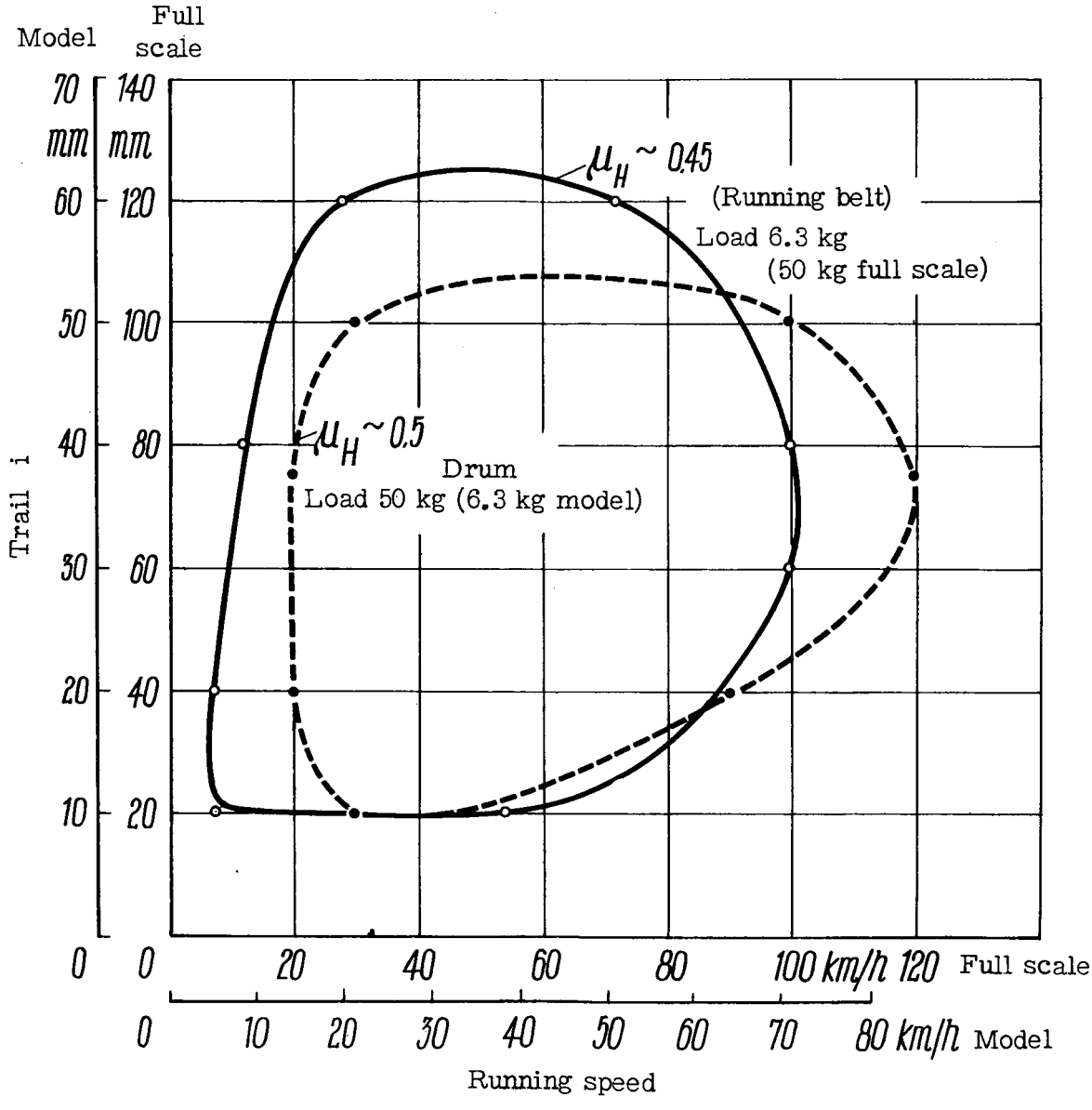

Figure 48.- Comparison of the ranges of tail-wheel shimmy of full-scale wheel on drum and of model wheel on running belt.

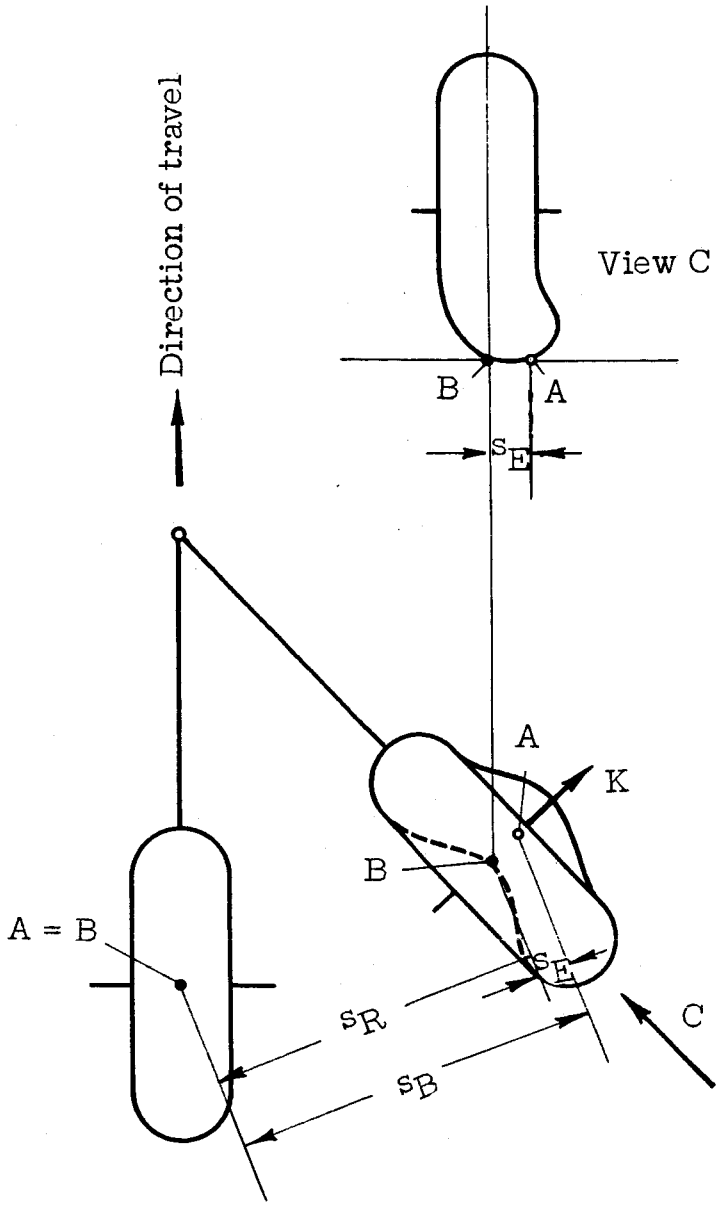

s_R lateral path of wheel center
s_B lateral path of point of ground contact } $s_B = s_R + s_E$
s_E lateral deformation of tire
K lateral force on ground perpendicular to plane of tire
A center of contact area
B ground projection of wheel-center point

Figure 49.- Representation of the lateral paths and deformations in shimmy.

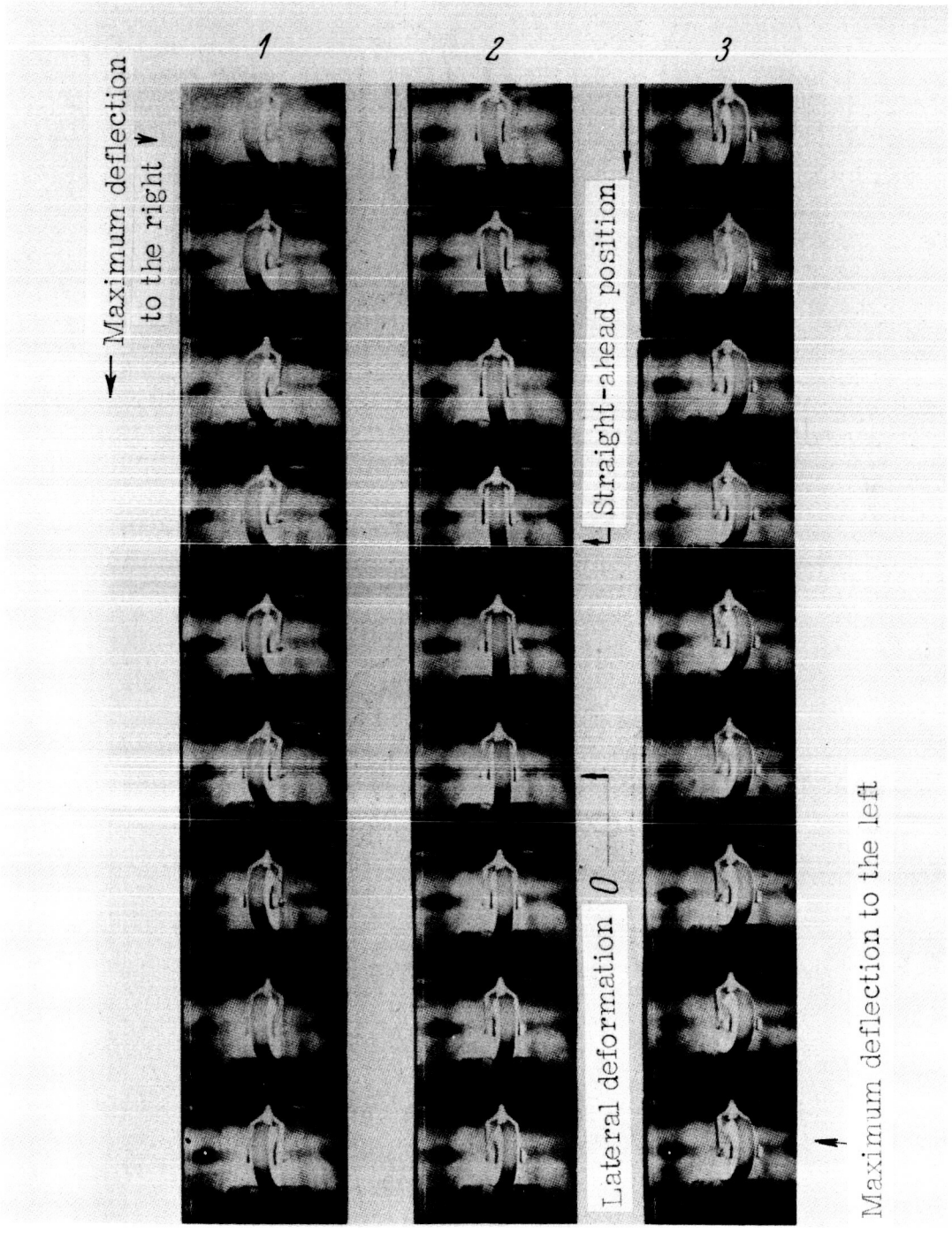

Figure 50.- Lateral deformation of a full-scale tire on a shimmying tail wheel on the rotating drum. Tire pressure 2.5 atmospheres gage inflation pressure. Change in direction of the lateral deformation 0.004 to 0.005s after passage through straight-ahead position.

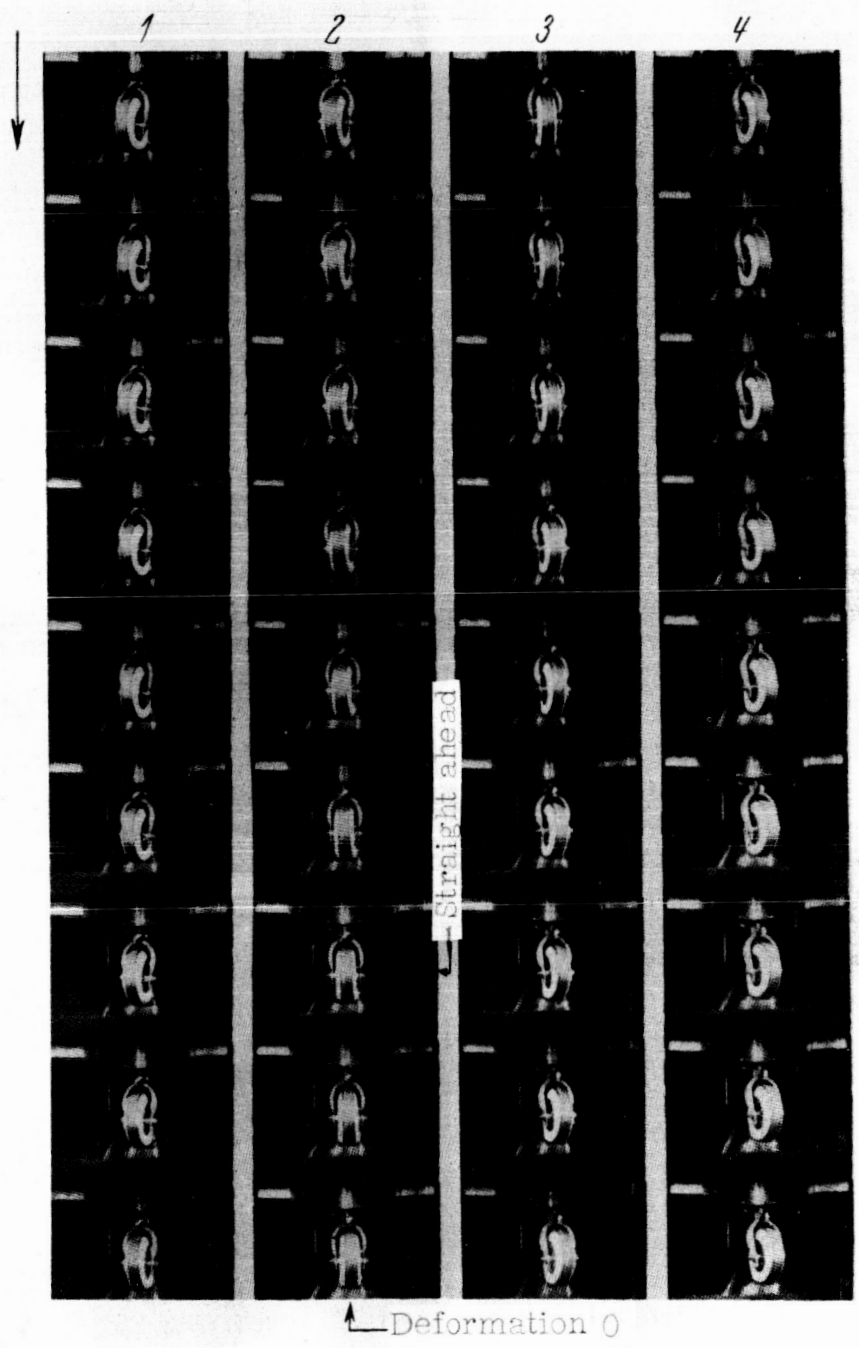

Figure 51.- Lateral deformation of a pneumatic tire on a shimmying model wheel on the running belt. High tire-inflation pressure (1.6 atmospheres gage inflation pressure). Change in direction of the lateral deformation 0.004s after passage through straight-ahead position.

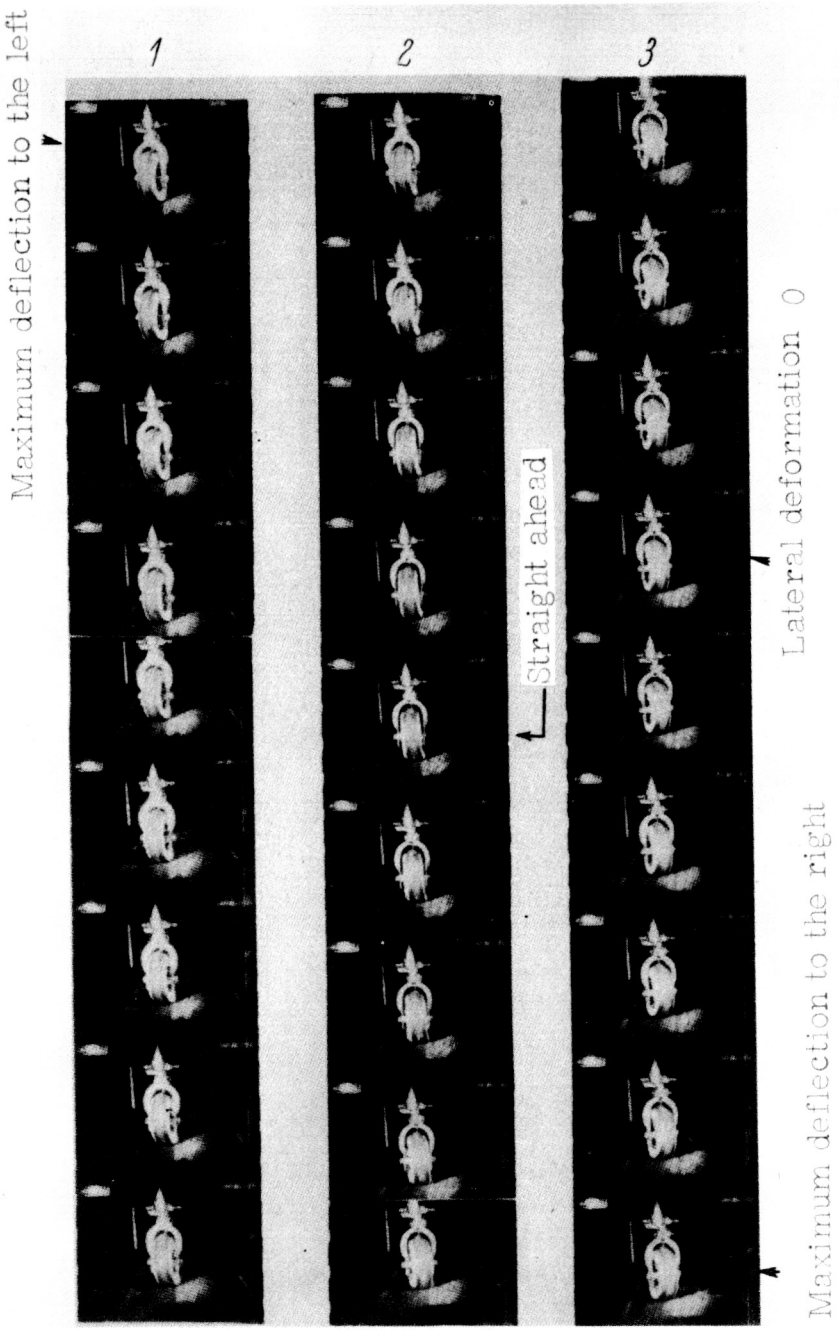

Figure 52.- Lateral deformation of a pneumatic tire on a shimmying model wheel on the running belt. Low tire inflation pressure (0.8 atmospheres gage inflation pressure). Change in direction of the lateral deformation 0.014s after passage through straight-ahead position.

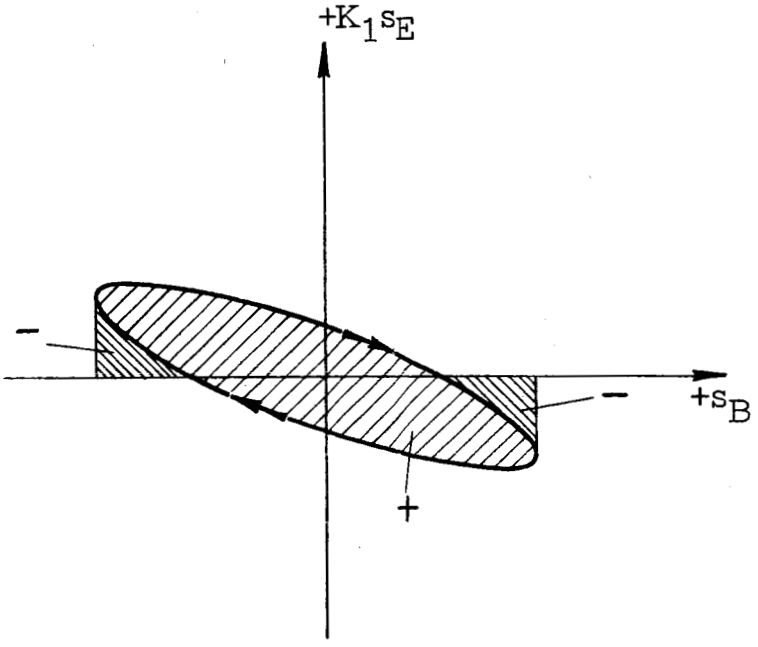

Figure 53.- Energy diagram from the variation of tire deformation according to slow-motion pictures.